SPECTROSCOPIC FUNCTION-STRUCTURE ANALYSIS OF THE SERCA-PLB COMPLEX

A DISSERTATION
SUBMITTED TO THE FACULTY OF
UNIVERSITY OF MINNESOTA
BY

XIAOQIONG DONG

IN PARTIAL FULFILLMENT OF THE REQUIREMENTS
FOR THE DEGREE OF
DOCTOR OF PHILOSOPHY

DAVID D. THOMAS, ADVISER

JUNE, 2014

Acknowledgements

First and foremost, I would like to thank my adviser, **Dr. David Thomas**, for recruiting me to the lab and for advising me. He has been inspiring and encouraging, challenging me beyond what I thought I could accomplish. In him, I saw what a true scientist is, always enthusiastic, energetic, and hard-working. I would not have finished my PhD journey without his support and guidance.

I would like to thank **Dr. Ji Li** and **Dr. Elizabeth Lockamy**, who mentored me when I first joined the lab. They taught me the wet lab and fluorescence techniques that are instrumental in my thesis work, and presentation skills that I will benefit from throughout my science career.

I am also thankful to **Dr. Christine Karim**, for inspiring scientific discussions. I want to thank **Dr. Razvan Cornea** for his enthusiastic help with protein labeling, small lectures on fluorophores, and career advice. I am grateful to **Dr. Zachary James**, for his help with molecular biology and protein expression, which led to a breakthrough of my research presented in Chapter 4. I appreciate the friendship with **Jesse McCaffrey**. I want to thank him especially for proofreading my dissertation.

It is hard to think of anyone in the Thomas lab who hasn't helped me along the way. Many thanks to **Dr. Gregory Gillispie**, **Kurt Peterson**, **Dr. Joseph Muretta**, and **Karl Petersen**, for technical assistance of fluorescence instrumentation and data analysis. I want to thank **Dr. Mike Autry** for his encyclopedic knowledge of the SERCA-PLB field and stimulating discussions. I am thankful to **Octavian Cornea** and **Sarah Blakely**

for all the administrative assistance. I also want to thank the Thomas lab members who I have been fortunate to work with: **Dr. Bengt Svensson, Dr. Naa-Adjeley Ablorh, Holly Langer, and Dr. Piyali Guhathakurta**.

Dedication

To my grandparents, Xiuxiang Zheng and Xiuzhang Dong.

To my parents, Ruifang Dong and Zhiyi Zang.

Abstract

Cardiomyocyte contraction is controlled by intracellular Ca^{2+} concentrations. Action potential opens the voltage-gated calcium channel in the sarcolemma and triggers the calcium-induced calcium-release mechanism to release Ca^{2+} stored in the sarcoplasmic reticulum (SR) through ryanodine receptors. For muscle relaxation to occur, Ca^{2+} must be removed from the cytosol. Most of the activator Ca^{2+} is sequestered back into the SR by sarco(endo)plasmic reticulum Ca^{2+}-ATPase (SERCA). In ventricular myocytes, SERCA is regulated by a small integral membrane protein, phospholamban (PLB). PLB binds and inhibits SERCA, and this inhibition is physiologically relieved by either micromolar Ca^{2+} in systole, or by phosphorylation at Ser16 or Thr17 through β-adrenergic stimulation. A decline in SERCA activity is implicated in heart failure irrespective of etiologies. Recent gene therapies for heart failure emphasize enhancing SERCA activity by decreasing PLB inhibition. However, the structural mechanism of relief of inhibition still remains elusive. This thesis work is motivated to elucidate the structural basis for SERCA regulation by PLB, hence providing more information for the design of next generation gene and drug therapies.

This thesis work uses time-resolved fluorescence resonance energy transfer (TR-FRET) to probe the structures of the SERCA-PLB complex in its activated or inhibited forms. In the first project, we investigated the function effect of the equilibrium of PLB cytoplasmic domain between an ordered ***R*** state and a disordered ***T*** state on SERCA regulation. We varied the lipid headgroup charges to perturb this equilibrium through

electrostatic interactions with the positively charged PLB cytoplasmic domain. TR-FRET measurements, in conjunction with functional data and electron paramagnetic resonance experiments, established the correlation of the ***T/R*** equilibrium with PLB inhibitory potency. In the second project, we studied the structures of the SERCA-PLB complex under physiological conditions that relieve inhibition. TR-FRET distance measurements between cytoplasmic domains of SERCA and PLB revealed that phosphorylation of PLB at Ser16 relieves SERCA inhibition mainly by shifting the ***T/R*** equilibrium toward the less inhibitory ***R*** state, and partially by dissociating the complex. Micromolar Ca^{2+} probably relieves inhibition through structural rearrangements within the transmembrane domain of the complex. In the last project discussed in this thesis, we used western blot to quantify different phosphorylation states of PLB in pig cardiac SR. PLB can be phosphorylated at either Ser16 or Thr17, generating four phosphorylation states: unphosphorylated, phosphorylated only at Ser16, phosphorylated only at Thr17, or phosphorylated at both sites. We also found that each PLB phosphorylation state has a distinct inhibitory potency for SERCA.

Table of Contents

List of Tables

List of Figures

List of Equations

Chapter 1 Introduction

1.1 Calcium Cycling in Cardiomyocytes

In cardiomyocytes, when the action potential depolarizes the sarcolemma in T-tubules, Ca^{2+} enters the cytoplasm mainly through membrane-potential dependent L-type calcium channels (Figure 1), contributing to the early phase of the action potential plateau. The sodium calcium exchanger (NCX), residing on sarcolemma, may also contribute a small portion of Ca^{2+} influx with concurrent countertransport of Na^{+}. [2] The influx of Ca^{2+} raises the cleft Ca^{2+} concentration, which activates ryanodine receptors (RyRs) to release Ca^{2+} from the sarcoplasmic reticulum (SR). This is the calcium-induced

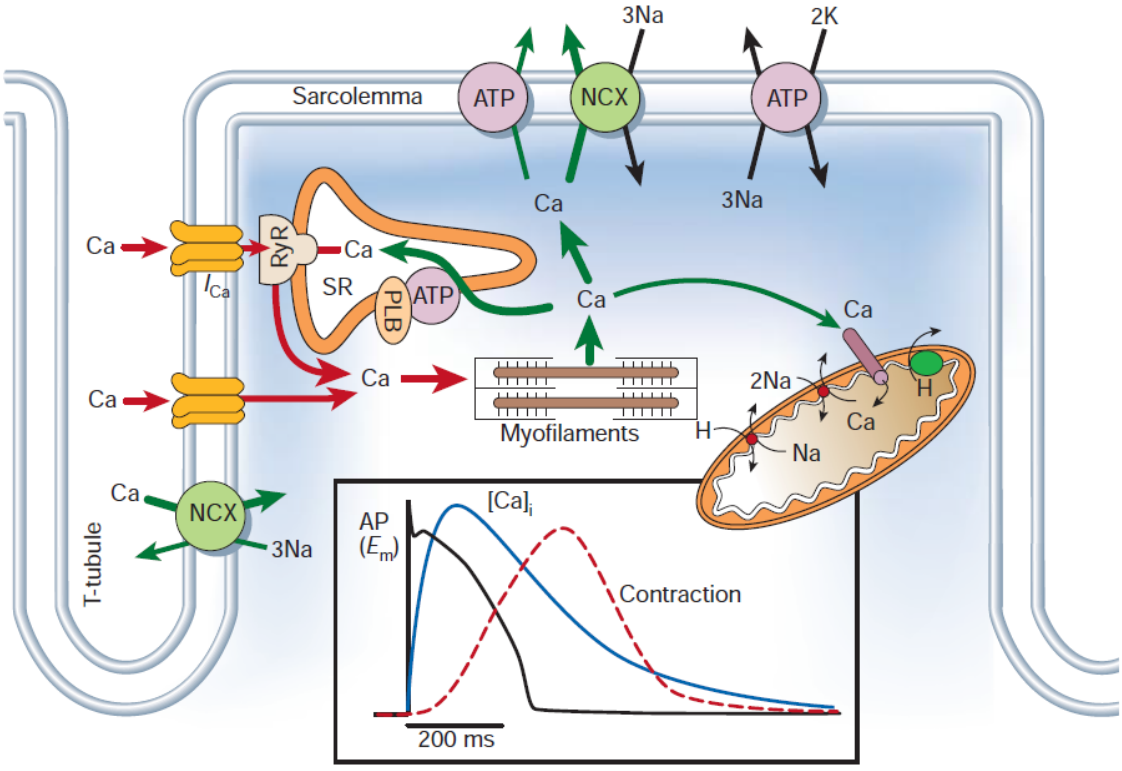

Figure 1 Calcium cycling in ventricular cardiomyocytes. Ca^{2+} enters the cell during action potential, and triggers Ca^{2+} release from the SR by calcium-induced calcium release mechanism. Elevated cytosolic Ca^{2+} concentration triggers the muscle contractile machinery. Activator Ca^{2+} is sequestered into the SR by SERCA, extruded by NCX on sarcolemma and plasma membrane Ca^{2+}-ATPase, and imported into mitochondria by a Ca uniporter. Figure taken from [1].

calcium-release mechanism. Approximately 50-60% of the total SR Ca^{2+} is released and the cleft [Ca^{2+}] is raised to 200-300 μM. [3] Ca^{2+} diffuses from the cleft to the cytosol and binds to troponin C (TnC), which triggers the conformational change of the troponin/tropomyosin complex, exposing the myosin binding sites on actin. The myosin head then binds to and pulls actin at the expense of ATP, causing muscle contraction.

For muscle relaxation to occur, Ca^{2+} needs to be removed from cytosol. This is achieved through sarco(endo)plasmic reticulum Ca^{2+}-ATPases (SERCA), NCX, plasma membrane Ca^{2+}-ATPase (PMCA), and Ca^{2+} uniporter on mitochondria (Figure 1). In murine ventricles, 90-95% of the activator Ca^{2+} is removed by SERCA, and only 5-8% by NCX. In contrast, in ventricles of rabbit, dog, cat, guinea pig, ferret, and human, the breakdown is 70% by SERCA and 25-28% by NCX. [1] 1% is extruded from the cytosol by PMCA. The remaining 1% is imported by a Ca^{2+} uniporter into mitochondria, where Ca^{2+} regulates ATP production. [4]

1.2 SERCA

SERCA is a P-type ATPase localized both in endoplasmic reticulum (ER) and SR. In muscle cells, SERCA harnesses the energy in the γ-phosphate of ATP and actively transports Ca^{2+} across the SR membrane against the concentration gradient at an approximate rate of 2 Ca^{2+} per ATP hydrolyzed. In mammals, three genes encode SERCA, namely SERCA1, SERCA2 and SERCA3, producing more than 10 isoforms. [5] SERCA1a is expressed in adult fast-twitch muscle. [6,7] SERCA2a is predominantly expressed in cardiac muscle and slow-twitch skeletal muscle. [8,9] SERCA3 isoforms are ubiquitously expressed in both nonmuscle and muscle tissue. [10,11] Both the structure and function of SERCA isoforms are highly conserved. SERCA2a protein is about 84%

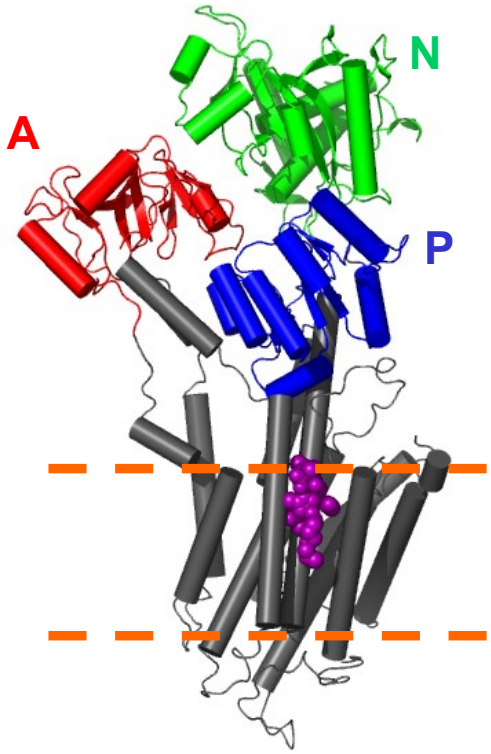

Figure 2 Crystal structure of SERCA. (1IWO). SERCA consists of ten transmembrane helices (grey) and three cytoplasmic domains, namely nucleotide-binding domain (green), actuator domain (red), and phosphorylation domain (blue). This crystal structure is stabilized by thapsigargin (purple). Structure resolved in [13] and rendered in VMD [14].

identical to SERCA1a protein, and these two isoforms are functionally identical. Both of them can be regulated by phospholamban (PLB), which is an endogenous inhibitor of SERCA2a. SERCA1a and SERCA2a also have similar affinity for Ca^{2+}, maximum velocity of Ca^{2+} uptake and pH dependence [12]. SERCA1a is predominantly used in *in vitro* studies because of its abundance relative to SERCA2a in muscle tissue.

SERCA1a consists of ten transmembrane helices (M1-M10) and three cytoplasmic domains: the actuator (A) domain, the nucleotide-binding (N) domain, and the phosphorylation (P) domain (Figure 2). [13] The first crystal structure of SERCA with two Ca^{2+} ions bound was not obtained until 2000 by Toyoshima's group. [15] Since then, a plethora of SERCA crystal structures stabilized with inhibitors and substrate analogues

has been obtained. [13,16,17,18,19,20] These crystal structures constitute a whole spectrum of SERCA catalytic intermediates, laying the structural foundation for probing calcium transport mechanism.

During an enzymatic cycle, SERCA transports 2 Ca^{2+} and countertransports 2-3 protons with 1 ATP hydrolyzed. [21] SERCA alternates between E1 (with high affinity for Ca^{2+}) and E2 (with high affinity for protons) intermediates in a cyclical manner. Recent crystal structures suggest that under physiological conditions, all intermediates have bound nucleotide, leading to a revised scheme of SERCA Ca^{2+} transport cycle (Figure 3). [22] The Ca^{2+} transport cycle starts with the transition from a proton-bound non-phosphorylated E2 state (H_nE2:ATP) to a calcium-bound E1 intermediate (Ca_2E1-ATP). The binding of 2 cytosolic Ca^{2+} is accompanied by the release of 2-3 protons. The transporter then rapidly autophosphorylates Asp351, forming a high-energy phosphorylated [Ca_2]E1~P:ADP intermediate with occluded Ca^{2+}. This is followed by the conformational change of SERCA back to the E2 state, the low-energy phosphorylated [Ca_2]E2P:ATP form. [23] ADP, the product of the autophosphorylation reaction, is replaced by ATP at this step. In the next step, Ca^{2+} is released into the SR lumen in exchange of 2-3 protons, forming H_nE2P:ATP intermediate. After closure of the luminal channel, these protons are occluded inside the transmembrane domain in the [H_n]E2-P:ATP transition state. Finally, the ATPase releases the phosphate and returns to the starting state.

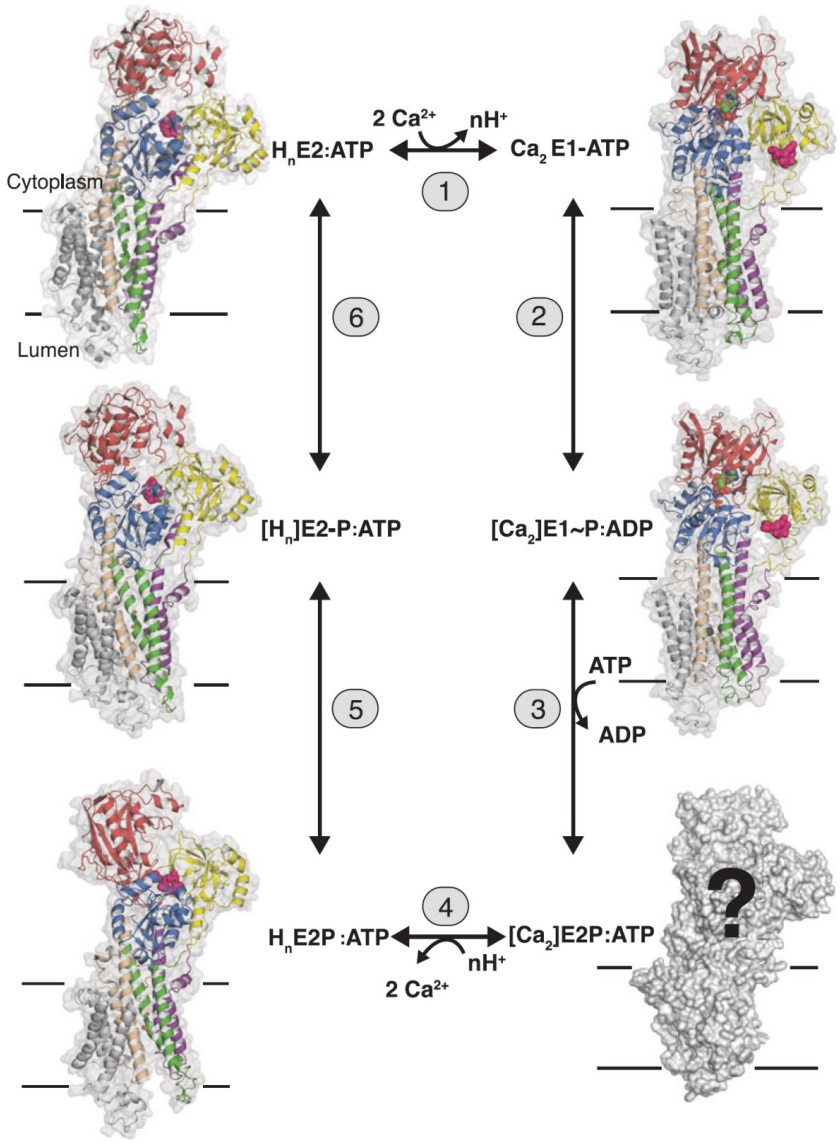

Figure 3 SERCA enzymatic cycle represented by SERCA1a crystal structures. The enzymatic cycle consists of the following reactions: (1) the exchange of protons for cytoplasmic Ca^{2+} ions; (2) phosphorylation at Asp351; (3) the conversion of $[Ca_2]$E1~P:ADP to $[Ca_2]$E2P:ATP (the structure of the latter is still unknown); (4) exchange of Ca^{2+} with luminal protons; (5) the formation of the proton occluded transition state; (6) the release of phosphate group. Figure taken from [22].

1.3 Phospholamban (PLB)

Phospholamban is an endogenous inhibitor of SERCA2a in cardiac and slow-twitch skeletal muscle. [24,25,26] Unphosphorylated PLB inhibits SERCA by decreasing its apparent Ca^{2+} affinity. [27] This inhibition is relieved either by micromolar Ca^{2+} or by phosphorylation of PLB. Two sites on PLB can be phosphorylated under physiological conditions. One is Ser16 which is phosphorylated by cAMP-dependent protein kinase A (PKA), and the other is Thr17 by calcium/calmodulin-dependent protein kinase II (CaMKII).

Wild-type PLB equilibrates between monomers and homopentamers, which are stabilized by a leucine-isoleucine zipper. [29,30,31] Shifting the equilibrium toward the

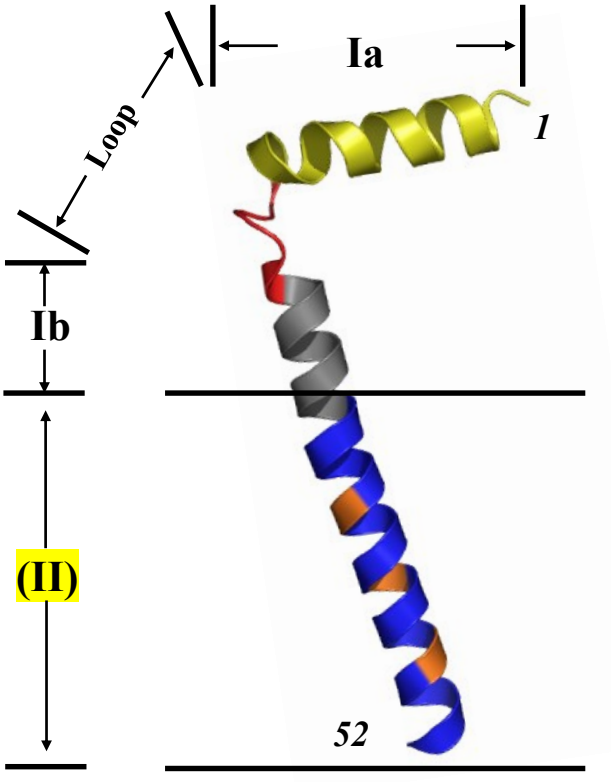

Figure 4 NMR structure of monomeric PLB.PLB consists of domain Ia (yellow), loop (red), domain Ib (grey) and domain II (blue). The three cysteine residues in the transmembrane domain are mutated to alanine, phenylalanine and alanine (orange) to prevent formation of PLB homopentamer. Structure resolved in [28] and rendered in VMD [14].

monomers is positively correlated with SERCA inhibition, suggesting that the monomeric form is the active species. [32,33,34,35,36] The pentamer is considered to be a storage or buffer form for the active monomers, although an electron microscopy study showed physical interaction between pentameric PLB and SERCA. [37] To eliminate PLB-PLB interactions and simplify SERCA-PLB measurements in our experiments, I used a monomeric form of PLB, with the three cysteines mutated to Ala, Phe and Ala, respectively (Figure 4). Electrophysiological studies suggested that pentameric PLB is an ion channel [38,39], but this is contradicted by NMR structures showing that the pore formed by PLB pentamer is not large enough to accommodate ions [40,41].

Mutagenesis studies at cardiomyocyte, organ, and intact animal levels found that phosphorylation of PLB by PKA at Ser16 and by CaMKII at Thr17 is the major mediator of the positive inotropic and lusitropic effects of the β1-adrenergic stimulation in the mammalian heart. [42,43,44] The increase in SERCA2a activity and Ca^{2+} uptake elicited by phosphorylation of these sites, leads to an increase in the rate of muscular relaxation, SR Ca^{2+} load, and SR Ca^{2+} release. In association with L-type Ca^{2+} channel and RyR2 phosphorylation, these processes mediate the enhanced contractility produced by β1 stimulation. [42].

Ser16 was believed to be the predominant phosphorylation site in the β1-adrenergic response. Phosphorylation at Ser16 was sufficient in mediating the maximal cardiac response to β-agonists. [45,46] Additional phosphorylation at Thr17 phosphorylation did not further activate SERCA. [47] Studies using mice with CaMKII inhibition showed unaltered response to isoproterenol. [48] However, the importance of Thr17 phosphorylation was found under pathological conditions, including ischemia-reperfusion

injuries, hypercapnic acidosis, and stunned hearts. [42,49] The two prerequisites for Thr17 phosphorylation are (a) stimulation of CaMKII signaling pathways and (b) inhibition of protein phosphatase 1, which dephosphorylates PLB at both Ser16 and Thr17. The above mentioned pathological situations activate CaMKII by increasing intracellular [Ca^{2+}] and acidosis-induced phosphatase inhibition. [49] Thr17 phosphorylation, but not Ser16 phosphorylation, was found to increase transiently during the early phase of reperfusion in ischemia/reperfusion injuries, and at the onset of acidosis. [50,51,52] Further mutagenesis studies used mice with S16A (not phosphorylatable at Ser16) and T17A (not phosphorylatable at Thr17) mutants. They demonstrated that Thr17 phosphorylation was essential for recovery of Ca^{2+} transients and contractility in the stunned heart. [52,53]

However, quantitation and systematic study of the inhibitory potency of different phosphorylation states of PLB are still lacking. In Chapter 5, we used quantitative western blot to measure the levels of PLB in pig cardiac SR. We also used an enzyme-coupled assay to measure the SERCA inhibition by different phosphorylation states of PLB in a controlled environment.

1.4 The SERCA-PLB Complex

The structure of the SERCA-PLB complex has been probed with various experimental methods, but the high-resolution crystal structure is still elusive. Early attempts were made with crosslinking and mutagenesis studies. James *et al* used a cross-linking agent and showed that K3 of PLB lies within 15 Å of both K397 and K400 in the sequence Lys-Asp-Asp-Lys-Pro-Val-402 in the N domain of SERCA2a, which was later confirmed by a mutagenesis study. [54,55] In the SERCA transmembrane domain,

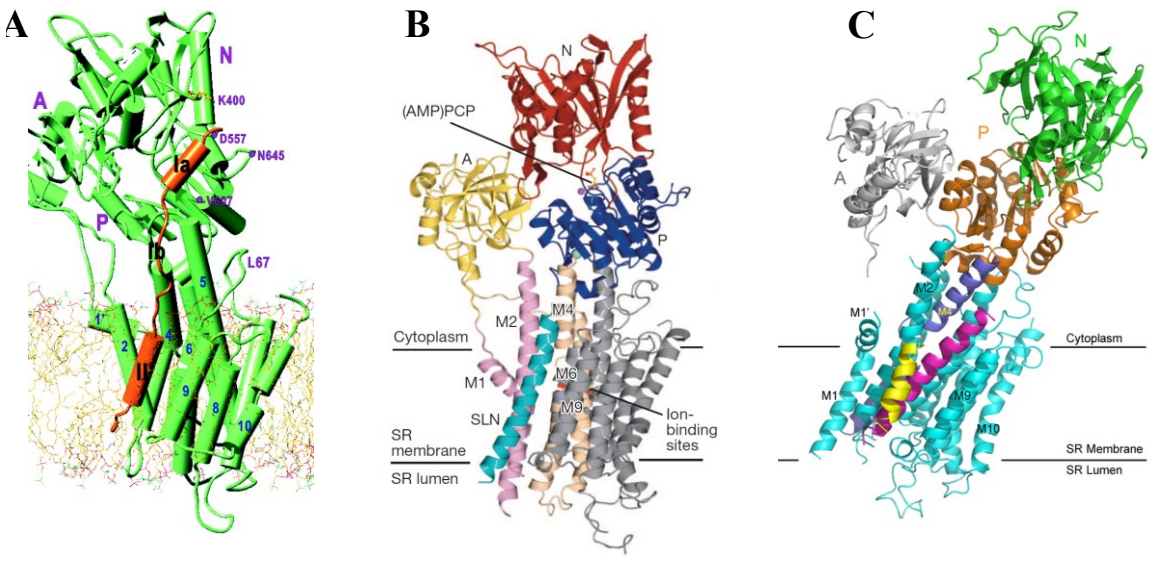

Figure 5 Structures of SERCA-SLN and SERCA-PLB complexes. A. Computational model of the SERCA-PLB complex. SERCA is shown in green and PLB in orange. Figure from [65]. **B**. Crystal structure of the SERCA-SLN complex. Sarcolipin (SLN) is shown in cyan. Figure from [66]. **C**.Crystal structure of the SERCA-PLB complex. Figure from [67]. The PLB that interacts with SERCA is shown in magenta. A small portion of the transmembrane domain of a second PLB (yellow) is also observed in the electron density.

mutations in M4 and M6 were found to have diminished ability to interact functionally with PLB. [56] On the PLB side, charged and hydrophobic residues from Glu2 to Ile18 in the cytoplasmic domain are essential for functional regulation of SERCA. [57,58] The transmembrane domain of PLB is sufficient to inhibit SERCA. [59,60] Mutations on one side of the transmembrane domain frequently disrupt its interaction with SERCA, and mutations on the other side eliminate the ability to form pentamers, although some residues forming the leucine/isoleucine zipper were also shown to interact with SERCA residues. [31,61,62,63,64] Several low resolution cryo-EM structures have been published, with varying SERCA to PLB stoichiometry of the complex. [30,37]

Based on constraints given by a plethora of SERCA crystal structures, mutagenesis and cross-linking studies, two computational models of the SERCA-PLB complex were proposed. These two models are very similar, with the one from Toyoshima's group

receiving more NMR experimental support. [65,68,69,70] In this model (Figure 5A), the transmembrane domain of PLB lies in a groove formed by M2, M4, M6 and M9 of SERCA, and the cytoplasmic domain lies in the hydrophobic groove in the N domain, as previously determined by the cross-linking study. [54,65] The cytoplasmic domain of PLB was unwound and extended to fit steric and biochemical constraints. Both of these models predict that PLB binds the E2 form of SERCA, the reason being that the binding groove on SERCA's transmembrane domain is closed in $E1 \cdot Ca_2$ form. The crystal structures of SERCA in complex with sarcolipin (SLN), a homologue to the PLB transmembrane domain present in heart atria and fast-twitch skeletal muscles, were published simultaneously by two groups (Figure 5B). [66,71] The two co-crystal structures of SERCA-SLN found that SLN binds in a groove formed by M2, M6, and M9. This is the same groove predicted by the previous SERCA-PLB computational model, and confirmed later by a crystal structure of SERCA in complex with a superinhibitory PLB mutant (PLB4) (Figure 5C). [65,67] However, in this crystal structure, only a portion of the transmembrane domain of PLB4 was resolved. The cytoplasmic domain as well as the C-terminus was not visible by electron density mapping. This structure also showed a small fragment of a second PLB4 tagging along with the PLB4 which physically interacts with SERCA. In all these structures, SLN and PLB bind to SERCA at the same site and trap SERCA into a previously unknown structure, more resembling the E1 state than the E2 state.

The structural mechanism of SERCA regulation by PLB remains controversial. The canonical "Dissociation Model" states that PLB binds SERCA to inhibit it, and dissociates from SERCA to relieve inhibition. This model was supported by crosslinking

and co-immunoprecipitation studies showing that either Ca^{2+} alone, or phosphorylation at Ser16 alone, or the combination of both, decrease physical interaction between SERCA and PLB.[54,72,73,74,75,76,77] However, new spectroscopic studies suggested the "Subunit Model", where neither Ca^{2+} nor phosphorylation of PLB dissociate the complex, but rather induce structural rearrangements within the complex. Specifically, EPR and NMR studies found that the cytoplasmic domain of PLB exists in a dynamic equilibrium between two states, an ordered ***T*** state, and a disordered ***R*** state. [78,79,80,81,82] Shifting the equilibrium toward ***R*** state by phosphorylation at Ser16, PLB mutants, or charged lipids, is sufficient to relieve inhibition. [82,83,84] The relief of inhibition by micromolar Ca^{2+} does not require dissociation either. FRET between SERCA and PLB showed little or no dissociation caused by Ca^{2+}. [85,86] Crosslinking and crystallography studies showed that PLB and SLN bind to the same groove on the SERCA transmembrane domain. [66,67,71,77] Two recent crosslinking studies found that SLN remains bound to SERCA throughout the enzymatic cycle. [76,77] It is thus proposed that SLN undergoes positional rearrangement to avoid clashes with the binding groove on SERCA in the calcium bound form. [66] It is possible that as the conformation of SERCA accommodates the binding of SLN and PLB in the absence of Ca^{2+}, the conformation of SERCA would also adapt to accommodate PLB in the presence of Ca^{2+}. The transmembrane domain of PLB probably repositions in a similar fashion as SLN, which explains the absence of dissociation between SERCA and PLB detected by FRET at high [Ca^{2+}]. [85,86] The local rearrangement is probably specific to each protein, which may explain the decreased crosslinking from PLB homologous site to SERCA [72,73,76].

To elucidate the structural basis for SERCA regulation by PLB and to test whether dissociation is necessary for relief of inhibition, we used charged lipids (Chapter 3), phosphorylation at Ser16 of PLB, and Ca^{2+} (Chapter 4) to perturb the function of the SERCA-PLB complex. TR-FRET revealed that the activity of SERCA-PLB complex is mainly controlled by the ***T/R*** equilibrium of the PLB cytoplasmic domain.

1.5 Heart Disease and the SERCA-PLB Complex

No SERCA mutation has been found to be directly correlated to human heart disease. But genetic variance of the PLB gene underlies several forms of human cardiomyopathy, although the frequency in the population is rare. Abnormal PLB level is probably a cause of cardiac malfunction. The first reported mutation in the PLB promoter region was found in a Japanese female patient with familial hypertrophic cardiomyopathy, probably due to increased transcriptional activity caused by this point mutation. [87] Later, another point mutation causing enhanced promoter activity was identified in Caucasian and Greek patients with dilated cardiomyopathy. [88] A case of a 2.5 year old girl with dilated cardiomyopathy was reported earlier this year, and genetic testing found chromosome duplication, where PLB was included. [89] Decreased PLB levels are also pathogenic. The PLB promoter mutant with decreased transcriptional activity was linked to late-onset hypertrophic cardiomyopathy in a Spanish family. [90] A virtually PLB null phenotype was discovered in two Greek families with inherited dilated cardiomyopathy. This point mutation results in L39Stop with absence of expression. [91]

Dominant R9C missense mutation was found to be correlated with inherited human dilated cardiomyopathy. Transgenic PLN-R9C mice recapitulated human heart failure with premature death. [92] Later, mutations at R9, R9L and R9H, were found to

be related to dilated cardiomyopathy in Brazilian population. [93] Detailed biochemical and biophysical studies found that R9C, R9L and R9H all elude phosphorylation by PKA, and R9C and R9L do not inhibit SERCA. [94,95] R9C was also found to stabilize the PLB pentamer by formation of disulfide bonds and eludes PKA phosphorylation. [95] Another study attributed the disease-causing ability of lethal R9C, R9L, R9H and R14del to hydrophobicity imbalance of PLB cytoplasmic domain. [58] R14del was found in patients with inherited dilated cardiomyopathy in Greek and German populations.[96,97] A later study using a transgenic mouse model found that R14Del is misrouted to the sarcolemma, where it activates Na/K-ATPase, leading to the activation of cardiac remodeling pathways. [98]

Calcium mishandling is one of the prominent features of heart failure, partially due to decreased SERCA2a activity regardless of heart failure etiology. [99,100,101,102] The failing heart expresses lower levels of SERCA2a [1,27]. SERCA2a activity is further decreased by increased inhibition of PLB due to (a) PLB protein levels decreased by a smaller proportion than the protein levels of SERCA in the failing hearts, therefore the ratio of PLB to SERCA increased [101,103]; and (b) the phosphorylation level is also decreased in human failing myocardium, either at Ser16 [104,105], Thr17 [106], or both [107,108]. Enhancing SERCA2a activity to restore Ca^{2+} homeostasis has been one of the primary targets of the recent gene therapies for heart failure. Moreover, these gene therapies showed promising results in both human patients and animal heart failure models.

One strategy to enhance SERCA2a activity is to directly increase SERCA2a expression in failing hearts. SERCA2a gene transfer in a number of heart failure models

showed preservation of systolic function and improvement of ventricular remodeling [109], restoration of the normal state of cardiac energetics [110,111], decrease in ventricular arrhythmias [112,113,114,115], and enhancement of coronary flow through activation of eNOS in endothelial cells [116]. CUPID (The Calcium Up-Regulation by Percutaneous Administration of Gene Therapy In Cardiac Disease) study is a first-in-human clinical gene therapy trial using an adeno-associated virus serotype (AAV1) vector to deliver SERCA2a gene in patients with advanced heart failure. It now has progressed to phase IIb clinical trial. [117] Lower number of cardiovascular events and significantly decreased risk of recurrent cardiovascular events were found in the group of patients who received high-dose of SERCA2a gene. No safety concerns were noted during the 3-year follow-up. [118] The success of these animal and human studies further validates SERCA2a as a promising therapeutic target for heart failure.

Another strategy to enhance SERCA2a activity is to decrease inhibition by PLB, either by decreasing PLB protein expression or by increasing PLB phosphorylation level. Ablation of PLB expression by genetic PLB knock-out or decrease PLB expression by RNAi resulted in improved contractility at cellular levels and suppressed progression of heart failure in animal models. [119,120,121] Expression of S16E-PLB, a phosphomimetic form, improved systolic and diastolic LV function in hamster, rat and sheep heart failing models. [122,123,124] Recent efforts to increase PLB phosphorylation level by inhibiting its dephosphorylation in heart failure models also showed promising results. This is done by introducing constitutively active truncated inhibitor-1, the inhibitor of protein phosphatase 1, which dephosphorylates PLB.[125,126,127,128,129]

Chapter 2 Fluorescence

2.1 Fluorescence Theories

Fluorescence is the emission of light from an excited singlet state to the ground singlet state. The concept of fluorescence is best described by a Jablonski diagram (Figure 6). The singlet ground, first, and second electronic states are depicted by S_0, S_1, and S_2, respectively. Fluorophores at each of these electronic states can exist in a number of vibrational energy levels, depicted by 0, 1, and 2. At room temperature, thermal energy is not adequate to populate the excited vibrational states or the electronic state of S_1.

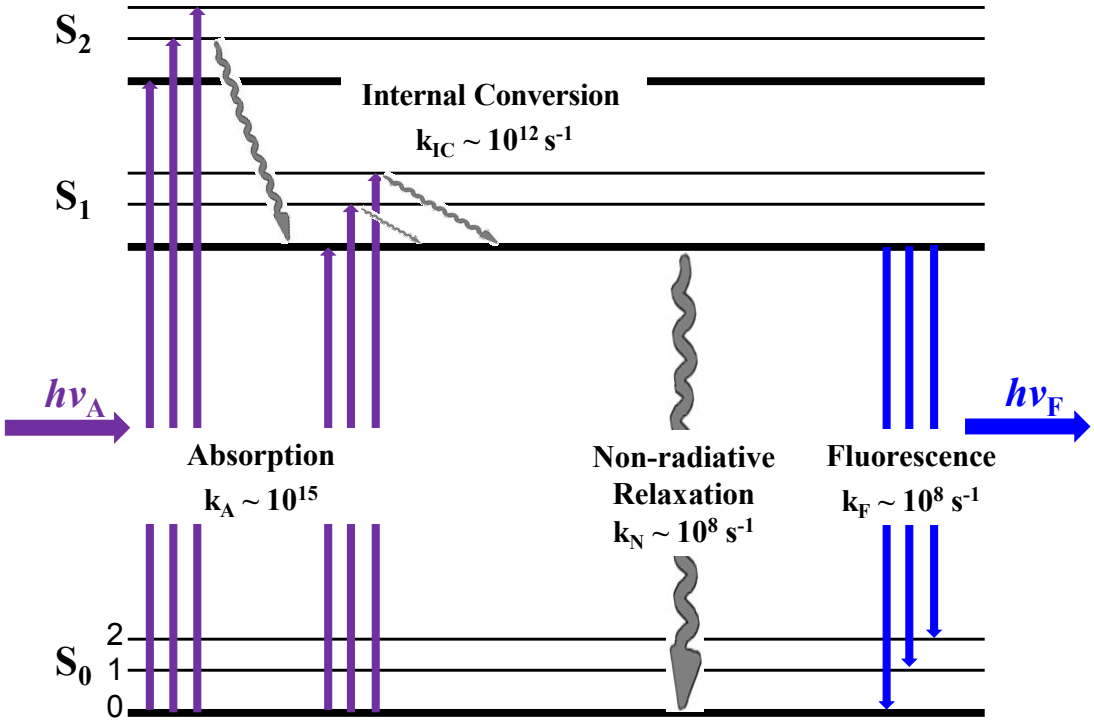

Figure 6 Jablonski diagram. The fluorophore is excited to the higher energy state by absorption of a photon (hv_A). Then it rapidly relaxes to the lowest vibrational state of S_1. From there, the fluorophore returns to the ground state either through non-radiative relaxation, or by emission of a photon (hv_F).

Therefore light is used to excite the fluorophore from the lowest vibrational state of S_0 to some higher vibrational level of either S_1 or S_2. The transition time is about 10^{-15} s, too short for significant displacement of nuclei. This is the Franck-Condon principle. Then the fluorophores rapidly relax to the lowest vibrational level of S_1, a process called internal conversion, with a rate of 10^{12} s^{-1} or higher. Fluorescence emission generally occurs quickly ($k_F \sim 10^8$ s^{-1}) from the lowest vibrational state of S1 to different vibrational states of the ground state. The spacing of the vibrational energy levels of the excited states is similar to that of the ground state. Hence the emission spectrum is typically a mirror image of the absorption spectrum of the S_0 to S_1 transition. Figure 6 also shows that the energy of emission is typically less than that of absorption, a phenomenon called Stokes shift. The excited fluorophore can either emit a photon at a rate of k_F, or relax to the ground state non-radiatively at a rate of k_N. The fluorescence quantum yield is the ratio of the number of photons emitted to the number absorbed. The fraction of fluorophores that decay through emission, and hence the quantum yield, $\emptyset_F$, is given by

$$\emptyset_F = \frac{k_F}{k_F + k_N} \qquad \textbf{Equation 1}$$

The lifetime of the excited state is defined by the average time the molecule spends in the excited state prior to return to the ground state. The lifetime is

$$\tau = \frac{1}{k_F + k_N} \qquad \textbf{Equation 2}$$

Fluorescence measurements can be broadly classified into two types of measurements: steady-state and time-resolved. Steady-state measurements are performed with constant illumination and the intensity of emission spectrum is recorded. The

steady-state measurements can be easily done and for this reason it is the most common type. However, several key fluorophore parameters cannot be resolved by the steady-state method. For example, an ensemble of fluorophores with different lifetimes due to different environments cannot be resolved by steady-state fluorescence. Time-resolved fluorescence can resolve fluorophore ensembles, making it generally advantageous. Time-resolved measurements are done with pulsed excitation light, and the intensity decay is recorded on the nanosecond timescale. Suppose fluorophores are excited with an infinitely sharp pulse of light, resulting in an initial population (n_0) of fluorophores in the excited states. If we use n(t) to denote the number of excited molecules at time t, then

$$\frac{dn(t)}{dt} = -(k_F + k_N)n(t) \qquad \textbf{Equation 3}$$

This results in an exponential decay of the excited state population

$$n(t) = n_0 \exp(-t/\tau) \qquad \textbf{Equation 4}$$

Because the fluorescence intensity I(t), which we observe in a fluorescence experiment, is proportional to n(t), then Equation 4 can be written as

$$I(t) = I_0 \exp(-t/\tau) \qquad \textbf{Equation 5}$$

2.2 Time-Correlated Single-Photon Counting (TCSPC)

TCSPC is the most common method to measure time-resolved fluorescence. It is a sensitive technique for recording low-level light signals with picosecond resolution and high precision. The principle of TCSPC is shown in Figure 7. The sample is excited with a pulse of light, and the expected fluorescence decay waveform is shown at top. The time is measured between the excitation pulse and the observed photon (Figure 7 Middle) and stored in a histogram (Figure 7 Bottom). The conditions are adjusted so that less than 1 photon is detected per 100 excitation pulses.

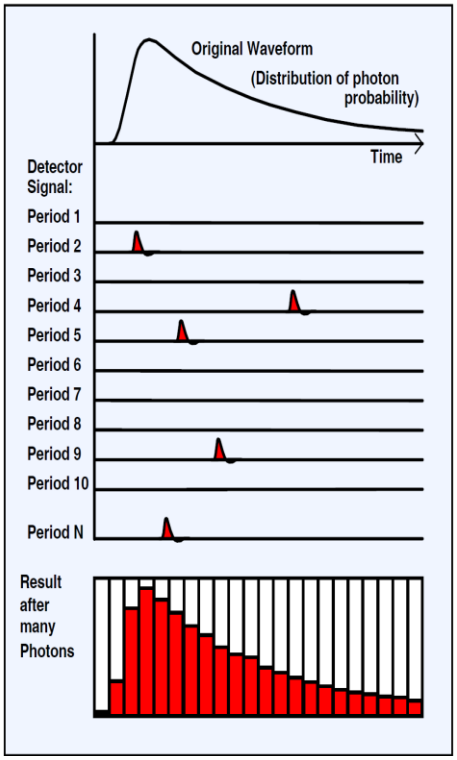

Figure 7 Principle of fluorescence measurement by TCSPC. Figure taken from **[130].**

The most common configuration of a TCSPC instrument is in the reversed start-stop configuration (Figure 8). After excitation of the fluorophores, the detector, photomultiplier tube (PMT), detects the arrival of the emitted photon and delivers a pulse. Then the pulse is fed to a constant fraction discriminator (CFD) to accurately mark the arrival time of the photon. The output of this CFD starts a time-to-amplitude

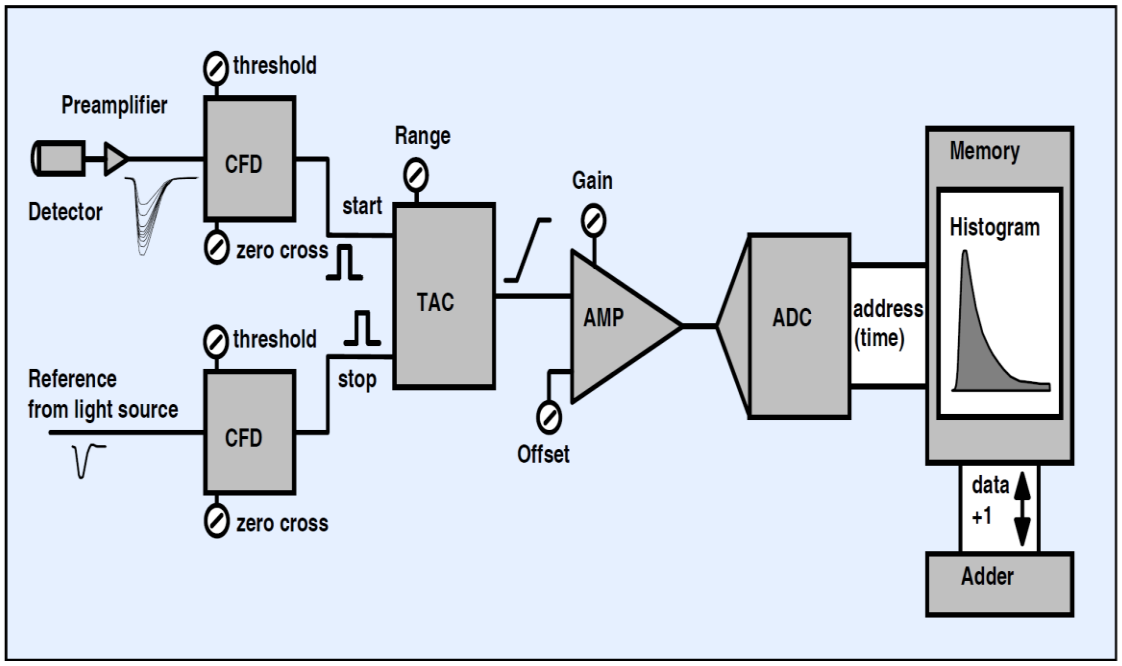

Figure 8 Reversed start-stop configuration of TCSPC. Figure taken from **[130].**

converter (TAC), which generates a voltage ramp where the voltage increases linearly with time on the nanosecond timescale. A second CFD is used to obtain a timing reference pulse from the excitation pulse. The light in the reference channel is delayed by a defined time period by transmitted through a defined length of optic cable. The TAC is stopped by the output from the reference CFD. The TAC now contains a voltage in linear relationship with the arrival time of the emitted photon. The TAC output voltage is then amplified by a biased amplifier and then fed to the analog-to-digital converter (ADC).

This process is repeated numerous times to generate a histogram of the arrival time (Figure 7 Bottom).

2.3 Fluorescence Resonance Energy Transfer (FRET)

FRET is a non-radiative transfer of energy from a donor fluorophore in the excited state to an acceptor molecule in the ground state (Figure 9). The emission spectrum of the donor fluorophore must overlap with the absorption spectrum of the acceptor molecule for FRET to occur. Energy is transferred through long-range dipole-dipole interactions, without the appearance of a photon. For this reason, the term

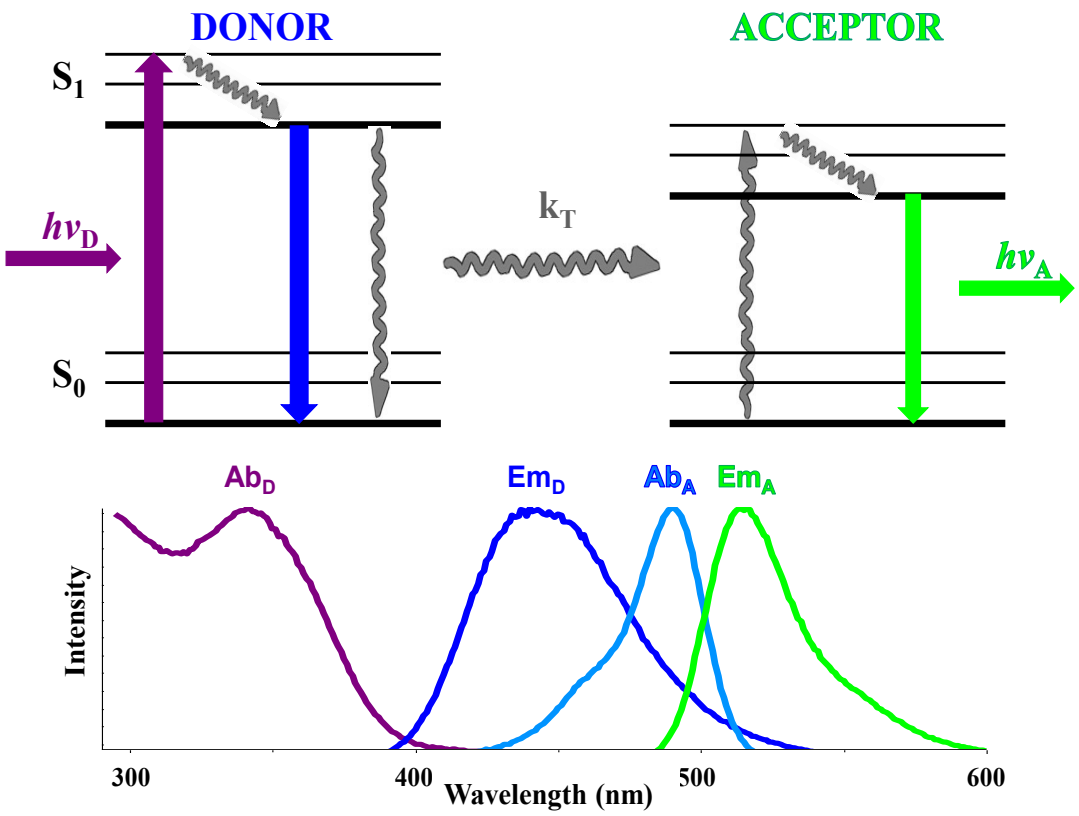

Figure 9 Schematic representation of FRET. Adapted from Dr. David Thomas's lecture notes. Bottom: absorption (Ab_D) and emission (Em_D) spectra of Alexa Fluor 350 as a donor, and the absorption (Ab_A) and emission (Em_A) spectra of iodoacetamidofluorescein as an acceptor.

"Resonance Energy Transfer" or "Förster Resonance Energy Transfer" is sometimes preferred.

The FRET efficiency (E) is the fraction of photons absorbed by the donor which are transferred to the acceptor. This fraction is given by

$$E = \frac{k_T(r)}{\tau_D^{-1} + k_T(r)} \quad \textbf{Equation 6}$$

where τ_D is the lifetime of the donor in the absence of an acceptor, and $k_T(r)$ is the rate of energy transfer as a function of the donor-to-acceptor distance (r). In time-resolved FRET experiments, E is measured as the fractional decrease in lifetime:

$$E = 1 - \frac{\tau_{DA}}{\tau_D} \quad \textbf{Equation 7}$$

where τ_D is the lifetime of the donor in the absence of an acceptor, and τ_{DA} is the lifetime of the donor which transfers energy to a nearby acceptor. The rate of energy transfer, $k_T(r)$, is given by

$$k_T(r) = \frac{1}{\tau_D}\left(\frac{R_0}{r}\right)^6 \quad \textbf{Equation 8}$$

where R_0 is the Förster distance, the distance at which FRET efficiency is 50%. [131]. Substituting into Equation 6, the FRET E can be directly expressed in terms of D-A distance r,

$$E = \frac{R_0^6}{R_0^6 + r^6} \quad \textbf{Equation 9}$$

The Förster distance (Å) is given by

$$R_0 = 9.78 \times 10^3 (\kappa^2 n^{-4} \emptyset_D J(\lambda))^{1/6} \quad \textbf{Equation 10}$$

where κ^2 is a factor describing the relative orientation in space of the transition dipoles of the donor and acceptor. κ^2 is usually assumed to be equal to 2/3, which is appropriate for dynamic random averaging of the donor and acceptor. n is the refractive index of the medium. It is usually assumed to be 1.4 for biomolecules in aqueous solutions. $\emptyset_D$ is the quantum yield of the donor in the absence of acceptor. J(λ) is the overlap integral which expresses the degree of spectral overlap between the donor emission and the acceptor absorption:

$$J(\lambda) = \frac{\int_0^\infty F_D(\lambda)\varepsilon_A(\lambda)\lambda^4 d\lambda}{\int_0^\infty F_D(\lambda) d\lambda} \quad \textbf{Equation 11}$$

Förster distance falls in the range of 20 to 90 Å, which is comparable to the size of biomolecules. Hence FRET is frequently used to measure distances between two sites within a biomolecule or within a complex. For this reason, FRET is described as a "spectroscopic ruler". [132]

Chapter 3 Structural and Functional Dynamics of an Integral Membrane Protein Complex Modulated by Lipid Headgroup Charge

Ji Li, Zachary M. James, Xiaoqiong Dong, Christine B. Karim, and David D. Thomas.

Department of Biochemistry, Molecular Biology, and Biophysics, University of Minnesota

Originally published in *Journal of Molecular Biology*, vol. 418, pp. 379 – 89. Reprinted with permission from Elsevier.

Xiaoqiong Dong contributed to SERCA purification and labeling, co-reconstitution, activity assays and TR-FRET experiments. Ji Li designed all the experiments, purified and labeled SERCA, performed activity assays and TR-FRET, and wrote the manuscript. Zachary M. James performed the EPR experiments. Christine B. Karim synthesized and purified PLB. David D. Thomas edited the final manuscript and contributed ideas to the project.

3.1 Chapter Overview

We have used membrane surface charge to modulate the structural dynamics of an integral membrane protein, phospholamban (PLB), and thereby its functional inhibition

of the sarcoplasmic reticulum Ca-ATPase (SERCA). It was previously shown by EPR, in vesicles of neutral lipids, that the PLB cytoplasmic domain is in equilibrium between an ordered ***T*** state and a dynamically disordered ***R*** state, and that phosphorylation of PLB increases the ***R*** state and relieves SERCA inhibition, suggesting that ***R*** is less inhibitory. Here we sought to control the ***T***/***R*** equilibrium by an alternative means – varying the lipid headgroup charge, thus perturbing the electrostatic interaction of PLB's cationic cytoplasmic domain with the membrane surface. We resolved the ***T*** and ***R*** states not only by EPR in the absence of SERCA, but also by time-resolved fluorescence resonance energy transfer (TR-FRET) from SERCA to PLB, thus probing directly the SERCA-PLB complex. Compared to neutral lipids, anionic lipids increased both the ***T*** population and SERCA inhibition, while cationic lipids had the opposite effects. In contrast to conventional models, decreased inhibition was not accompanied by decreased binding. We conclude that PLB binds to SERCA in two distinct structural states of the cytoplasmic domain, an inhibitory ***T*** state that interacts strongly with the membrane surface, and a less inhibitory ***R*** state that interacts more strongly with the anionic SERCA cytoplasmic domain. Modulating membrane surface charge provides an effective way of investigating the correlation between structural dynamics and function of integral membrane proteins.

3.2 Introduction

The functions of integral membrane proteins depend on the interplay of protein structure and dynamics with the lipid environment [133]. In the present study, we use the lipid environment as a tool to perturb the system, followed by measurement of structure, dynamics, and function, to elucidate mechanistic principles. We vary membrane surface

electrostatics by manipulating lipid headgroup charge, which has been shown to be a powerful approach in the analysis of peripheral membrane proteins [134].

The sarcoplasmic reticulum Ca-ATPase (SERCA) actively transports Ca from the cytoplasm to the SR lumen and initiates muscle relaxation. In the cardiomyocyte, an integral membrane protein phospholamban (PLB) [135] regulates SERCA activity by decreasing SERCA's apparent Ca affinity [136]. This inhibition can be relieved by elevated Ca^{2+} or by phosphorylation of PLB in response to β-adrenergic stimulation [137]. Decreasing this inhibitory regulation relieves cardiomyopathy, so elucidating the interaction mechanism between SERCA and PLB is essential for understanding cardiac pathology and for devising new cardiac therapies [138].

PLB exists in equilibrium between monomeric and pentameric forms, but the monomer is the principle species that binds to and inhibits SERCA [139], so we used the monomeric AFA-PLB mutant (C36A/C41F/C46A) [28,78] throughout this study. The high-resolution structural dynamics of free PLB monomer in a lipid bilayer has been determined using nuclear magnetic resonance (NMR) and electron paramagnetic resonance (EPR) [28,78,83,140]. PLB consists of an N-terminal cytoplasmic helix, a loop, and a transmembrane helix (Figure 10). The top of the TM helix (domain Ib) is hydrophilic, directly interacts with lipid headgroups, and is more dynamic than the rest of the TM helix (domain II) [78,140,141]. EPR of TOAC, a spin label attached rigidly to the peptide backbone, shows that the cytoplasmic domain of PLB (Ia and Ib) is in equilibrium between an ordered ***T*** state and a dynamically disordered (partially unfolded) ***R*** state (sometimes called "excited state"), while the transmembrane helix is quite stable [78]. The cytoplasmic domain is associated with the membrane surface in ***T*** but

dissociated in ***R*** [78]. Phosphorylation of PLB induces a shift in the ***T***/***R*** equilibrium toward ***R***, suggesting that ***R*** is less inhibitory than ***T*** [83,142].

Numerous high-resolution structures of SERCA in its enzymatic cycle have been obtained from X-ray diffraction [15,22], but there is no high-resolution structure of the SERCA-PLB complex. Based on crosslinking, mutagenesis and structures of free SERCA and free PLB, a docking model has been constructed, in which the cytoplasmic domain of PLB extends above the membrane surface and interacts with the cytoplasmic domain of SERCA [65]. Conventional models hypothesize that dissociation of this inhibitory SERCA-PLB complex is necessary for the relief of SERCA inhibition, either by high Ca, phosphorylation of PLB, mutagenesis of PLB, or addition of a PLB antibody [75,143], but EPR and NMR studies suggest that PLB remains bound to SERCA in both ***T*** (inhibitory) and ***R*** (less-inhibitory) states [69,83,144]. However, none of these spectroscopic studies probed specifically the bound SERCA-PLB complex.

To help resolve this controversy, in the present study we have probed directly the structure of the SERCA-PLB complex, and we systematically tuned the structural dynamics of the cationic cytoplasmic domain of PLB by adjusting membrane surface charge using charged lipids. We first used EPR [83,145] of TOAC-PLB in the absence of SERCA, to show that we can control the ***T***/***R*** equilibrium using lipid headgroup charge. We then used time-resolved fluorescence resonance energy transfer (TR-FRET) [146] to directly measure SERCA-PLB binding and simultaneously resolve the ***T*** and ***R*** structural states of the SERCA-PLB complex (see section 3.6 for a brief introduction to FRET). We performed ATPase assays to determine the correlation of these observations with PLB inhibitory function. With this combined approach we constructed a revised model for the

structural and functional regulation of the SERCA-PLB complex. This approach has implications far beyond SERCA, demonstrating that variation of membrane surface electrostatics, in conjunction with high-resolution spectroscopy, is a potentially powerful approach to systematically tune the structural and functional dynamics of integral membrane proteins.

3.3 Results

We used lipid headgroup charge as a means of perturbing electrostatically the structural equilibria of the SERCA-PLB system. The advantage of this approach is that it does not alter the native chemical compositions of the proteins, compared with conventional modifications such as mutagenesis, phosphorylation, and crosslinking. All lipids used have the same unsaturated fatty acid chains, di(C18:1), but varying headgroups and charges: phosphatidyl choline (PC, 0), phosphatidyl ethanolamine (PE, 0), phosphatidyl glycerol (PG, −1), phosphatidyl serine (PS, −1), ethyl-phosphocholine (EPC, +1), and trimethyl-ammonium-propane (TAP, +1) (Figure 10). We hypothesized that the principal effect of this variation of membrane surface charge would be to perturb the equilibrium between the ***T*** state (membrane bound and highly ordered) and the ***R*** state (dissociated from the membrane and highly disordered). If our hypothesis is true, negatively charged lipids should increase the ***T*** state population and SERCA inhibition (Figure 10, top left), while positively charged lipids should have the opposite effects (Figure 10, top right). In this work, membranes were composed of PC, PE, and L at molar ratios 4/1/1, where L is PS, PG, PC, EPC, or TAP (Figure 10, bottom). PC and PE are in all samples, because they are the major constituent lipids in cardiac SR and are important

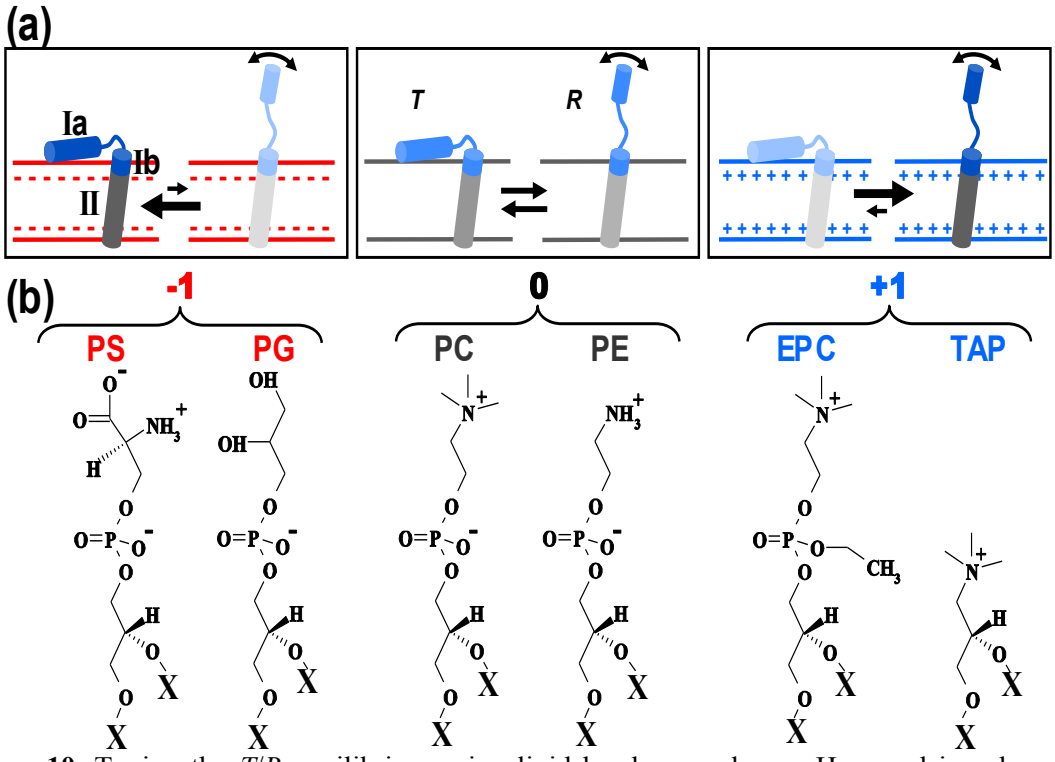

Figure 10. Tuning the *T*/*R* equilibrium using lipid headgroup charge. Here and in subsequent figures, red indicates negative charge, blue positive. (a) The cationic cytoplasmic domain (Ia and Ib) of monomeric PLB is in equilibrium between an ordered ***T*** state and a dynamically disordered ***R*** state, while domain II is stable [78]. (b) Structures of lipid headgroups and their net charges. All lipids have the same fatty acid chain, X = $C_{18:1}$ (oleic acid).

for SERCA activity and PLB-dependent regulation in reconstituted membranes [147,148]. The molar ratios of SERCA/PLB/lipid, when one or both proteins were present, were 1/10/700, which results in a functional regulation of SERCA by PLB that matches that in the native environment [85,149].

EPR shows that the PLB structural distribution depends on lipid headgroup charge. We have previously shown that the TOAC spin label, rigidly coupled to the peptide backbone at position 11 on PLB, clearly resolves the ***T*** and ***R*** states [78,83,145]. Therefore, we used this EPR approach to determine the effect of lipid headgroup charge on the ***T***/***R*** equilibrium (Figure 11). The ***T*** state is dynamically restricted, resulting in a broad peak at lower field, while the dynamically disordered ***R*** state results in a sharp peak

at higher field (Figure 11a). The positions and shapes of the two components did not change significantly with lipid headgroup charge, indicating that only the populations of the two states were affected. The mole fraction of PLB in the ***R*** state (X_R) was determined by digital analysis of EPR spectra as described previously [145] (Figure 11b). X_R is about 0.20 in zwitterionic PC, while anionic PS and PG decrease X_R substantially and cationic EPC and TAP increase X_R (Figure 11). These results strongly support the hypothesis in Figure 10: the ***T***/***R*** equilibrium is influenced by the electrostatic interaction between the cationic cytoplasmic domain of PLB and the membrane surface charge; anionic lipid headgroups attract the cationic PLB cytoplasmic domain to the membrane surface, stabilizing the membrane-associated ***T*** state, while cationic lipid headgroups repel the cationic PLB cytoplasmic domain from the membrane surface, stabilizing the ***R*** state.

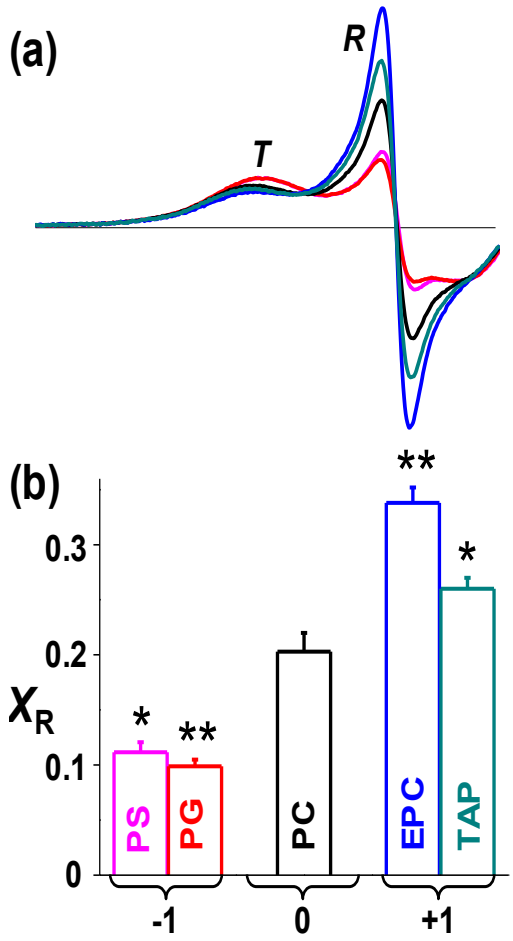

Figure 11. Effect of lipid headgroup charge on EPR of 11-TOAC spin-labeled PLB in lipid bilayers, with lipid composition and abbreviations as defined in Figure 10 (color scheme indicated in Figure 10b). (a) Low-field portion (3305 to 3341 G) of the spectrum resolves two distinct dynamic states of the PLB cytoplasmic domain, an ordered ***T*** state and a dynamically disordered ***R*** state. (b) Mole fraction of ***R*** state (X_R). Mean ± SEM (n = 3). Students *t*-test, compared with PC: * $p < 0.05$, ** $p < 0.01$.

TR-FRET from SERCA to PLB resolves two structural states of the SERCA-PLB complex. To further resolve the structure of the SERCA-PLB complex, we performed TR-FRET to measure the distance between IAEDANS-labeled SERCA (AEDANS-SERCA, donor) and Dabcyl-labeled PLB (Dabcyl-PLB, acceptor). The Förster distance (R_0) between this pair is 3.2 nm [85]. IAEDANS labels SERCA specifically at Cys674, with the molar ratio of bound dye to SERCA = 1.02 ± 0.05 [150]. Synthetic AFA-PLB was labeled by attaching Fmoc-Lys(Dabcyl)-OH to the N-terminus

at the last step of synthesis [149]. The time-resolved fluorescence of AEDANS-SERCA without (donor only, $F_D(t)$) or with Dabcyl-AFA-PLB (donor plus acceptor, $F_{D+A}(t)$) was measured by direct waveform recording using a high-performance time-resolved fluorescence instrument [151] (see section 3.5) (Figure 12a), then analyzed (Equation S14 - Equation S20) using non-linear fitting software. Conventional steady-state FRET only measures the ensemble-averaged interprobe distance. The principal advantage of TR-FRET is that it resolves directly the fraction X_b of the donor that has acceptor bound, thus reporting directly the structure of the SERCA-PLB complex (Equation S17 - Equation S20). Within this bound complex, TR-FRET also resolves multiple structural states, as defined by Gaussian interprobe distance distributions, each characterized by the center (R_i), width ($FWHM_i$), and mole fraction (x_i) (Equation S17 - Equation S20) [146,152]. For the bound complex in PC, two Gaussian components are necessary and sufficient to fit $F_{DA}(t)$ (Figure 12b, Figure S17). The shorter interprobe distance (R_1) is 1.75 ± 0.03 nm, with width $FWHM_1$ = 0.99 ± 0.07 nm and mole fraction x_1 = 0.77 ± 0.02. The longer interprobe distance (R_2) is 3.03 ± 0.02 nm, with $FWHM_2$ being 1.67 ± 0.24 nm, and $x_2 = 1 - x_1$ = 0.23 ± 0.02. The fraction of SERCA bound to PLB (Equation S20), is X_b = 0.82 ± 0.01 in PC, indicating that 82% of SERCA is bound to PLB. These results support the model that the complex between SERCA and PLB is in equilibrium between two structural states (Figure 12), as is PLB in the absence of SERCA (Figure 11).

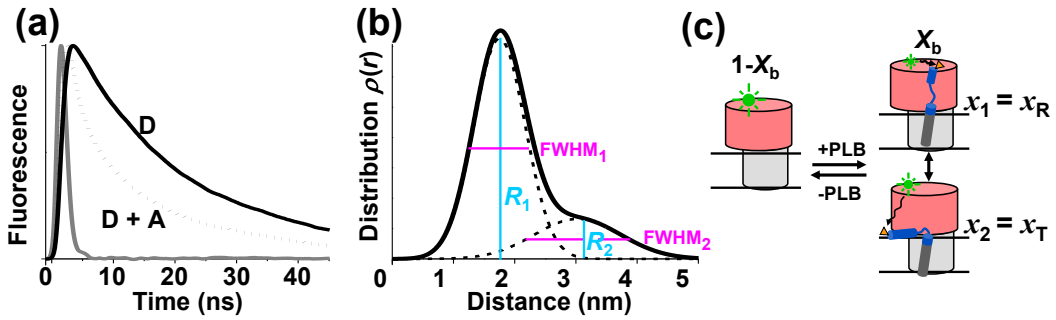

Figure 12. TR-FRET from AEDANS-SERCA (donor) to Dabcyl-PLB (acceptor) in PC. (a) Example of TR fluorescence, measured by direct waveform recording in PC membranes. D = donor-only, D+A = donor plus acceptor. Gray = instrument response function (IRF). (b) SERCA-PLB interprobe distance distribution determined from data in a, containing two Gaussian components (solid curve = sum of two dashed curves), centered at R_1 and R_2. (c) TR-FRET data resolves free SERCA (left, mole fraction 1-X_b) from PLB-bound SERCA-PLB (right, X_b). Two structural states of the bound SERCA-PLB complex are resolved (b), consistent with the model shown here. x_1 and x_2 are the mole fractions of the two states, corresponding to bound ***T*** and ***R*** states, as shown below.

Ensemble average FRET shows that the average interprobe distance between SERCA and PLB is affected by lipid headgroup charge. Ensemble-average FRET efficiency $\langle E_{D+A} \rangle$ (Figure 13a) was calculated using the average lifetime (Equation S16), which is equivalent to (but more precise than) FRET efficiency measured by fluorescence intensity under steady illumination [153]. Compared to zwitterionic PC, anionic PS and PG decreased FRET, suggesting an increase in the average interprobe distance, while cationic EPC and TAP increased the ensemble-average FRET, suggesting a decreased average interprobe distance (Figure 13a). These results suggest that the proximity between SERCA and PLB is affected by the electrostatic interaction between the lipid headgroup and the PLB cytoplasmic domain. However, this ensemble average measurement has no structural resolution, so it can not distinguish a change in binding from a change in the structure of the complex. Only TR-FRET can resolve the ambiguity.

Lipid headgroup charge modulates the distribution of the two structural states of the SERCA-PLB complex. TR-FRET waveforms were fitted as described in

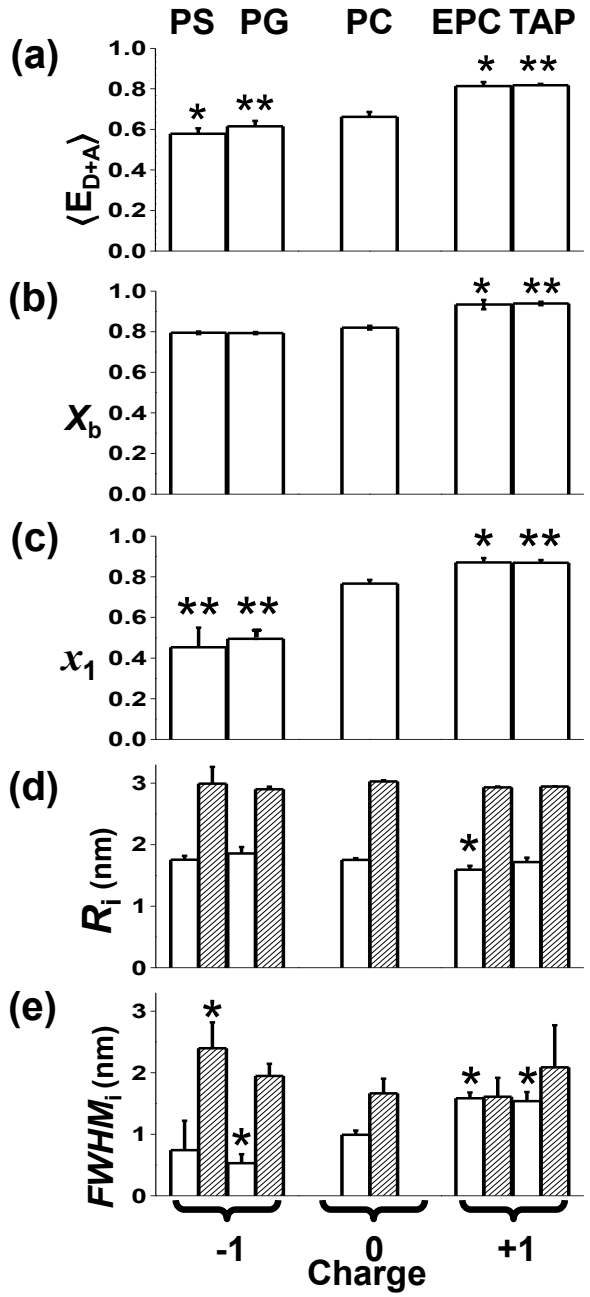

Figure 13. Effects of lipid charge on SERCA-PLB structural distribution, determined from TR-FRET. Two-Gaussian components distance distributions were determined as in Figure 12. Students *t*-test, compared with PC: * $p < 0.05$, ** $p < 0.01$. (a) Ensemble average FRET. (b) Mole fraction of SERCA bound to PLB. (c) Mole fraction of the short distance state ($x_1 = x_{\mathbf{R}}$). (d) Centers R_1 (open) and R_2 (shaded) of the two distance distributions. (e) Widths.

Figure 12. In all cases, across the five different lipid compositions, two structural states were found to be necessary and sufficient to fit the data. The independently determined parameters (Figure 13b-e) were the fraction of SERCA bound to PLB (X_b) and mole fractions of bound states (x_1 and x_2) (Figure 12c), along with the structural characteristics of each bound state (R_1, $FWHM_1$, R_2, $FWHM_2$) (Equation S14 - Equation S20) (Figure 12b). Membrane surface charge only slightly affects the binding (X_b) between SERCA and PLB (Figure 13b). In PS, PG and PC, X_b is ~ 0.8, while in EPC and TAP, X_b is ~ 0.9. Thus, most SERCA has PLB bound, and these small effects cannot explain the substantial dependence of $\langle E_{D+A} \rangle$ on charge (Figure 13a). The two structural states have consistent properties, justifying their being treated as 'states.' The central interprobe distances of the two SERCA-PLB structural states were found to be quite invariant, with a short distance R_1 ~ 1.8 nm, and a long distance R_2 ~ 3.0 nm (Figure 13d). Some of the widths ($FWHM_i$, defining the structural heterogeneity) of the distance distributions are slightly dependent on lipid headgroup charge (Figure 13e).

The most prominent effect of membrane surface charge is to shift the equilibrium between the two structural states (Figure 13c). Compared to zwitterionic PC (x_1 = 0.77 ± 0.02), anionic PS and PG decrease x_1 to 0.45 ± 0.10 and 0.49 ± 0.05 respectively. Cationic EPC and TAP increase x_1 to 0.87 ± 0.02 and 0.87 ± 0.01 respectively. Thus in both isolated PLB (EPR in Figure 11) and in the SERCA-PLB complex (TR-FRET in Figure 13), the electrostatic interaction between the cytoplasmic domain of PLB and the membrane surface charge shifts the structural equilibrium between two structural states. Based on a comparison between EPR and TR-FRET data, it appears that population 1, the short distance state detected by TR-FRET, corresponds to the ***R*** state, while population 2

corresponds to the ***T*** state, as depicted in Figure 12c. Negative surface charge attracts the positively charged PLB cytoplasmic domain and thus increases the fraction ($x_2 = x_T$) of the membrane-associated bound ***T*** state (long interprobe distance), while positively charged headgroups have the opposite effect and thus increase the bound ***R*** state fraction ($x_1 = x_R$).

SERCA activity in the absence of PLB depends on lipid headgroup charge. To establish control values, the ATPase activity of SERCA alone was measured at different pCa, and the pCa-dependence was fitted using Equation 12. There were no significant effects on the V_{max} (activity at saturating Ca), but there were significant effects of headgroup charge on pK_{Ca}, defining the apparent Ca affinity (Table 1). Compared to PC (zwitterionic), PS and PG (anionic) increase pK_{Ca}, while EPC and TAP (cationic) decrease it.

Table 1. Lipid charge effects on SERCA activity (Equation 12). (Mean ± SEM. n ≥ 4)

Lipid (charge)	pK_{Ca}	V_{max}
PS (-)	6.81 ± 0.01	1.65 ± 0.03
PG (-)	6.73 ± 0.02	1.55 ± 0.12
PC (0)	6.68 ± 0.02	1.65 ± 0.19
EPC (+)	6.53 ± 0.03	1.46 ± 0.10
TAP (+)	6.51 ± 0.02	1.66 ± 0.19

Lipid headgroup charge affects SERCA inhibition by PLB. The inhibitory function of PLB is defined by its shift of the apparent SERCA Ca affinity, ΔpK_{Ca} (Figure 14a, Equation 13). In order to compare the inhibitory potency of PLB in various lipid environments, ΔpK_{Ca} was normalized to the value obtained with PC (Figure 14b). The results show that PLB is more inhibitory in the presence of anionic lipids PS and PG, and less inhibitory in the presence of cationic lipids EPC and TAP. Previous results showed that PLB phosphorylation, which decreases inhibition of SERCA, increases the

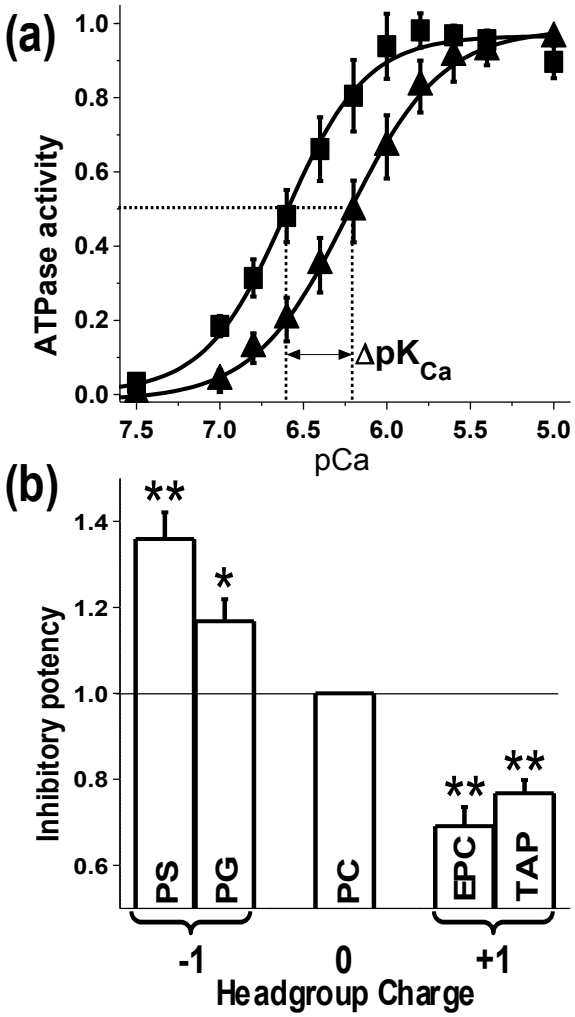

Figure 14 Effects of lipid headgroup charge on SERCA inhibition. (a) Activity of SERCA in PC without (■) and with (▲) AFA-PLB. Solid curves are the best fit using Equation 12. Error bars are SEM (n = 4). (b) Inhibitory potency, defined as ΔpK_{Ca} normalized to the value for PC (mean ± SEM. n = 4-6). Students *t*-test, compared with PC: * $P < 0.05$, ** $P < 0.01$.

population in the dynamically disordered ***R*** state [83]. The results of Figure 14b show that membrane surface charge modulates PLB's effect on SERCA by an analogous mechanism, confirming the conclusion above that the ***R*** state corresponds to the structural state having the shorter interprobe distance (population 1 in Figure 12 and Figure 13).

3.4 Discussion

Bimodal structure of the SERCA-PLB complex resolved by TR-FRET. Using EPR, we demonstrated that anionic lipids attract the cationic cytoplasmic domain of PLB to the membrane surface and thus increase the population of the membrane-associated ***T*** state, while cationic lipids do the opposite, increasing the ***R*** state population (Figure 11). We then used TR-FRET to resolve two distinct structural states of the bound SERCA-PLB complex (Figure 13) and observed a similar effect, with the ***R*** state assigned to the population having the shorter interprobe distance (Figure 13). Membrane surface charge shifts the equilibrium between the ***T***/***R*** states with little or no effect on the two structural states themselves (Figure 13d). This supports a model in which the cytoplasmic domain of the SERCA-bound ***T*** state is membrane associated, while that of the SERCA-bound ***R*** state loses contact with the membrane surface and contacts the SERCA cytoplasmic domain (Figure 12c).

Mechanism of SERCA regulation. As we systematically varied the membrane surface charge, we observed a strong correlation between the population of the ***R*** state and PLB inhibitory function (Figure 15a). This finding is consistent with previous results showing that phosphorylation of PLB, which decreases SERCA inhibition, also increases x_R [83], as do some loss-of-inhibition mutations in PLB [154]. In the current study, we show that varying the membrane surface charge serves not only to relieve inhibition (positive charge increases x_R), but also to increase inhibition (negative charge decreases x_R). Thus we obtain convincing evidence that this correlation between structural

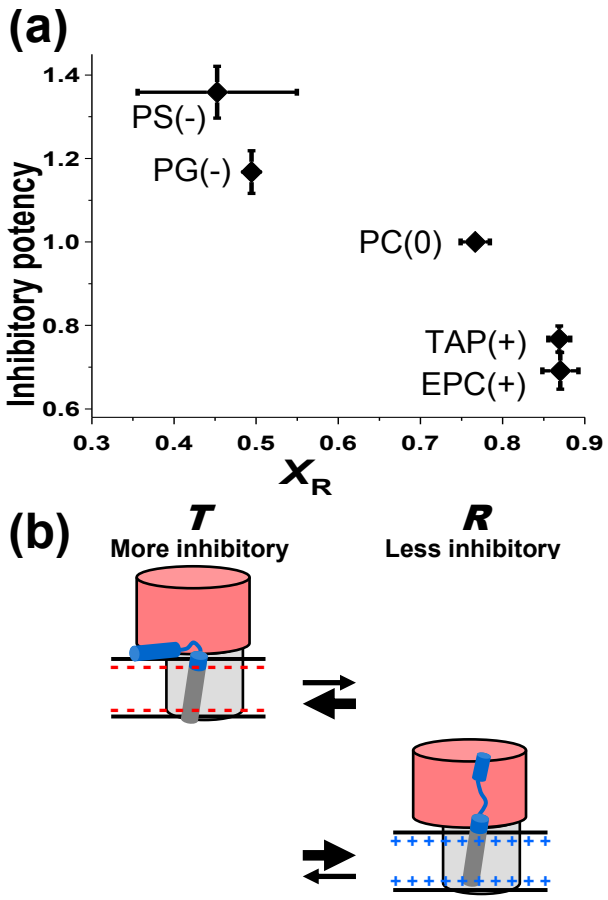

Figure 15. Correlation of inhibitory potency with the *T*/*R* equilibrium. (a) As the fraction of SERCA-PLB complex in the *R* state (x_R) increases, in response to increasing membrane surface charge, the inhibitory potency of PLB (defined in Figure 14) decreases. (b) Model consistent with the data. Both *T* and *R* states bind to SERCA. The membrane-associated ***T*** state is more inhibitory than the extended ***R*** state. Negative surface charge shifts the equilibrium toward ***T***, increasing inhibition (top), while positive surface charge does the opposite (bottom).

dynamics and function holds even in the absence of PLB covalent modification (e.g., phosphorylation or mutation): it is primarily the ***T***/***R*** equilibrium that determines SERCA function (Figure 15b).

Structural dynamics, not SERCA affinity, determines the inhibitory potency of PLB. TR-FRET clearly resolves free SERCA from the bound SERCA-PLB complex (Figure 12c), and shows that relief of inhibition does not arise from a change in X_b, the fraction of SERCA bound to PLB (Figure 13b). In both neutral (PC) or anionic lipids (PS, PG) (Figure 13b), 80% of the SERCA is bound to PLB ($X_b \sim 0.8$), but PLB is more inhibitory in anionic lipids (Figure 14b). Cationic lipids (EPC and TAP) actually increase slightly the fraction of SERCA bound to PLB ($X_b \sim 0.9$, Figure 13b), but PLB inhibitory function decreases (Figure 14b). This is opposite from the effect expected if relief of inhibition were due to dissociation of the complex. Therefore, the functional effects are due to structural changes within the bound SERCA-PLB complex (Figure 15b), not to changes in SERCA-PLB affinity. It has been shown that the transmembrane helix of PLB without the cytoplasmic domain is sufficient to inhibit SERCA activity [60], so the role of the cytoplasmic domain is to relieve this inhibition when it is in the ***R*** state. Future studies must investigate how the dynamic disorder of the ***R*** state propagates allosterically to the transmembrane domain, interrupting the inhibitory interaction of the transmembrane domain with SERCA. This will have important implications for therapeutic engineering in this system, since it offers the hope of designing mutant proteins or drugs that stabilize the non-inhibitory ***R*** state and thus relieve SERCA inhibition, without the need to dissociate PLB from SERCA [149,154].

Relationship to previous work. The fraction x_R is much greater when PLB is bound to SERCA (Figure 12, Figure 13c) than when it is free (Figure 11); this is consistent with previous studies by EPR [83,144] and crosslinking [65], all of which suggest that SERCA decreases PLB's interaction with the membrane surface. This is presumably due in part to the negative charge of the SERCA cytoplasmic domain (indicated by red color in Figure 12c and Figure 15b), which attracts the positively charged PLB cytoplasmic domain. Thus a negatively charged membrane surface competes most effectively for PLB binding (Figure 13c). Previous NMR results suggested that several residues around Lys3 on PLB are in contact with SERCA [69]. NMR also provides more detailed structural insight into the interactions between PLB and the membrane surface, involving both hydrophobic and hydrophilic side chains [81,155]. Previous NMR results showed that the anionic PG increases the population of the restricted ***T*** state of PLB in the absence of SERCA [81], consistent with the EPR results here (Figure 11).

Implications for SERCA regulation in native SR. The primary purpose of our manipulation of the lipid environment in this study was to perturb the structural and functional dynamics of SERCA-PLB through a mechanism distinct from PLB phosphorylation. However, it is also important to ask how these results relate to conditions in native cardiac SR. Our lipid headgroup composition is similar to that of cardiac SR, where PC is predominant (53%), followed by PE (27%) and PS (10%) [156]. However, most (76%) of the negatively charged PS headgroups face the lumen [156], so it is unlikely that they interact significantly with the cytosolic domain of PLB. Thus, since virtually all of the lipids facing the cytosol are neutral, it is likely that the conditions

in cardiac SR are best mimicked by our sample in which all lipids are neutral, where 77% of the SERCA-PLB complex is in the less inhibitory ***R*** state (Figure 15a). These results suggest that in cardiac SR, a minor population of PLB in the ***T*** state is enough to inhibit SERCA substantially. At first glance, this seems surprising, but it means that phosphorylation of PLB need only shift about 23% of PLB to the ***R*** state to maximally activate SERCA. This is analogous to the poised equilibrium in the regulatory light chain of smooth muscle myosin, where phosphorylation causes just a 22% shift in the dynamic structural equilibrium but results in profound activation [146].

Lipid headgroup charge as a research tool to tune the structural and functional dynamics of integral membrane proteins. It has been an effective strategy to vary the physical properties of the hydrophobic core of the membrane, such as the hydrophobic thickness and fluidity [157,158], to investigate the structural and functional dynamics of integral membrane proteins. The composition of lipid headgroups is also critical for the function of membrane proteins [134], including SERCA [147,159]. Researchers have varied the zwitterionic and anionic lipid compositions to mimic native membrane environments [160,161]. Cationic lipids, on the other hand, do not occur naturally and have been used primarily as tools in liposomal transfection [162] and lipid transfer [163]. The present study introduces them as agents to perturb the structure and function of membrane proteins. Using lipids with anionic, zwitterionic, and cationic headgroups, we controlled the surface electrostatics and tuned successfully the structural dynamics of an integral membrane protein complex. Compared to altering the protein structure through direct chemical modifications such as mutagenesis, phosphorylation, lipidation, methylation, and crosslinking, this method preserves the chemical integrity of

the proteins involved. Although the present study focuses on charge variation, it is clear from the data that charge is not the only headgroup property that affects structural dynamics and function in the SERCA-PLB system – the two anionic lipids do not cause identical effects; neither do the two cationic lipids. Nevertheless, despite substantial variation in headgroup size and shape, the correlations of structure and function with charge are clear (Figure 15).

3.5 Materials and Methods

Sample preparation and assays. SERCA was purified from rabbit skeletal muscle using reactive red in 0.1% octaethylene glycol monododecyl ether ($C_{12}E_8$) [85]. Purified SERCA was labeled with AEDANS as previously described [85] and flash frozen in sucrose buffer (300 mM sucrose, 20 mM 3-(N-morpholino) propanesulfonic acid (MOPS), pH 7.0, 4 °C). The dye-to-protein ratio was determined by measuring the absorbance at 334 nm (ε = 6100 M^{-1} cm^{-1}) in a denaturing buffer (0.1 M NaOH, 1% sodium dodecyl sulfate). Solid-phase peptide synthesis and HPLC purification were used to prepare AFA-PLB, as previously reported [78,83]. Fluorescence Labeling at the N-terminus was accomplished by incorporation of Fmoc-Lys(Dabcyl)-OH during peptide synthesis. Fmoc-TOAC-OH (2,2,6,6-tetramethylpiperidine-1oxyl-4-amino-4-carboxylic acid) was incorporated in the AFA-PLB sequence at position 11, as previously reported [164]. Characterization was accomplished by mass spectrometry (MALDI-TOF) and Edman protein sequencing. PLB concentrations were measured with the BCA assay (Pierce) and by amino acid analysis. Functional reconstitution of SERCA and/or PLB was performed as described previously [35,83], adapted for systematic variation of lipid composition. The final molar ratio of SERCA/PLB/lipid was 1/10/700, with either one or

both proteins present. The molar lipid composition was PC/PE/L = 4/1/1, where L = PS (−), PG (−), PC (0), EPC (+) and TAP (+).

Ca-ATPase activity was measured at 25 °C as a function of pCa using an enzyme-linked ATPase assay in a microplate reader [85]. The data were fitted by

$$V = \frac{V_{max}}{1 + 10^{-n(pK_{Ca} - pCa)}} \qquad \textbf{Equation 12}$$

where V_{max} is the maximum ATPase rate, pK_{Ca} is the apparent Ca affinity, and n is the Hill coefficient. The inhibitory potency of PLB was defined as the decrease in the apparent Ca^{2+} affinity of SERCA:

$$\Delta pK_{Ca} = pK_{Ca}(-PLB) - pK_{Ca}(+PLB) \qquad \textbf{Equation 13}$$

EPR spectroscopy. EPR spectra were acquired with a Bruker EleXsys E500 spectrometer equipped with a 4122 SHQ cavity. A quartz dewar and Bruker N_2 temperature controller were used to maintain the samples at 25 ± 0.1 °C. Spectra were acquired using 12.6 mW microwave power, 100 kHz modulation frequency with 1 G peak-to-peak amplitude, and a 120 G sweep width. Mole fractions of populations, resolved by rotational dynamics, were determined by fitting the spectra to numerical simulations [83].

FRET spectroscopy. Fluorescence waveforms were acquired using a high-performance time-resolved fluorescence (HPTRF) spectrometer constructed in this laboratory [151], which uses direct waveform recording (DWR) rather than the conventional method of time-correlated single-photon counting (TCSPC). As shown previously, when identical samples are studied, this DWR instrument offers 105 times higher throughput than TCSPC, while providing at least comparable performance in signal/noise, accuracy, and resolution of distinct components [151]. AEDANS-SERCA

was excited using a passively Q-switched microchip YAG laser (NanoUV-355; JDS Uniphase), at 355 nm with a pulse repetition frequency of 10 kHz. The high energy (1 mJ / pulse) narrow (~ 1 ns full width at half maximum) laser pulses are highly uniform in shape and intensity. Emitted photons pass through a polarizer set to the magic angle (54.7°), followed by an interference bandpass filter (Semrock 470/22 nm), detection with a photomultiplier tube (PMT) module (H5773-20, Hamamatsu), and digitization (Acqiris DC252, time resolution 0.125 ns). TR-FRET waveforms were analyzed as described previously [146] and described in SI. For all FRET samples analyzed, two Gaussian distance distributions were necessary and sufficient to fit the data (Figure S17).

3.6 Supplementary Information

TR-FRET data analysis. Fluorescence waveforms were analyzed using a non-linear least-squares fitting as described previously [146,165]. The observed donor-only waveform $F_{Dobs}(t)$ was fitted by a simulation $F_{Dsim}(t)$, consisting of a multiexponential decay $F_D(t)$ convolved with the instrument response function IRF(t) (Figure 12a, acquired from light scattering).

$$F_D(t) = \sum_{i=1}^{n} A_i \exp(-t/\tau_{Di}) ,$$

$$F_{Dsim}(t) = \int_{-\infty}^{+\infty} IRF(t-t') F_D(t') dt', \qquad \textbf{Equation S14}$$

where τ_{Di} are the donor-only fluorescence lifetimes. The ensemble-average lifetime is given by:

$$\langle \tau_D \rangle = \sum_{i=1}^{n} A_i \tau_{Di} / \sum_{i=1}^{n} A_i \qquad \textbf{Equation S15}$$

The observed donor + acceptor waveform $F_{D+Aobs}(t)$ was sometimes fitted to a multiexponential function using the same approach. The ensemble-average FRET efficiency, which is equivalent to the result of a steady-state fluorescence measurement [153], is given by:

$$\langle E_{D+A} \rangle = 1 - \langle \tau_{D+A} \rangle / \langle \tau_D \rangle . \qquad \textbf{Equation S16}$$

To resolve structural states, a distribution of donor-acceptor distances $\rho(r)$ was assumed:

$$F_{DA}(t) = \int_{-\infty}^{+\infty} \rho(R) \cdot \sum_{i=1}^{n} A_i \exp[(-t/\tau_{Di})(1+[R_{0i}/R]^6)]dR, \qquad \textbf{Equation S17}$$

where R_{0i} is the lifetime-weighted Förster distance [146] (in Å):

$$R_{0i}^6 = 9780^6 J\kappa^2 n^{-4} k_{rad} \tau_{Di} \qquad \textbf{Equation S18}$$

where J is the overlap integral between the donor emission and acceptor absorption spectra, n is the refractive index (1.4), κ^2 is the orientation factor (2/3, assuming random orientation), and k_{rad} is the radiative decay rate for the donor. The value of k_{rad}, which is assumed to be invariant for each donor, is the ratio of the quantum yield Q_D over the average lifetime of the donor $\langle \tau_D \rangle$ (Equation S15) and was measured previously to be 0.0257 ns^{-1} for AEDANS [146]. Equation S18 follows directly from the Förster theory's assumption [131,146] that the energy transfer rate constant k_T (= $R_{0i}^6 R^{-6}/\tau_{Di}$) depends on the donor-acceptor distance R but not on the donor-only lifetime τ_{Di}. Here we also

assume that the orientation factor κ^2 does not change from one structural state to another, but this is justified by low fluorescence anisotropy values that were observed. R_0 between AEDANS-SERCA and Dabcyl-PLB is 3.2 nm [85].

The distance distribution $\rho(r)$ (Equation S17) was assumed to be a sum of n Gaussian components, each corresponding to a structural state of the SERCA-PLB complex, with its central distances R_j, widths $FWHM_j$, and mole fractions $\boldsymbol{x}_j$

$$\rho(R) = \sum_{j=1}^{n} \boldsymbol{x}_j \, \sigma_j^{-1}(2\pi)^{-1/2} \exp(-[(R-R_j)/(2\sigma_j)]^2,$$

$$\sigma_j = FWHM_j/[2*(2 \ln 2)^{1/2}], \qquad \textbf{Equation S19}$$

$$\sum_{j=1}^{n} \boldsymbol{x}_j = 1$$

The observed waveform $F_{D+Aobs}(t)$ was fitted by $F_{D+Asim}(t)$:

$$F_{D+A}(t) = (1 - X_b)F_D(t) + X_b F_{DA}(t),$$

$$F_{D+Asim}(t) = \int_{-\infty}^{+\infty} IRF(t - t') \cdot F_{D+A}(t')dt', \qquad \textbf{Equation S20}$$

where X_b is the fraction of donor-labeled SERCA bound to and transferring energy to acceptor-labeled PLB. Thus binding (X_b) is determined independently of the mole fractions of resolved structural states (x_j in Equation S19).

Donor-only fluorescence decays are best fit with 3 exponential components. The donor-only fluorescence decay $F_D(t)$ (Figure S16a), was fitted with a multiexponential function (Equation S14), with the result that three lifetime components are necessary and sufficient to fit the data (Equation S14, n = 3), based on the residual

plots (data – fit, Figure S16b) and the χ^2 values (sum of residuals at each data point, Figure S16c). The results show clearly that the fit is improved by increasing n from 2 to 3, but not by increasing n from 3 to 4. The fitting results are summarized in Table S2. The donor-only fluorescence lifetime is not sensitive to the lipid environment (Table S3), presumably because the labeling site (Cys674) is elevated far from the membrane surface. Therefore, to increase precision in the FRET analysis, the three donor lifetime values were globally linked. The corresponding R_{0i} (Equation S18) values are listed in Table S3.

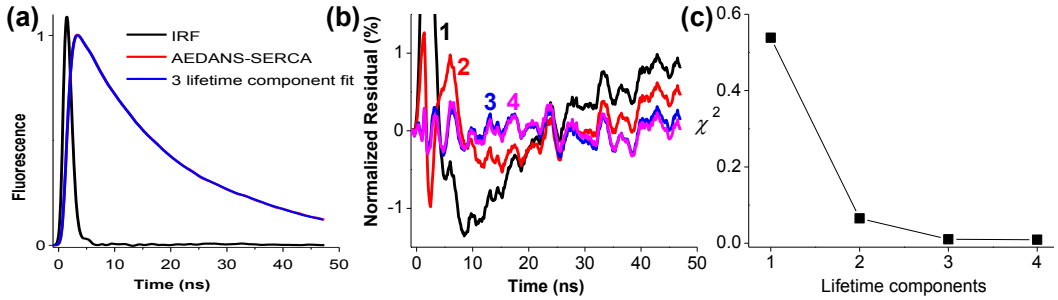

Figure S16. Fluorescence lifetime fit of IAEDANS-labeled SERCA. (a) Fluorescence data, fit and instrument respond function. (b) normalized residual plots ((data – fit) / max fit value) of fits with increasing number of lifetime components (Equation S14, n = 1-4).

Table S2. Fluorescence lifetime of AEDANS-SERCA in charged lipid vesicles, analyzed using Equation S14 and Equation S15 (mean ± SEM, N= 4).

Lipid (charge)	A_1	τ_1	A_2	τ_2	A_3	τ_3	$\langle \tau \rangle$
PS (-)	0.418 ± 0.016	0.112 ± 0.009	0.055 ± 0.004	4.96 ± 0.85	0.527 ± 0.018	18.9 ± 0.1	10.3 ± 0.3
PG (-)	0.412 ± 0.015	0.134 ± 0.017	0.055 ± 0.003	5.36 ± 0.46	0.532 ± 0.015	18.9 ± 0.1	10.4 ± 0.3
PC (0)	0.403 ± 0.009	0.13 ± 0.013	0.054 ± 0.001	5.27 ± 0.39	0.544 ± 0.009	18.9 ± 0.1	10.6 ± 0.2
EPC (+)	0.415 ± 0.01	0.124 ± 0.01	0.059 ± 0.002	4.88 ± 0.53	0.526 ± 0.011	18.8 ± 0.1	10.2 ± 0.2
TAP (+)	0.392 ± 0.013	0.134 ± 0.002	0.056 ± 0.003	4.37 ± 0.42	0.551 ± 0.01	18.8 ± 0.1	10.7 ± 0.2

Table S3. The three fluorescence lifetimes of AEDANS-SERCA were globally linked for all samples, and the three R_{0i} values were calculated using Equation S19 (mean ± SEM, N= 4).

	A_i	τ_i	R_{0i}
1	0.407 ± 0.09	0.122 ± 0.012	15.2 ± 0.3
2	0.052 ± 0.001	4.32 ± 0.25	27.6 ± 0.2
3	0.541 ± 0.01	18.7 ± 0.1	35.3 ± 0.1

Two structural states are necessary and sufficient to fit the TR-FRET data. To resolve structural states within the SERCA-PLB complex, we used $F_D(t)$ as input (Table S3), to fit $F_{D+Aobs}(t)$ and determine the interprobe distance distribution (Equation S17 – Equation S20). We tested models with one, two, and three Gaussian components (Equation S19, n = 1, 2, and 3). The goodness of fit was evaluated to minimize χ^2 (Figure S17). The fit was consistently improved by increasing the distance components (n in Equation S19) from 1 to 2, but not from 2 to 3 (Figure S17). Thus two Gaussian distance

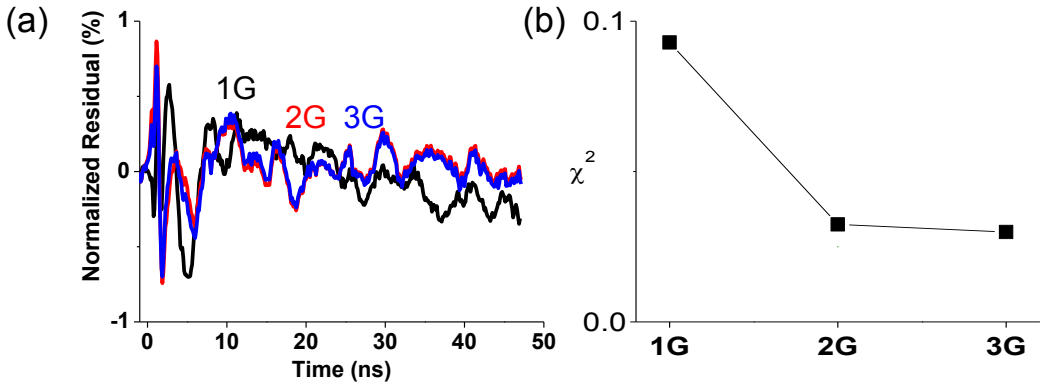

Figure S17. Time-resolved FRET resolves two structural states of the SERCA-PLB complex in zwitterionic lipid vesicles. Examples of the fluorescence waveforms of AEDANS-SERCA only (D) or co-reconstituted with Dabcyl-AFA (D+A) are in (Figure 12a). The instrument-response function (IRF in Figure 12a) was convolved with simulated decays (Equation S17 - Equation S20), then fitted to the experimental waveforms. (a) normalized residual plots show that 2G (Equation S19, n = 2) is better than 1G, while 3G doesn't improve the fit. (b) The χ^2 values confirm that the 2G model is necessary and sufficient to fit the data.

distributions are necessary and sufficient to fit the TR-FRET data, and we conclude that the SERCA-PLB complex adopts two distinct structural states. The results are summarized in Figure 12 and Figure 13. We also fit the data with a model-independent multiexponential function as in Equation S14, and found that a three-exponential function (Equation S14, $n = 3$) gave as good a fit as the double-Gaussian (Equation S19, $n = 2$). However, this fit did not allow us to quantitate binding from structural changes, nor did it provide a realistic physical view of this dynamic protein complex. This same two-Gaussian analysis was successfully applied previously to similar FRET data from smooth muscle myosin regulatory light chain [146] and the myosin relay helix [152], generating high-resolution structural information that was confirmed by independent molecular dynamics simulations [146] or by dipolar electron–electron resonance (DEER) EPR spectroscopy [152].

Support-Plane Analysis. We analyzed the χ^2 surface to estimate the uncertainty of the fitting parameters (Figure S18). To generate the χ^2 surface, the parameter of interest is fixed (x-axis), and all other parameters are allowed to vary to minimize χ^2 (y-axis). The red bar represents 67% confidence level. Thus the uncertainties are ± 0.01 nm for R_1 and R_2, ± 0.015 nm for $FWHM_1$, and ± 0.075 nm for $FWHM_2$. These uncertainties were typically comparable to or less than those obtained from the standard deviations of multiple experiments (Figure 13). Uncertainties in widths $FWHM_i$ are typically greater than those of the center distances R_i (Figure S18), and the same trend is seen in the error bars (SEM values) from multiple experiments (Figure 13).

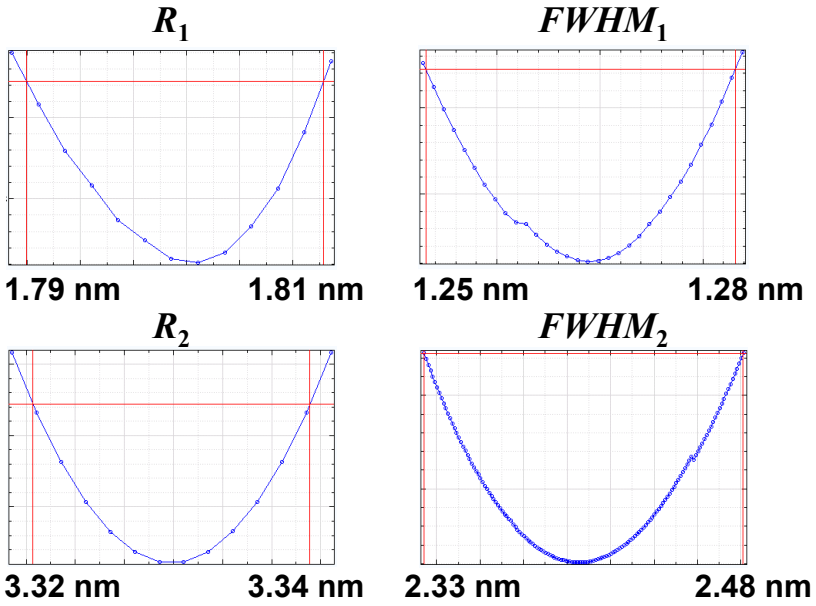

Figure S18. Uncertainty of fitting parameters estimated by χ^2 surface ("support-plane") analysis. This example is in PS vesicles. The intersection between the horizontal red line and the blue χ^2 surface represents 67% confidence level.

Chapter 4 Time-resolved FRET Reveals the Structural Mechanism of SERCA-PLB Regulation

Xiaoqiong Dong[1] and David D. Thomas[2]

[1]Department of Biomedical Engineering

[2]Department of Biochemistry, Molecular Biology and Biophysics, University of Minnesota, Minneapolis, Minnesota 55455, USA

Originally published in *Biochemical and Biophysical Research Communications*, vol.449, pp. 196-201. Reprinted with permission from Elsevier.

Xiaoqiong Dong did all the work and wrote the manuscript. David D. Thomas contributed ideas to the project and edited the final manuscript.

4.1 Chapter Overview

We have used time-resolved fluorescence resonance energy transfer (TR-FRET) to characterize the interaction between phospholamban (PLB) and the sarcoplasmic reticulum (SR) Ca-ATPase (SERCA) under conditions that relieve SERCA inhibition. Unphosphorylated PLB inhibits SERCA in cardiac SR, but inhibition is relieved by either micromolar Ca^{2+} or PLB phosphorylation. In both cases, it has been proposed that inhibition is relieved by dissociation of the complex. To test this hypothesis, we attached fluorophores to the cytoplasmic domains of SERCA and PLB, and reconstituted them functionally in lipid bilayers. TR-FRET, which permitted simultaneous measurement of SERCA-PLB binding and structure, was measured as a function of PLB phosphorylation

and [Ca^{2+}]. In all cases, two structural states of the SERCA-PLB complex were resolved, probably corresponding to the previously described *T* and *R* structural states of the PLB cytoplasmic domain. Phosphorylation of PLB at S16 completely relieved inhibition, partially dissociated the SERCA-PLB complex, and shifted the *T/R* equilibrium within the bound complex toward the *R* state. Since the PLB concentration in cardiac SR is at least 10 times that in our FRET measurements, we calculate that most of SERCA contains bound phosphorylated PLB in cardiac SR, even after complete phosphorylation. 4 μM Ca^{2+} completely relieved inhibition but did not induce a detectable change in SERCA-PLB binding or cytoplasmic domain structure, suggesting a mechanism involving structural changes in SERCA's transmembrane domain. We conclude that Ca^{2+} and PLB phosphorylation relieve SERCA-PLB inhibition by distinct mechanisms, but both are achieved primarily by structural changes within the SERCA-PLB complex, not by dissociation of that complex.

4.2 Introduction

A hallmark of heart failure is dysregulation of intracellular Ca^{2+} handling [99], primarily caused by inadequate removal of Ca^{2+} from the cytosol by the sarco(endo)plasmic reticulum Ca^{2+}-ATPase (SERCA) [166], which actively sequesters Ca^{2+} back into the sarcoplasmic reticulum (SR) at a ratio of 2 Ca^{2+} per ATP hydrolyzed [167]. In the heart, SERCA is regulated by phospholamban (PLB), a single-pass integral membrane protein. Unphosphorylated PLB inhibits SERCA by decreasing its apparent Ca^{2+} affinity [136]. Under physiological conditions, this inhibition is relieved by either micromolar Ca^{2+} or by phosphorylation of PLB, primarily by protein kinase A (PKA) at

S16 [168]. Recent gene therapies targeting increased SERCA activity show promise for alleviation of heart failure [169]. Ablation of PLB or introduction of phosphomimetic mutant S16E-PLB suppress progression of heart failure in animal models [120,123,124]. Overexpression of SERCA2a, the cardiac isoform, has successfully completed Phase IIa clinical trials [170]. These studies validate the SERCA-PLB complex as a potent therapeutic target for heart failure. However, rational design of improved therapies is hampered by uncertainty regarding the mechanism by which PLB regulates SERCA.

Two structural mechanisms for relief of SERCA inhibition have been proposed. The dissociation model hypothesizes that PLB dissociates from SERCA to relieve inhibition. This model is supported by crosslinking and co-immunoprecipitation studies that found decreased physical interaction between SERCA and PLB at either micromolar Ca^{2+} or after phosphorylation at S16 by PKA [54,72,73,74,75,76]. However, recent spectroscopic studies support the subunit model, in which inhibition of SERCA is relieved by structural rearrangements within the SERCA-PLB complex, not by dissociation. Electron paramagnetic resonance (EPR) and fluorescence resonance energy transfer (FRET) studies showed that PLB remains bound to SERCA when the pump is activated [85,86,171,172]. EPR and NMR studies showed that the cytoplasmic domain of PLB exists in equilibrium between a *T* state that is ordered and an *R* state that is dynamically disordered [78,80,145]. Phosphorylation shifts the equilibrium toward the *R* state and relieves inhibition [83]. FRET studies showed that variation of lipid headgroup charge shows a strong correlation between the population of the *R* state and SERCA-PLB activation, without dissociation, further validating the subunit model [84]. That study showed the power of time-resolved (TR) FRET to distinguish between changes in

structure and association. In the present study, we have used TR-FRET, using fluorophore-labeled SERCA and PLB reconstituted in lipid bilayers, to resolve the effects of both micromolar Ca^{2+} and PLB phosphorylation on the structure and stability of the SERCA-PLB complex. These results provide definitive insights into the molecular mechanisms underlying relief of inhibition in cardiac SR.

4.3 Materials and Methods

SERCA purification and labeling

Crude SR vesicles were prepared from the fast-twitch skeletal muscle of New Zealand white rabbits [173]. SERCA was further purified from crude SR vesicles using reactive-red chromatography [174]. For FRET studies, purified SERCA was labeled with 5-iodoacetamidofluorescein (IAF) (Invitrogen, CA) specifically and completely at C674 [175].

Expression, purification, phosphorylation and labeling of PLB

Native PLB equilibrates between monomers and homopentamers [139]. To simplify the analysis and focus on the SERCA-PLB interaction, a monomeric mutant of PLB was used, with the three cysteine residues (C36, C41 and C46) in the transmembrane domain mutated to alanine, phenylalanine, and alanine, respectively [176]. Site-directed mutagenesis was performed to mutate Y6 to C for thiol-reactive fluorophore attachment. This site was chosen because Y6 is not involved in the interaction with SERCA [69]. Recombinant PLB was expressed in *E. coli* and purified as previously published [177]. For site-directed fluorophore labeling, lyophilized PLB

powder was dissolved at a concentration of 0.2 mM in 20 mM MOPS, 1% octyl β-D-glucopyranoside (OG), pH 7.0. Alexa Fluor® 350 C_5 maleimide (Invitrogen, CA) freshly dissolved in DMSO was then added at 10-fold molar excess. The reaction was allowed to proceed at room temperature for 1 hour, and the labeled PLB was purified by reversed-phase HPLC. For phosphorylation studies, labeled PLB was phosphorylated as described previously [139] and purified by reversed-phase HPLC. Complete labeling and phosphorylation of PLB was confirmed by ESI-MS. The concentration of PLB was measured by the BCA assay.

Co-reconstitution of SERCA and PLB

SERCA and PLB were co-reconstituted into lipid vesicles using 4:1 1,2-dioleoyl-*sn*-glycero-3-phosphocholine (DOPC)/1,2-dioleoyl-*sn*-glycero-3-phosphoethanolamine (DOPE) (mol/mol) to yield unilamellar vesicles [148]. Ca^{2+}-ATPase activity and FRET measurements were performed immediately after co-reconstitution. The final buffer composition of FRET samples was 50 mM MOPS, 50 mM KCl, 5 mM $MgCl_2$, 1 mM EGTA, pH 7.0, with varying concentrations of $CaCl_2$ to yield the desired free Ca^{2+} concentration (pCa 8.0, 6.4, or 5.4).

Ca^{2+}-ATPase functional measurements

To ensure that labeled SERCA and PLB remain functional, we measured the ATPase activity of co-reconstituted samples at 25^{o} C, using an NADH-linked enzyme-coupled assay [148,149]. The Ca^{2+}-dependent rate of ATP consumption was fitted to the Hill equation,

$$V = V_{max}/[1+ 10^{-n\,(pKCa - pCa)}], \qquad \textbf{Equation 21}$$

where $pCa = -\log_{10}[Ca^{2+}]$, V_{max} is the limiting activity at saturating calcium, pK_{Ca} is the pCa value where $V = 0.5V_{max}$, and *n* is the Hill coefficient. The inhibition of SERCA by PLB is shown as ΔpK_{Ca}, the shift of pK_{Ca} upon addition of PLB.

Time-resolved fluorescence resonance energy transfer (TR-FRET) measurements

SERCA and PLB were labeled with fluorophores at the sites shown in Figure 19**A.** PLB was labeled with Alexa Fluor 350 maleimide (donor) at Y6C, and SERCA was labeled with IAF (acceptor) at C674. The quantum yield of bound Alexa Fluor 350 maleimide was measured in 20 mM MOPS, 1% OG, pH 7.0, using quinine sulfate dehydrate (AnaSpec, CA) as the standard, yielding a quantum yield of 0.48 for PLB, 0.80 for phosphorylated PLB (pPLB). The corresponding R_0 values [178] are calculated to be 4.6 nm and 5.0 nm, respectively. The time-resolved fluorescence decay of co-

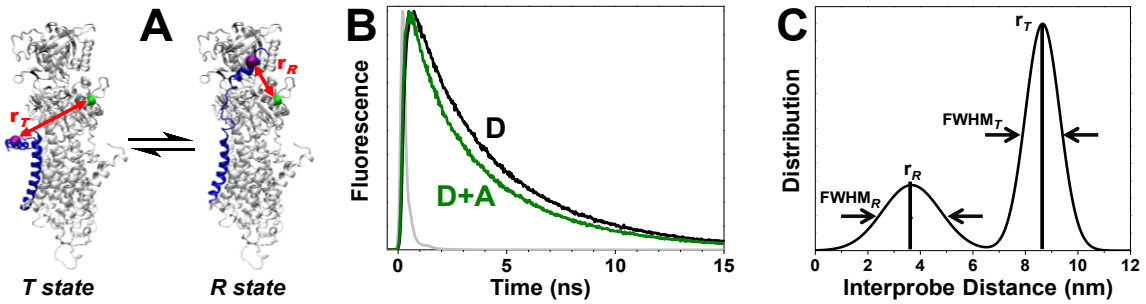

Figure 19: TR-FRET experimental design. **A** Models of SERCA-PLB complex. SERCA (silver)-bound PLB (blue) is proposed to exist in an equilibrium between *T* and *R* states, as shown previously by EPR [83]. There is no high-resolution structure of the SERCA-PLB complex, but a model for the *R* state (right) is from [65], and the *T* state model (left) is based on the NMR structure of PLB. The labeling sites on SERCA (C674) and PLB (Y6C) are shown as green and magenta spheres, respectively. The interprobe distances in *T* and *R* states are denoted as r_T and r_R, respectively. Image created in VMD [14]. **B** Representative fluorescence waveforms. D. donor only. D+A, donor plus acceptor. Grey indicates instrument response function. **C** Interprobe distance distributions resolved from fluorescence waveforms in **B**. Two Gaussian distance distributions were resolved. The shorter and longer distances correspond to *R* and *T* states, respectively [84].

reconstituted samples was measured by time-correlated single-photon counting (Becker-Hickl, Berlin, Germany), following excitation at 385 nm using a subnanosecond pulsed diode laser (PicoQuant, Berlin, Germany), filtering the emitted light using a 440/40 filter (Semrock, NY), and detection with a PMH-100 photomultiplier (Becker-Hickl). The instrument response function (IRF, Figure 19B) was recorded from water. TR-FRET data was analyzed as previously published [84]. The observed donor-only waveform (Figure 19B) was fitted by a simulation $F_{Dsim}(t)$, consisting of a multi-exponential decay $F_D(t)$ convoluted with the IRF

$$F_D(t) = \sum_{i=1}^{n} A_i \exp(-t/\tau_{Di})$$

Equation 22

$$F_{Dsim}(t) = \int_{-\infty}^{+\infty} IRF(t-t')F_D(t')dt'$$

where τ_{Di} is the fluorescence lifetime of the *i*th component. In this study, two exponentials were sufficient to fit the donor-only waveform (Figure S23). The waveform of the samples containing donor and acceptor (Figure 19B), was fitted by $F_{D+A,sim}(t)$:

$$F_{D+A}(t) = (1 - x_{DA})F_D(t) + x_{DA}\sum_{i=1}^{m} F_{DA,j}(t)$$

Equation 23

$$F_{D+A,sim}(t) = \int_{-\infty}^{\infty} IRF(t-t')F_{D+A}(t')dt',$$

where x_{DA} is the mole fraction of donor-labeled PLB that is bound to acceptor-labeled SERCA, and $F_{DA,j}(t)$ is the fluorescence waveform of the *j*th donor-acceptor complex. We found that m=2 was sufficient (Figure S25).

$$F_{DA}(t) = \int_{-\infty}^{+\infty} \rho(R)\sum_{i=1}^{n} A_i \exp\{(-t/\tau_{Di})[1 + (R_{oi}/R)^6]\}dR$$

Equation 24

where R_{oi} is the Förster distance of Alexa Fluor 350 and IAF, and ρ(R) is the distance distribution function, assumed to be sum of Gaussians, each with a mole fraction x_j, a center r_j and a full width at half maximum ($FWHM_j$) (Figure 19C):

$$\rho(R) = \sum_{j=1}^{2} x_j \left(\frac{1}{\sigma_j \sqrt{2\pi}}\right) \exp\left[-\frac{(R - r_j)^2}{2\sigma_j^2}\right]$$

Equation 25

$$\text{where } \sigma_j = \frac{FWHM_j}{2\sqrt{2 \ln 2}}$$

We assumed that PLB and pPLB populate the same two states, because the distance parameters resolved from independent fittings are similar for PLB and pPLB (Figure S24) and this assumption does not change the goodness of the fit (Figure S25). Our previous FRET studies showed that the shorter distance observed between probes on the SERCA and PLB cytoplasmic domains is the *R* state (correlating with decreased inhibition), while the longer distance is due to the *T* state, in which the PLB cytoplasmic domain interacts with membrane surface and hence increases interprobe distance [84]. Therefore, we refer the parameters of the shorter distance with a subscript *R*, and those of the longer distance with a subscript *T* (Figure 19).

Statistical Analysis

Data is presented as the mean ± SE. For comparison between two groups, a student's *t*-test was performed. A *p*-value less than 0.05 was taken as significant.

4.4 Results

Function of labeled SERCA and PLB.

To confirm that the labeled proteins preserve their functions, we co-reconstituted SERCA and PLB into lipid vesicles and measured the Ca^{2+}-dependent ATPase activity. The function of unlabeled PLB is characterized by inhibition of SERCA (decreasing pK_{Ca}) and reversal after phosphorylation at S16 by PKA (Figure 20). For unlabeled SERCA, pK_{Ca} = 6.43 ± 0.02, unlabeled PLB shifted pK_{Ca} to 6.32 ± 0.003, and unlabeled pPLB restored pK_{Ca} to 6.39 ± 0.02. Labeled proteins demonstrated similar results (Figure 20). The pK_{Ca} of acceptor-labeled SERCA is 6.45 ± 0.02, donor-labeled PLB shifted it to 6.32 ± 0.003, and phosphorylated donor-labeled PLB shifted it back to 6.45 ± 0.01. Therefore, the fluorophore-labeled SERCA and PLB retained their functions, and these samples should provide reliable information of the conformational rearrangement induced by phosphorylation of S16 by PKA.

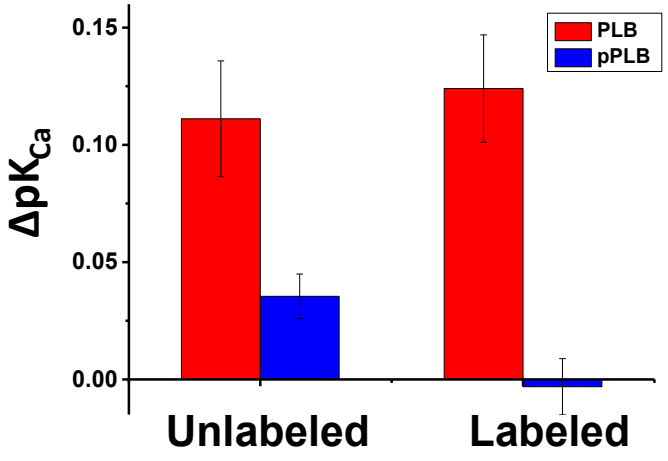

Figure 20: Functional effect of PLB phosphorylation (as measured by ΔpK_{Ca}) is not affected by FRET labeling of SERCA and PLB. The molar ratio of Lipid:PLB:SERCA is 700:5:1. n ≥ 3.

TR-FRET within the SERCA-PLB complex.

Time-resolved fluorescence of donor-labeled PLB was measured in the presence of either unlabeled or acceptor-labeled SERCA with a PLB to SERCA molar ratio of 0.2. The fluorescence waveforms were then fitted by the equations described in Materials and Methods. TR-FRET data was fitted to two Gaussian distance distributions [84], assuming that PLB and pPLB populate the same two structural states (Figure S24 and Figure S25). The shorter distance, r_R, is 3.52 ± 0.42 nm and the longer distance, r_T, is 8.27 ± 0.27 nm (Figure 21A&B). The distance between the labeling sites predicted by the SERCA-PLB model is 2.69 nm (Figure 19A right) [65]. Crosslinking showed previously that K3 of PLB was within 1.5 nm of SERCA K400 [54]. The distance between C674 and K400 predicted by a crystal structure in the absence of Ca is 3.48 nm (3B9R) [20], consistent with our measurement for r_R. The fraction of pPLB that binds to SERCA (x_{DA}) decreased significantly from that of PLB, from 0.99 ± 0.01 to 0.50 ± 0.06 (Figure 21C), indicating that the SERCA-PLB complex partially dissociates after PLB phosphorylation. Within the bound population, the fraction of the *R* state, x_R, is substantially increased after PLB

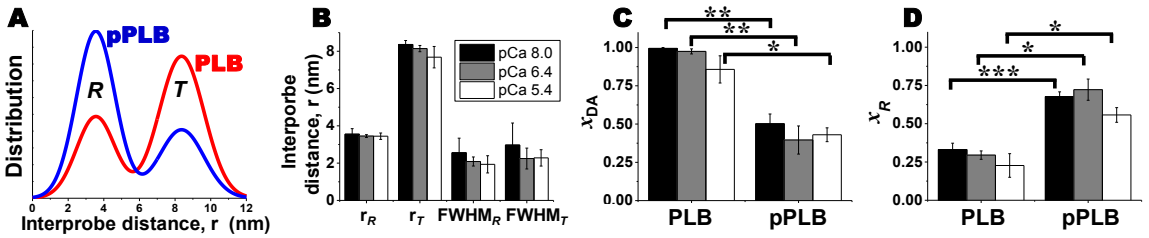

Figure 21: TR-FRET shows that phosphorylation of PLB partially dissociates the SERCA-PLB complex and shifts the population to the shorter distance distribution. A: Two Gaussian distance distributions (two structural states of SERCA-PLB, *R* and *T*) were needed to fit the TR-FRET data. Red: PLB. Blue: pPLB. B: Centers (r) and widths (FWHM) of distance distributions. C: Compared to PLB, phosphorylated PLB decreased the mole fraction of SERCA-bound PLB (x_{DA}), but did not abolish it. D: The mole fraction of the short distance component (x_R) increased after phosphorylation. SERCA: PLB = 5. Lipid : SERCA = 200. n ≥ 3. * p<0.05, ** p<0.01, ***p<0.001.

phosphorylation, from 0.33 ± 0.04 to 0.68 ± 0.04 (Figure 21A&C), indicating a substantial shift of the *T/R* equilibrium toward the *R* state.

Interprobe distances were measured at three Ca^{2+} concentrations, and no significant effects of Ca^{2+} were observed in binding or structure (Figure 21, Table S4). These results show clearly that PLB remains bound to SERCA after the E2 (Ca-free) to E1 (Ca-bound) transition. This result is consistent with previous FRET findings that the SERCA-PLB complex does not dissociate at physiological Ca^{2+} concentrations [85,86].

4.5 Discussion

We have performed TR-FRET on fluorophore-labeled SERCA and PLB co-reconstituted into lipid vesicles, to probe the structural mechanism for relief of inhibition by PLB phosphorylation and by micromolar Ca^{2+}. The functions of the proteins were preserved after covalent modification with fluorophores (Figure 20). TR-FRET analysis showed that phosphorylation of PLB partially dissociates the SERCA-PLB complex and shifts the SERCA-bound PLB toward the less inhibitory *R* state. Ca^{2+} does not dissociate the complex or perturb the *T/R* equilibrium (Figure 21).

The mechanism of relief of inhibition due to PLB phosphorylation has been controversial. Phosphorylation of PLB has been found to perturb the physical interaction between SERCA and PLB, as detected by decreases in crosslinking [74] and co-immunoprecipitation [75]. One study in living cells, using fluorescent fusion proteins, reported that phosphomimetic PLB mutations decreased FRET between SERCA and PLB [179], while another study reported increased FRET upon PLB phosphorylation [172]. Due to the steady-state nature of these FRET measurements, it is not clear whether

changes in FRET were due to changes in SERCA-PLB association or to changes in the donor-acceptor distance within the complex. In the present study, this ambiguity was removed by the detection of time-resolved fluorescence, which simultaneously and independently resolves changes in binding and structure [84]. TR-FRET showed that 40-50% of PLB remains bound to SERCA after phosphorylation (Figure 21C), even though phosphorylation completely relieves SERCA inhibition (Figure 20). Therefore, the activity of the SERCA-pPLB complex is comparable to that of SERCA alone, and the relief of inhibition in the bound complex must be due to a structural change within the SERCA-pPLB complex.

To assess the physiological significance of the two observed effects – dissociation and structural change, it is important to compare the composition of our reconstituted samples with those in cardiac SR. In the present study with a fluorescent donor on PLB, acceptor-labeled SERCA was in 5-fold excess over PLB, to maximize the precision of FRET measurements. However, in cardiac SR, as in our functional measurements (Figure 20), PLB is in large excess (3-5 fold) over SERCA [26]. Based on the affinity of SERCA for pPLB indicated from Figure 21, and on the known concentrations of SERCA and PLB in cardiac SR [26,180], 76 ± 2% of SERCA in cardiac SR contains bound pPLB, even after complete phosphorylation of PLB (Table S5). This is consistent with EPR and NMR findings that pPLB remains bound to SERCA [80,171], with allosteric relief of inhibition achieved by shifting the *T/R* equilibrium toward the *R* state [80,83]. The present study clearly supports this "subunit" model for SERCA regulation (Figure 22, left) over the dissociation model.

Although both dissociation and subunit models have been proposed to explain the mechanism of relief of inhibition by micromolar Ca^{2+} [72,73,76,85,86], our TR-FRET data showed no Ca-dependent changes in either binding or structure (Figure 21B, C, D), clearly ruling out the dissociation model, but also showing clearly that Ca^{2+} relieves SERCA-PLB inhibition by a different mechanism from that of phosphorylation. This result is consistent with previous steady-state FRET studies showing little or no dissociation of PLB from SERCA due to Ca^{2+} [85,86]. Ca^{2+} is known to induce structural changes in its activation of SERCA [181,182], but these changes apparently do not perturb the distance between our labeling sites in the cytoplasmic domains of SERCA and PLB. This conclusion is consistent with structural models, since the distance between SERCA C674 (our acceptor labeling site) and K400 (proposed to lie in the binding groove of the PLB cytoplasmic domain, where our donor is located), changes only from 3.48 nm in the Ca-free crystal structure to 3.41 nm in the Ca-bound structure [16,20]. Since SERCA inhibition by PLB is caused by interaction of the transmembrane domains of the two proteins [60], we propose that Ca-induced structural changes in the SERCA transmembrane domain disrupt this inhibitory interaction, without changing interactions of the cytoplasmic domains, and without producing a substantial decrease in SERCA-PLB affinity (Figure 22, right). This rearrangement of transmembrane helices would explain the Ca-induced decrease in crosslinking between the transmembrane domains of SERCA and PLB [72,73,76].

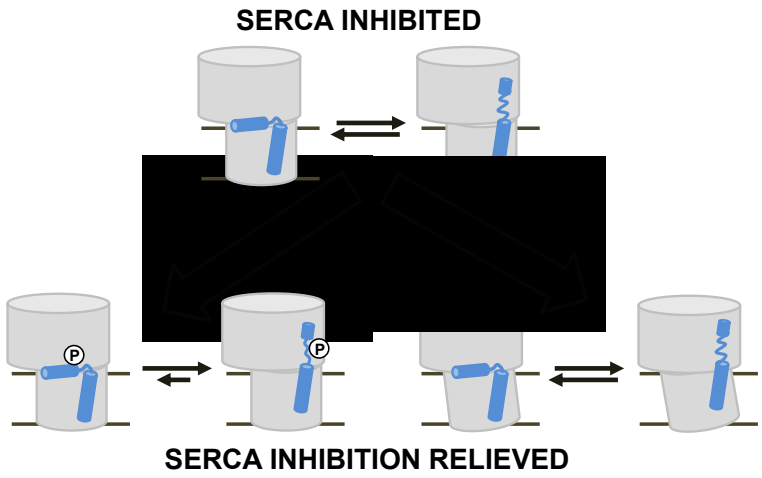

Figure 22: Two mechanisms to relieve SERCA inhibition by PLB in cardiac SR. Phosphorylation shifts the PLB cytoplasmic domain toward the dynamically disordered *R* state. Micromolar Ca^{2+} induces a structural change in the SERCA transmembrane domain.

In summary, we conclude that phosphorylation of PLB and Ca^{2+} relieve SERCA inhibition through different mechanisms (Figure 22), neither of which relies primarily on dissociation of the SERCA-PLB complex. PLB phosphorylation acts by promoting the dynamic disorder of the PLB cytoplasmic domain, while Ca^{2+} acts by changing the structure of the transmembrane domain of SERCA. Both mechanisms must disrupt the inhibitory interactions between the two transmembrane domains, by distinct mechanisms that remain to be elucidated (Figure 22).

4.6 Supplementary Materials

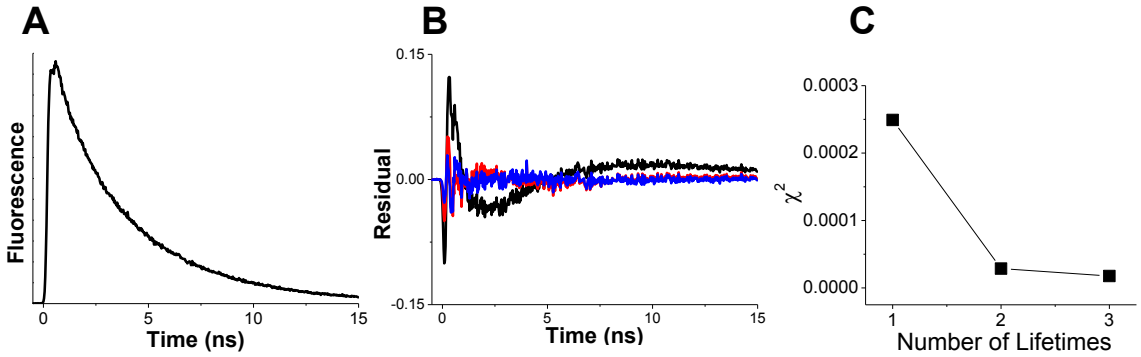

Figure S23: Two lifetimes are sufficient to fit the time-resolved fluorescence data. Both residual and χ^2 values decreased significantly from 1 lifetime to 2 lifetimes, but did not improve appreciably with a third lifetime. A Time-resolved fluorescence waveform of a donor only sample. B Residual plots of 1 lifetime (black), 2 lifetimes (red), and three lifetimes (blue). C χ^2 values with 1, 2, or 3 lifetimes.

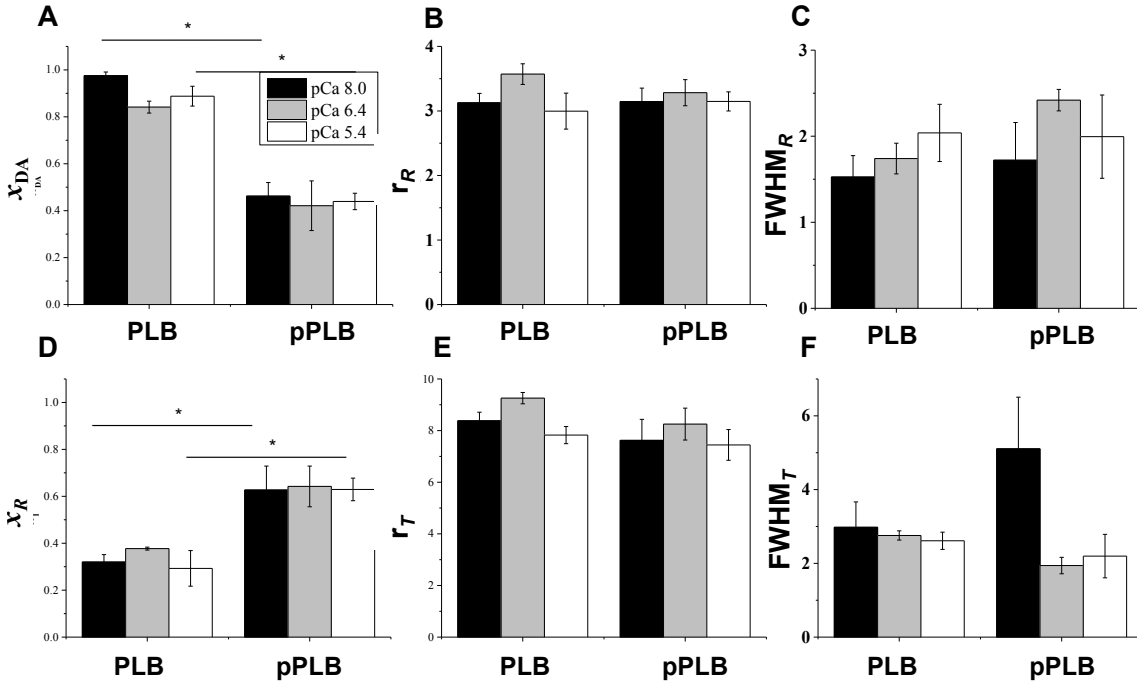

Figure S24: Results from independent fits, assuming that PLB and pPLB populate different structural states, each characterized by a 2-Gaussian interprobe distance distribution (Equation 25, illustrated in Figure 19C). Phosphorylation (A) partially dissociates the complex (deceases x_{DA}, defined in Equation 23), and (D) increases the population of the *R* state within the complex (increases x_R). The centers (r_R and r_T) and widths ($FWHM_R$ and $FWHM_T$) resolved from independent fits are similar in the presence and absence of phosphorylation. This observation justifies the global fits in Figure 21, where we assumed that PLB and pPLB populate the same *R* (r_R and $FWHM_R$) and *T* (r_T and $FWHM_T$) states. $*p < 0.05$.

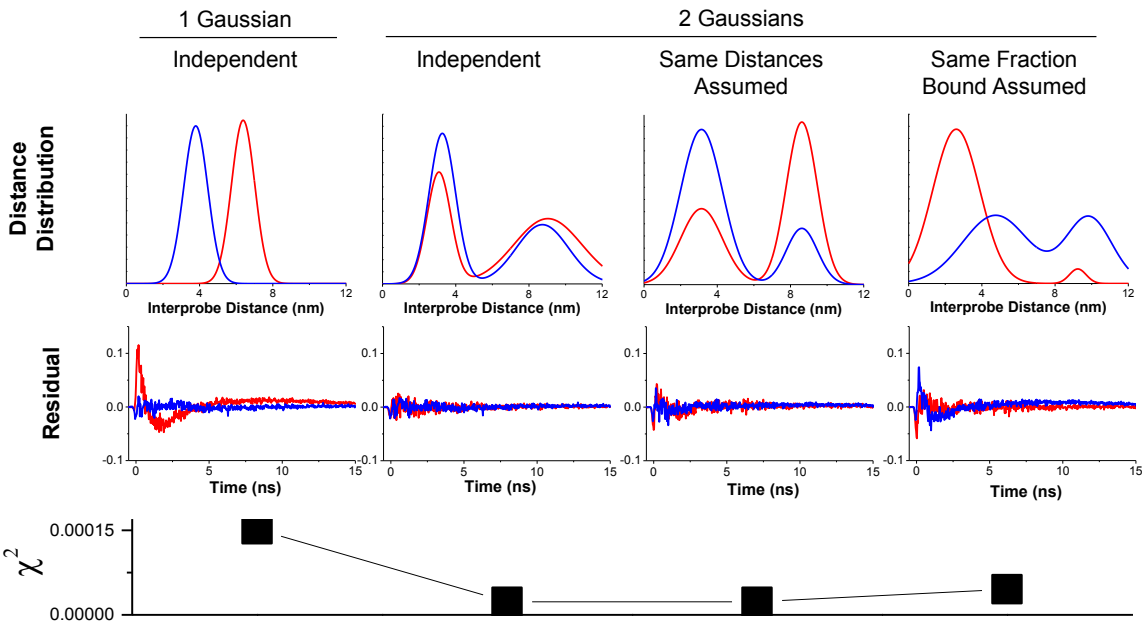

Figure S25: Comparisons among different fitting models, for PLB (red) and pPLB (blue). The residual and χ^2 values are greatly improved from 1 Gaussian to 2 (Equation 24 & Equation 25). With the same distances assumed (The same two structural states are present for PLB and pPLB, only the mole fractions change.), the χ^2 value did not change compared to that of the independent 2-Gaussian fitting (Figure S24). However, when we forced the fraction bound (x_{DA}) to be the same, the residual and χ^2 value worsened appreciably. Therefore, we reported the results of 2 Gaussian fitting with same distances assumed in Figure 21.

Table S4 Interprobe distances.

		x_{DA}	x_T	r_T (nm)	$FWHM_T$ (nm)	x_R	r_R (nm)	$FWHM_R$ (nm)
pCa 8.0	PLB	1.00 ± 0.01 **	0.67 ± 0.04 ***	8.37 ± 0.21	2.97 ± 1.18	0.33 ± 0.04	3.55 ± 0.30	2.56 ± 0.78
	pPLB	0.50 ± 0.06	0.32 ± 0.03			0.68 ± 0.03		
pCa 6.4	PLB	0.97 ± 0.02 **	0.71 ± 0.03 *	8.14 ± 0.17	2.25 ± 0.56	0.29 ± 0.03	3.45 ± 0.08	2.09 ± 0.24
	pPLB	0.40 ± 0.09	0.28 ± 0.07			0.72 ± 0.07		
pCa 5.4	PLB	0.86 ± 0.09 *	0.77 ± 0.08 *	7.68 ± 0.57	2.28 ± 0.44	0.23 ± 0.08	3.44 ± 0.17	1.94 ± 0.46
	pPLB	0.43 ± 0.05	0.44 ± 0.05			0.56 ± 0.05		

* p <0.05, ** p < 0.01, *** p < 0.001 compared to pPLB at the same Ca^{2+} concentration. Assumed that PLB and pPLB populate the same R (r_R and $FWHM_R$) and T (r_T and $FWHM_T$) states.

Table S5 Mole fraction of SERCA containing bound pPLB, x_B

Samples	$[SERCA]_t$	$[pPLB]_t$	x_B
TR-FRET	5	1	0.09 ± 0.01
Activity Assay	1.4	7	0.53 ± 0.03
Cardiac SR	6.5	22.7	0.76 ± 0.02

PLB was assumed to be completely phosphorylated. $[SERCA]_t$ and $[pPLB]_t$ are the total concentrations, expressed in molecules per 1000 lipids. For the TR-FRET samples, x_B = 0.09 was calculated from x_{DA}, the fraction of donor-labeled pPLB molecules containing bound SERCA (Figure 21C), using $x_B = x_{DA}[pPLB]_t / [SERCA]_t$. (No statistically significant difference was found as a function of pCa, so we used the average value of x_{DA} = 0.45 ± 0.04 for pPLB in Figure 21C). The concentrations of total SERCA ($[SERCA]_t$) and total pPLB ($[pPLB]_t$) are either controlled in the samples for TR-FRET and activity assays, or estimated from reported values in cardiac SR [26,183]. SERCA-SERCA and PLB-PLB interactions are neglected, since they are much weaker than SERCA-PLB interactions [36]. The SERCA and pPLB binding affinities are assumed to be the same under the three conditions. K_d is calculated to be 6.0 ± 0.8 per 1000 lipids, using the parameters resolved from TR-FRET data and the equation

$$K_d = \frac{[SERCA][pPLB]}{[SERCA\text{-}pPLB]}$$

The fractions of pPLB-bound SERCA in the activity assay and in cardiac SR are estimated using the following equations:

$$[SERCA\text{-}pPLB] = \frac{([SERCA]_t + [pPLB]_t + K_d) - \sqrt{([SERCA]_t + [pPLB]_t + K_d)^2 - 4[SERCA]_t[pPLB]_t}}{2}$$

$$x_B = \frac{[SERCA\text{-}pPLB]}{[SERCA]_t}$$

Chapter 5 Distinct Functional Effects of Phospholamban Phosphorylation States

Naa-Adjeley D. Ablorh, Xiaoqiong Dong, Zachary M. James, David D. Thomas, and Christine B. Karim

Department of Biochemistry, Molecular Biology and Biophysics, University of Minnesota, Minneapolis, Minnesota 55455

Submitted to *Journal of Biological Chemistry*

Xiaoqiong Dong performed the activity assays. Naa-Adjeley D. Ablorh did the western blot and wrote the manuscript. Zachary M. James purified SERCA. David D. Thomas contributed ideas to the project and edited the manuscript. Christine B. Karim synthesized PLB, helped design the experiments, and edited the manuscript.

5.1 Chapter Overview

We have studied the differential effects of phospholamban (PLB) phosphorylation states on the activity of the sarcoplasmic reticulum (SR) Ca-ATPase (SERCA). It has been shown that unphosphorylated PLB (UPLB) inhibits SERCA and that phosphorylation of PLB at S16 or T17 relieves this inhibition in cardiac SR. However, the levels of the four phosphorylation states of PLB (UPLB, singly phosphorylated P16-PLB and P17-PLB, and doubly phosphorylated 2P-PLB) have not been measured quantitatively in cardiac SR, nor have their functional effects on SERCA been determined directly. Therefore, we

synthesized all four PLB species and used them as standards to establish a quantitative immunoblot assay. This assay was used to determine the mole fractions of all four PLB phosphorylation states in pig cardiac SR. To determine directly the functional effects of each PLB species, we co-reconstituted each of the synthetic peptides in phospholipid vesicles with SERCA1a, and measured the Ca^{2+} dependence of SERCA activity. SERCA inhibition, measured as the decrease in apparent Ca^{2+} affinity, was maximally relieved by P16-PLB, followed by 2P-PLB, followed by P17-PLB. Thus, phosphorylation at T17 showed the least capacity to relieve SERCA inhibition, and actually decreased the effect of phosphorylation at P16 on the same PLB. These results show that each PLB phosphorylation state uniquely alters Ca^{2+} homeostasis, with important implications for cardiac health, disease and treatment.

5.2 Introduction

The role of PLB and PLB phosphorylation in cardiac calcium homeostasis - During cardiac relaxation, the sarcoplasmic reticulum calcium ATPase (SERCA) actively transports calcium into the SR. The resulting electrochemical gradient supplies most of the driving force for passive Ca^{2+} efflux into the cytosol during contraction [1]. In cardiac sarcoplasmic reticulum (CSR), SERCA forms a complex with its inhibitor, phospholamban (PLB) [1,67,137,184]. It has been shown that an increase in the ratio of unphosphorylated phospholamban (UPLB) to SERCA, by overexpression of PLB or decreased phosphorylation, decreases the apparent Ca^{2+} affinity (pK_{Ca}) of SERCA and leads to contractile dysfunction [185,186]. Phosphorylation at S16 and/or T17 [47,187] partially reverses this inhibition by increasing the apparent Ca^{2+} affinity of SERCA

[185,188,189]. Spectroscopic studies show that PLB phosphorylation induces structural rearrangement within the PLB/SERCA complex without changing the affinity of SERCA for PLB, which is essentially a subunit of SERCA under physiological conditions [171,190]. Having ruled out a dissociative mechanism for relieving SERCA inhibition, PLB phosphorylation emerges as the molecular switch that regulates SERCA activity [83]. However, this is a complex switch, because there are four distinct PLB phosphorylation states: UPLB (no phosphorylation, favored by protein phosphatase-1, PP1 [191,192,193]), P16-PLB (phosphorylation at Ser16 by protein kinase A [194]), P17-PLB (phosphorylation at Thr17 by CaMKII), and 2P-PLB (phosphorylation at both Ser16 and Thr17). Their regulation of SERCA depends on two factors: (a) the concentration of each state (b) the potency of each as a SERCA-bound inhibitor, ΔpK_{Ca}.

Quantitation of the four PLB phosphorylation states – It has been proposed that the concentration of each PLB phosphorylation state differs with the etiology of heart disease. Qualitative western blots have suggested that P16-PLB and P17-PLB concentration decrease in dilated cardiomyopathy [195] and that P17-PLB concentration increases in ischemia [196] and acidosis [197]. 2P-PLB has not been measured. Moreover, these trends can vary with age [198] and gender [199]. A complete phosphorylation profile for each age group, gender, and etiology of heart failure could guide rational design of disease-specific phosphomimetic mutants [172], targeted toward the proper PLB phosphorylation state. Such a phosphorylation profile can also evaluate PP1, CaMKII, and PKA as targets for small molecules [200,201]. Assessing the role of PLB phosphorylation states in cardiac pathology and treatment will require quantitation of their concentrations. Quantitation of PLB phosphorylation states has been hindered by

the availability of appropriate antibodies. Antibodies to 2P-PLB have become available only recently, and none of the PLB antibodies that are selective for other phosphorylation states are completely specific [202]. Thus, quantitation of PLB phosphorylation states has not been accomplished.

The functional effects of PLB phosphorylation states – The inhibitory potency of each phosphorylation state determines its functional effect at a given concentration. Previously, PP1, PKA, and CaMKII have been used in efforts to phosphorylate PLB selectively at S16 or P17, but complete and exclusive phosphorylation at one site was never achieved, so the only clear conclusion was that both P16-PLB and P17-PLB show decreased SERCA inhibition [47,203,204,205,206,207,208,209]. The effect of double phosphorylation (2P-PLB) is controversial. In one study, addition of a second phosphate increased the pK_{Ca} [210], while in two other studies, it had no effect [47,211]. Thus the inhibitory potencies of the four PLB phosphorylation states are yet to be determined.

The present study - In the present study, we have used solid-phase peptide synthesis to produce pure samples of each of the four PLB phosphorylation states, allowing the accurate quantitation of both the concentration and potency of each PLB phosphorylation state. To measure concentrations, the four synthetic peptides were used as standards to quantify antibody selectivity, enabling the accurate determination of all four species by immunoblot, despite the imperfect specificities of the four antibodies. To measure the potency of each PLB phosphorylation state, pK_{Ca} was measured after each of the four synthetic peptides was co-reconstituted with SERCA, guaranteeing complete, exclusive, and site-specific phosphorylation, as well as identical PLB/SERCA stoichiometry.

5.3 Experimental Procedures

Synthesis of the four phosphorylation states of PLB – The sequences of human UPLB, P16-PLB, P17-PLB, and 2P-PLB were prepared using Fmoc solid-phase peptide synthesis with or without incorporation of phosphorylated amino acids at specific sites [78,83]. Phosphorylation was accomplished by incorporation of Fmoc-Ser(PO(OBzl)OH)-OH for P16-PLB and Fmoc-Thr(PO(OBzl)OH)-OH for P17-PLB during peptide synthesis. 2P-PLB was prepared by incorporation of both phosphorylated amino acids at position S16 and T17 [78,83]. UPLB was prepared without incorporation of phosphorylated amino acids. Phospholamban was characterized by amino acid analysis and mass spectrometry [78].

SERCA1a was purified from rabbit skeletal muscle using reactive red in 0.1% octaethylene glycol monododecyl ether (C12E8) as previously described [85,174]. And the concentration was measured with the Pierce BCA assay [78,83].

Electrophoresis and immunoblot-Samples were dissolved in Laemmli buffer (Biorad) with 5% β-mercaptoethanol (BME), loaded onto a 10-20% Tris-Tricine gel (Biorad), and separated by SDS-PAGE at constant voltage (120V) at 25 ^{o}C for 90 minutes. Proteins were then transferred to 0.45 micron Immobilon-FL PVDF membranes (Millipore) in Towbin transfer buffer [212] for 50 minutes at constant current (300mA), blocked overnight in pure Odyssey blocking buffer (LI-COR Biosciences), and rinsed for 1 minute in ddH_2O. Each membrane was incubated with one primary antibody (Ab) per the manufacturer's instructions, washed 3 times for 15 minutes with TBST (Tris-buffered saline with 0.1% tween) and then incubated with a second primary antibody per the manufacturer's instructions, and washed 3 times for 15 minutes with TBST before

simultaneously adding two secondary antibodies LI-COR IR-680LT and LI-COR 800CW, directed against the appropriate animal, each at a dilution of 1:15,000 for 25 minutes. The membrane was then washed 3 times for 15 minutes with TBST, and the blots were stored in TBS (Tris-buffered saline). Proteins were detected and analyzed using the LI-COR Odyssey. The 700nm channel detected the IR-680LT and the IR-680RD. The 800nm channel detected the IR-800CW (LI-COR Biosciences). All incubation buffers consisted of 50% Odyssey blocking buffer (LI-COR Biosciences) and 50% TBS containing 0.1% Tween 20 (TBST) except the incubation of the antibody for 2P-PLB. This was incubated in 5% w/v BSA, 1X TBS, 0.1% Tween-20 at 4°C, per the manufacturer's instructions. Analysis by densitometry was accomplished with Odyssey software. The resolution was 169 μm and the focus offset was 0.0 mm. Boxes were drawn around an area that encompassed all PLB bands (monomeric and oligomeric). The background was local, determined as the average or median of the intensities at the top and the bottom of the box. The greatest linearity was obtained at a border width of 1 pixel.

Table 6. Primary antibodies. Indices (i) and (j) correspond to antibodies and PLB species, respectively in Equation 26.

Antibody	Epitope	Ab abbrev (i)	PLB selectivity (j)	reactivity	dilution	company
2D12	1-52	AbU (1)	UPLB (1)	Mouse	1:6000	Abcam
Ab12963	11-21	Ab16 (2)	P16-PLB and 2P-PLB (2)	Goat	1:1000	Santa Cruz Biotechnology
Ab17024-R	12-22	Ab17 (3)	P17-PLB and 2P-PLB (3)	Rabbit	1:1000	Santa Cruz Biotechnology
Ab8496	unknown	Ab2P (4)	2P-PLB (4)	Rabbit	1:2000	Cell Signaling Technology

**Cell Signaling Technology reports that the Ab8496 epitope has 100% sequence homology with pig and human, thus excluding E2D and K27N.*

Quantification of four phosphorylation states of PLB - Quantitation of the four phosphorylation states of PLB in pig cardiac SR was accomplished by an extension of our

previous method for quantitation of two states [202], using the antibodies given in Table 6**.** Antibodies entirely specific for each of these four species are not available, so it is necessary to start with four antibodies having partial selectivity, determine this selectivity quantitatively using purified synthetic standards, run the unknown on the same four blots, and then solve a system of four equations with four unknowns to determine the composition of the unknown sample (Equation 26):

$$I_i = \Sigma \varepsilon_{ij} c_j \text{ , I = 1, …4; j = 1, …4,} \qquad \textbf{Equation 26}$$

i refers to the primary antibody, and *j* refers to the phosphorylation state of the standard, as defined in Table 6. Thus ε_{ij} is the slope of the standard curve from phosphorylation state *j* (obtained using purified synthetic standards) from a blot using primary antibody *i*, and c_j is the concentration of the phosphorylation state *j* of PLB in the sample. The result is a 4x4 matrix of simultaneous equations, which was solved in MATLAB, to determine the unknown concentration c_j. The mole fraction of each PLB phosphorylation state (X_j) was calculated from

$$X_j = c_j/\Sigma c_j \text{ (j = 1, …4),} \qquad \textbf{Equation 27}$$

To validate the method, it was applied to mixtures of synthetic standards containing known concentrations of each phosphorylation state (Table 7). The PLB primary antibodies were all based on epitopes that exclude residues 2 and 27 (the only differences between human and pig sequences), so the method is equally valid for analysis of both species. Secondary antibodies Ab800CW (goat-anti mouse), Ab800CW (donkey-anti goat), and Ab680LT (goat anti-rabbit), were obtained from Li-COR Biosciences. Quantitation of SERCA was accomplished by SDS-page, stained with coomassie brilliant blue, using purified SERCA1a.

Table 7. Known Xj values (Equation 27) in mixtures of PLB standards

Mixture	U	P16	P17	2P	n
a	0.25	0.25	0.25	0.25	6
b	0.10	0.20	0.30	0.40	6
c	0.20	0.30	0.40	0.10	6
d	0.30	0.40	0.10	0.20	6
e	0.40	0.10	0.20	0.30	6

ATPase assay-Ca-ATPase activity was performed after reconstitution of SERCA with each of the four synthetic PLB standards [60,78,83,213,214]. PLB and SERCA were reconstituted in dioleoyl-phosphatidylcholine (DOPC) and dioleoyl-phosphatidylethanolamine (DOPE), at a molar ratio of 4:1 as previously described [148], at a molar ratio of PLB/SERCA/lipid of 5/1/700. Ca-ATPase activity was measured as a function of $[Ca^{2+}]$ using an NADH-coupled, enzyme-linked ATPase assay [84,85] at a temperature of 25^{o}C. The data were fitted by the Hill equation:

$$V = V_{max}/[1+ 10^{-n\,(pKCa\,-\,pCa)}] \qquad \textbf{Equation 28}$$

V_{max} is the maximum ATPase rate; pK_{Ca} is the apparent Ca affinity; and n is the Hill coefficient. Inhibitory potency of each PLB species is defined as ΔpK_{Ca}, the decrease in pK_{Ca} compared with that measured with SERCA in the absence of PLB.

Statistical analysis - For validation of the method, the accuracies of X_{PLB} values, performed on known mixtures of standards, were calculated as ΔX_{PLB}, which is equal to ΔX_{PLB}(apparent) - ΔX_{PLB}. Precision is expressed as SEM. X_{PLB} in pig CSR and pK_{Ca} in the co-reconstitutions were compared using one-way analysis of variance (ANOVA). A p-value of less than 0.05 was considered significant.

5.4 Results

Validation of immunoblot method – The assay was applied to five mixtures of synthetic standards containing known concentrations of each of the four PLB phosphorylation states (Table 7). Four identical gels, with the same concentrations of each pure synthetic PLB standard and equal volumes of the same five mixtures (Table 7) were run and blotted with four different antibodies. The mixtures were run in duplicate.

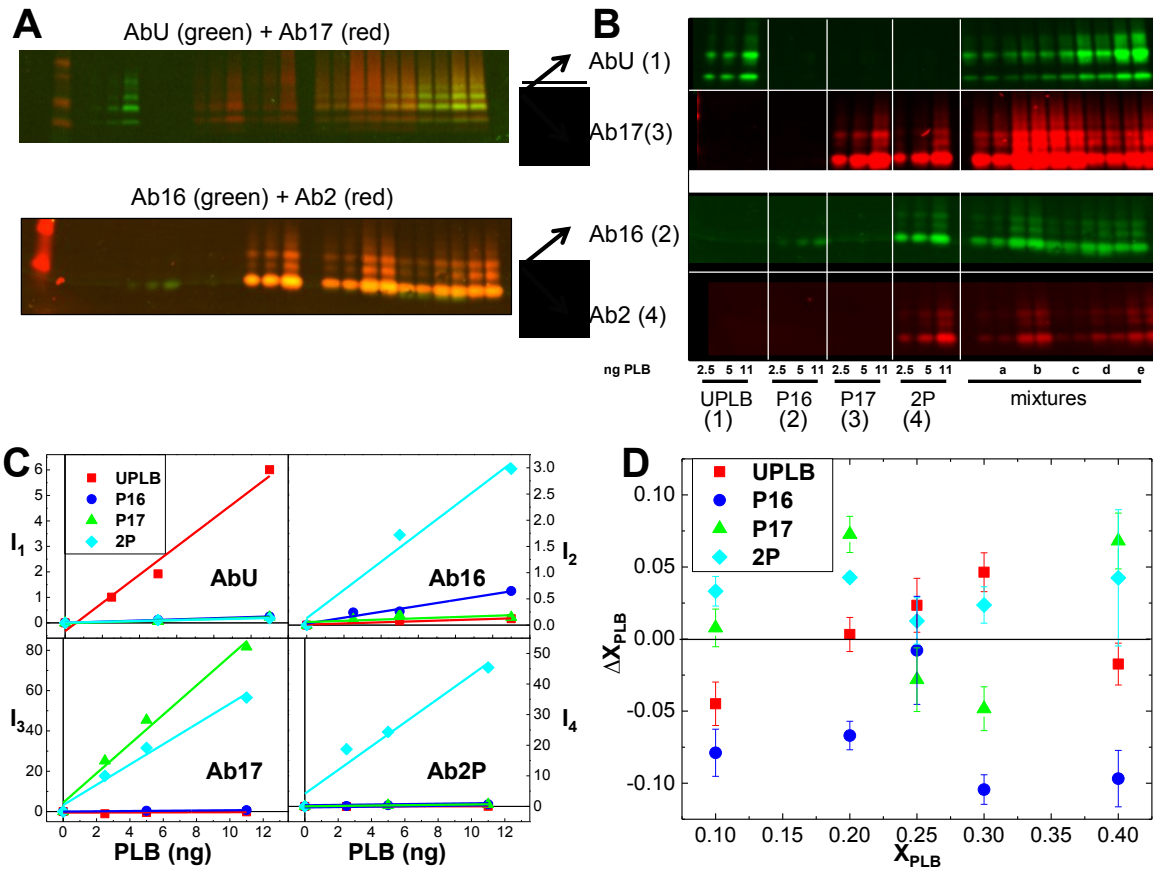

Figure 26. Validation of the method for calculating mole fractions (X_{PLB}, Equation 27) of all four PLB phosphorylation states. (A) Immunoblots stained with two primary antibodies. (B) Individual images from A. Numbers in parentheses indicate *i* and *j* values in Equation 26 and Table 6. (C) Standard curves produced from intensity values I_i (i indicates the antibody as in B), obtained from densitometry of standards in B. Slopes are the ε_{ij} values in Equation 26. (D) The error ΔX_{PLB}, obtained from mixtures (Table 7), plotted against the actual X_{PLB} for all four PLB phosphorylation states.

The use of fluorescent secondary antibodies made it possible to visualize two blots on the same membrane (Figure 26A), provided that the primary antibodies were produced in different animals. For the top blot in Figure 26A, mouse primary antibody (AbU) was paired with rabbit primary antibody (Ab17). For the bottom blot in Figure 26A, goat primary antibody (Ab16) was paired with rabbit primary antibody (Ab2P). Visualizing two different epitopes on one membrane required that the secondary antibodies emitted at resolved wavelengths. LI-COR800CW is conjugated to a dye detected at 800 nm, using a green pseudo-color for display. By contrast, LI-COR680LT is conjugated to a dye detected at 680 nm, using a red pseudo-color for display. In Figure 26A (top), the green signal corresponds to goat-anti-mouse-LI-COR-800CW secondary antibody bound to primary mouse antibody AbU, and the red signal corresponds to goat-anti-rabbit-LI-COR-680LT secondary antibody bound to primary rabbit antibody Ab17. In Figure 26A (bottom), the green signal corresponds to donkey-anti-goat-LI-COR-800CW secondary antibody bound to primary goat antibody Ab16, and the red signal corresponds to goat-anti-rabbit-LI-COR-680LT secondary antibody bound to primary rabbit antibody Ab2P. Figure 26B shows the red and green signals resolved in separate images.

Figure 26C shows standard curves obtained from the 2.5, 5, and 11 ng PLB standards in Figure 26B. In C, "I_i" indicates the primary antibody that was used to stain the corresponding blot in B (see Table 6), and the slopes of these standard curves are the ε_{ij} values in Table 6 and Equation 26. All slopes had a Pearson's r value of ≥ 0.95. These ε_{ij} values were used to calculate the mole fraction of each species in the five mixtures, and the results are compared with the known values, in Figure 26D and Table 8. ΔX_{PLB} is the difference between the measured and known mole fractions in the PLB mixtures. The

results show that the assay is remarkably accurate, with all 20 measurements coming within 0.1 of the correct value.

Table 8. ΔX_{PLB} values in mixtures of PLB standards, mean ± SEM (Figure 26D)

	UPLB	P16-PLB	P17-PLB	2P-PLB	n
a	0.02 ± 0.02	-0.01 ± 0.04	-0.03 ± 0.02	0.01 ± 0.02	6
b	-0.05 ± 0.02	-0.08 ± 0.02	0.01 ± 0.01	0.03 ± 0.01	6
c	0.00 ± 0.01	-0.07 ± 0.01	0.07 ± 0.01	0.04 ± 0.10	6
d	0.05 ± 0.01	-0.10 ± 0.01	-0.05 ± 0.00	0.02 ± 0.01	6
e	-0.02 ± 0.01	-0.10 ± 0.02	0.07 ± 0.02	0.04 ± 0.05	6

Application to Cardiac SR−The mole fractions (X_{PLB}), of all four phosphorylation states of PLB were measured in cardiac sarcoplasmic reticulum prepared from six pig hearts, using the method described in Figure 26. The greatest mole fraction was observed for P16-PLB (X_{P16} = 0.45 ± 0.008), followed by UPLB (X_{UPLB} = 0.35 ± 0.008), then the doubly phosphorylated 2P-PLB (X_{2P} = 0.12 ± 0.006); P17-PLB had the lowest concentration in CSR (X_{P17} = 0.08 ± 0.007) (Figure 27, right). ANOVA showed significant differences among all the mole fractions of PLB phosphorylation states. In summary, all four states are significantly populated, and the order of mole fractions is P16-PLB > UPLB >> 2P-PLB > P17-PLB.

Effects of specific phosphorylation states of PLB on SERCA activity − Synthetic human UPLB, P16-PLB, P17-PLB, and 2P-PLB were evaluated for their ability to inhibit SERCA (Figure 28). By fitting the data with Equation 28, the inhibition of Ca-ATPase activity was quantified by the decrease in pK_{Ca} (the negative log of the pCa value required for 50% activation) in Figure 28A. Each PLB phosphorylation state displayed a

significantly different value of pK_{Ca}, according to the ANOVA, showing that they are functionally distinct. As expected, UPLB, the constituent inhibitor of SERCA showed the largest decrease in pK_{Ca} compared to SERCA alone. When compared to UPLB + SERCA, P16-PLB had the largest increase in pK_{Ca}, followed by 2P-PLB and lastly, P17-PLB (Figure 28). Thus, the order of SERCA restorative potency of the phosphorylated derivatives of PLB is P16-PLB >> 2P-PLB > PThr17 (Figure 28).

5.5 Discussion

Quantitation of PLB phosphorylation states in cardiac SR− We have extended our previous quantitative immunoblot assays [202], which measured mole fractions of two PLB phosphorylation states, to measure mole fractions of all four PLB phosphorylation states (Figure 26). Our assay allows accurate quantitation even though Ab16 and Ab17 are not completely specific (Figure 26C). The use of the synthetic peptides and two-color immunoblots provides accurate concentrations of all four species in known mixtures

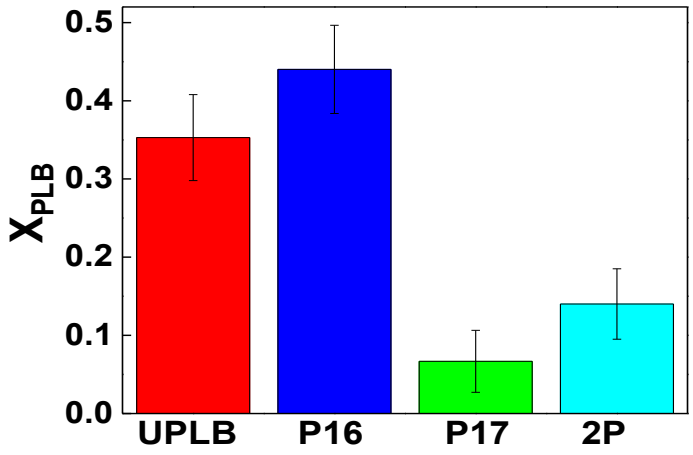

Figure 27. Mole fractions of PLB phosphorylation states in SR isolated from pig hearts. Mean ± SEM, *n* = 6 hearts.

(Figure 26D). We used this assay to determine the unknown concentrations of these phosphorylation states of PLB in pig cardiac SR, showing that all four states are present, with the concentration of P16-PLB comparable to that of UPLB, 4 times that of 2P-PLB, and 6 times that of P17-PLB (Figure 27). In the future, this assay can be used to investigate correlations between the mole fractions of PLB phosphorylation states (Figure 27) and cardiac physiology and pathology, as affected by CaMKII, PKA, and PP1.

Direct measurement of inhibitory potencies of all four PLB phosphorylation states - We have used four phosphorylation state-specific co-reconstitutions of PLB with SERCA to determine the inhibitory potencies of PLB phosphorylation states (Figure 28). Our *in vitro* system has facilitated the simultaneous control of PLB/SERCA stoichiometry and the purity of each PLB phosphorylation state, which is not feasible in cardiac tissue samples (Figure 27)[47]. While our assay utilizes SERCA1a from fast-twitch skeletal muscle, our measured potencies apply as well to the heart, where SERCA2a predominates, since these two isoforms have been shown to have identical regulatory interactions with PLB [215,216].

Each PLB phosphorylation state has a distinct effect on SERCA function (Figure 28, Table 9). These differences are not due to differences in affinity for SERCA, since the

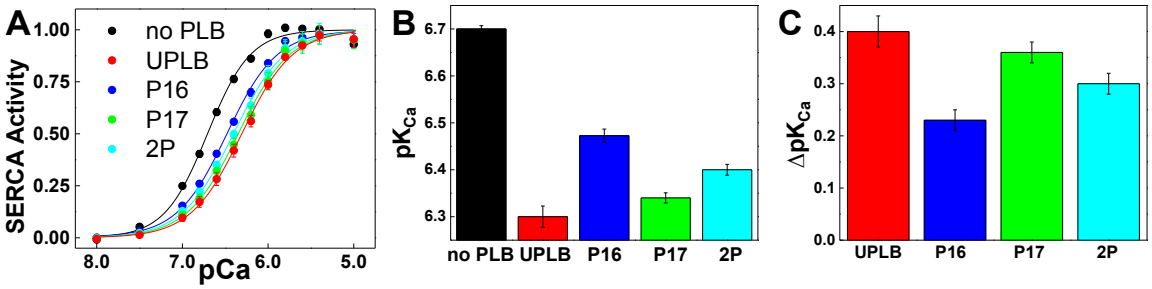

Figure 28. SERCA activity due to PLB phosphorylation states. SERCA (black), UPLB (red), P16-PLB (blue), P17-PLB (green), 2P-PLB (cyan). (A) Ca-ATPase data, showing best fits to Equation 28, with data normalized to the V_{max} value obtained in the fit. (B) pK_{Ca} values from A. (C) ΔpK_{Ca} values, relative to no PLB.

PLB/SERCA ratio of 5/1 used here was previously determined to be saturating, independent of PLB phosphorylation [149,171]. UPLB increased pK_{Ca} by 0.40, corresponding to an increase of K_{Ca} by a factor of 2.5. P16-PLB was the least inhibitory PLB species, increasing pK_{Ca} by only 0.23. Thus phosphorylation at P16 has the greatest effect in relieving SERCA inhibition. Intermediate results were observed for P17-PLB (ΔpK_{Ca} = 0.36) and for 2P-PLB (ΔpK_{Ca} = 0.30) (Figure 28, Table 9), showing that the effects of phosphorylation at the two sites are not additive, since double phosphorylation produces an effect intermediate between the two singly phosphorylated states of S16 phosphorylation when both S16 and T17 are phosphorylated on the same PLB (Figure 28, Table 9).

Implications for cardiac physiology and pathology − An established therapeutic goal in treatment of heart failure is SERCA activation [217]. Therefore, the low inhibitory potency of P16-PLB (Table 9) establishes it (not P17-PLB or P2-PLB) as the best template for loss-of-inhibition PLB mutants in gene therapy [123,149,172,218]. Similarly, these results suggest that activation of PKA should be therapeutically more effective than activation of CaMKII. In fact, elevation of CaMKII activity could reduce the benefits of

Table 9. Effect of PLB on SERCA activity (Figure 28), mean ± SEM.

Sample	K_{Ca} (μM)	pK_{Ca}	ΔpK_{Ca}	n
no PLB	0.20 ± 0.01	6.70 ± 0.01	0	4
UPLB	0.50 ± 0.09	6.30 ± 0.02	0.40 ± 0.03	4
P16-PLB	0.34 ± 0.04	6.47 ± 0.01	0.23 ± 0.02	4
P17-PLB	0.40 ± 0.04	6.34 ± 0.01	0.36 ± 0.02	4
2P-PLB	0.36 ± 0.40	6.40 ± 0.01	0.30 ± 0.02	4

PKA activation, since both P17-PLB and 2P-PLB are more inhibitory than P16-PLB (Table 9). This may explain why the P17-PLB elevation at the onset of ischemia fails to improve SERCA activity and cardiac function [197]. The low inhibitory potency of P17-PLB can also be therapeutically useful. For example, in acidosis and ischemia, where elevated CaMKII leads to arrhythmia, necrosis and apoptosis [197], treatment with small-molecule CaMKII inhibitors [219,220] can occur without appreciable decreases SERCA activity.

Conclusions We have used solid-phase peptide synthesis to produce pure samples of each of the four PLB phosphorylation states, making possible the accurate quantitation of both the concentration and potency of each PLB phosphorylation state. These four states are all present in pig cardiac tissue in different concentrations, and each has a distinct inhibitory effect on SERCA activity. Thus it is now feasible to determine these concentrations in human tissue samples and to relate them quantitatively to cardiac physiology and pathology, providing essential information for future therapeutic developments.

Chapter 6 Summary and Future Directions

6.1 Summary

The structural mechanism of SERCA regulation by PLB remains elusive. Two models have been proposed and each model has been supported with experimental results. The canonical "dissociation" model maintains that inhibition is caused by PLB binding to SERCA. For relief of inhibition to occur, PLB must dissociate from SERCA. The "subunit" model states that PLB acts as a subunit of the SERCA-PLB complex. The inhibitory potency of PLB is determined by its conformation within the complex.

This thesis work helps elucidate the structure-function relationship of the SERCA-PLB complex using TR-FRET. In Chapter 3, we confirmed that the cytoplasmic domain of PLB equilibrates between an ordered ***T*** state and a disordered ***R*** state. By modulating the ***T/R*** equilibrium by electrostatic interactions, we found that the inhibitory potency of PLB is strongly correlated with its structural state, but not with binding. This study clearly supported the subunit model and established that the ***T*** state is more inhibitory, and that the ***R*** state is less inhibitory. In Chapter 4, I studied the SERCA-PLB complex with physiological perturbations: phosphorylation of PLB at Ser16 and micromolar Ca^{2+}. TR-FRET measurements showed that Ser16 phosphorylation relieves inhibition both by dissociating the complex and by shifting the ***T/R*** equilibrium toward the less inhibitory ***R*** state, supporting both the dissociation model and the subunit model. In cardiac SR, the subunit model probably accounts for most of the relief of inhibition induced by phosphorylation. Ca^{2+} relieves inhibition through a different structural mechanism. Ca^{2+} is known to induce a SERCA conformational change but this protein

structural change did not affect the interaction between the cytoplasmic domains of SERCA and PLB. Hence, Ca^{2+} probably relieves inhibition by inducing structural rearrangements in the transmembrane domains of the complex.

PLB can be phosphorylated at two sites, Ser16 and Thr17, generating four phosphorylation states: unphosphorylated, phosphorylated at Ser16, phosphorylated at Thr17, and phosphorylated at both sites. In Chapter 5, using a quantitative western blot method, we found that all of the four phosphorylation states of PLB exist in pig cardiac SR. We also measured the function of SERCA in the presence of different phosphorylation states of synthetic PLB in co-reconstituted system, and found that each PLB species has a distinct inhibitory potency.

6.2 Future Directions

This thesis work helps resolve the seemingly contradictory models used to explain the structural mechanism of SERCA regulation by PLB. Results from Chapter 3 and 4 support the subunit model. However, the structural rearrangement in the transmembrane domain that disrupts the inhibitory interaction between SERCA and PLB remains elusive. Future spectroscopic studies should study the interactions in this critical region by attaching the labels in the transmembrane domain. Smaller probes, such as spin labels used in EPR studies, will be preferred because they have a small propensity for disturbing the function.

It is an interesting finding that different phosphorylation states of PLB have distinct functional effects. The structural aspects of unphosphorylated and Ser16

phosphorylated PLB have been extensively studied, which is not the case for Thr17 phosphorylated and doubly phosphorylated PLB. To discover the structural mechanisms underlying their distinct functions, the dynamics should be studied by EPR, and the specific interaction between SERCA and different phosphorylation states of PLB should be elucidated by time-resolved or single-molecule FRET.

We used a co-reconstituted system because the lipid compositions, protein species and protein concentrations can be accurately controlled. The results we observed in this artificial system will need to be confirmed by experiments done in their native environment. TR-FRET should be applied to SERCA and PLB fused with fluorescent proteins expressed in cardiomyocytes. With electrical pacing and other physiological stimuli, we should be able to study the SERCA-PLB complex in action.

Bibliography

[1] D.M. Bers, Cardiac excitation-contraction coupling, Nature 415 (2002) 198-205.

[2] C.R. Weber, K.S. Ginsburg, D.M. Bers, Cardiac submembrane [Na+] transients sensed by Na+-Ca2+ exchange current, Circ Res 92 (2003) 950-952.

[3] J.W. Bassani, W. Yuan, D.M. Bers, Fractional SR Ca release is regulated by trigger Ca and SR Ca content in cardiac myocytes, Am J Physiol 268 (1995) C1313-1319.

[4] J.W. Bassani, R.A. Bassani, D.M. Bers, Relaxation in rabbit and rat cardiac cells: species-dependent differences in cellular mechanisms, J Physiol 476 (1994) 279-293.

[5] M. Periasamy, A. Kalyanasundaram, SERCA pump isoforms: their role in calcium transport and disease, Muscle Nerve 35 (2007) 430-442.

[6] C.J. Brandl, S. deLeon, D.R. Martin, D.H. MacLennan, Adult forms of the Ca2+ATPase of sarcoplasmic reticulum. Expression in developing skeletal muscle, J Biol Chem 262 (1987) 3768-3774.

[7] C.J. Brandl, N.M. Green, B. Korczak, D.H. MacLennan, Two Ca2+ ATPase genes: homologies and mechanistic implications of deduced amino acid sequences, Cell 44 (1986) 597-607.

[8] D.H. MacLennan, C.J. Brandl, B. Korczak, N.M. Green, Amino-acid sequence of a Ca2+ + Mg2+-dependent ATPase from rabbit muscle sarcoplasmic reticulum, deduced from its complementary DNA sequence, Nature 316 (1985) 696-700.

[9] A. Zarain-Herzberg, D.H. MacLennan, M. Periasamy, Characterization of rabbit cardiac sarco(endo)plasmic reticulum Ca2(+)- ATPase gene, J Biol Chem 265 (1990) 4670-4677.

[10] S.E. Burk, J. Lytton, D.H. MacLennan, G.E. Shull, cDNA cloning, functional expression, and mRNA tissue distribution of a third organellar Ca2+ pump, J Biol Chem 264 (1989) 18561-18568.

[11] F. Wuytack, B. Papp, H. Verboomen, L. Raeymaekers, L. Dode, R. Bobe, J. Enouf, S. Bokkala, K.S. Authi, R. Casteels, A sarco/endoplasmic reticulum Ca(2+)-ATPase 3-type Ca2+ pump is expressed in platelets, in lymphoid cells, and in mast cells, J Biol Chem 269 (1994) 1410-1416.

[12] J. Lytton, M. Westlin, S.E. Burk, G.E. Shull, D.H. MacLennan, Functional comparisons between isoforms of the sarcoplasmic or endoplasmic reticulum family of calcium pumps, J Biol Chem 267 (1992) 14483-14489.

[13] C. Toyoshima, H. Nomura, Structural changes in the calcium pump accompanying the dissociation of calcium, Nature 418 (2002) 605-611.

[14] W. Humphrey, A. Dalke, K. Schulten, VMD: visual molecular dynamics, J Mol Graph 14 (1996) 33-38, 27-38.

[15] C. Toyoshima, M. Nakasako, H. Nomura, H. Ogawa, Crystal structure of the calcium pump of sarcoplasmic reticulum at 2.6 A resolution, Nature 405 (2000) 647-655.

[16] A.M. Jensen, T.L. Sorensen, C. Olesen, J.V. Moller, P. Nissen, Modulatory and catalytic modes of ATP binding by the calcium pump, Embo J 25 (2006) 2305-2314.
[17] C. Toyoshima, T. Mizutani, Crystal structure of the calcium pump with a bound ATP analogue, Nature 430 (2004) 529-535.
[18] C. Olesen, T.L. Sorensen, R.C. Nielsen, J.V. Moller, P. Nissen, Dephosphorylation of the calcium pump coupled to counterion occlusion, Science 306 (2004) 2251-2255.
[19] K. Obara, N. Miyashita, C. Xu, I. Toyoshima, Y. Sugita, G. Inesi, C. Toyoshima, Structural role of countertransport revealed in Ca(2+) pump crystal structure in the absence of Ca(2+), Proc Natl Acad Sci U S A 102 (2005) 14489-14496.
[20] C. Olesen, M. Picard, A.M. Winther, C. Gyrup, J.P. Morth, C. Oxvig, J.V. Moller, P. Nissen, The structural basis of calcium transport by the calcium pump, Nature 450 (2007) 1036-1042.
[21] F. Cornelius, J.V. Moller, Electrogenic pump current of sarcoplasmic reticulum Ca(2+)-ATPase reconstituted at high lipid/protein ratio, FEBS Lett 284 (1991) 46-50.
[22] J.V. Møller, C. Olesen, A.M. Winther, P. Nissen, The sarcoplasmic Ca2+-ATPase: design of a perfect chemi-osmotic pump, Q Rev Biophys 43 (2010) 501-566.
[23] S. Danko, T. Daiho, K. Yamasaki, X. Liu, H. Suzuki, Formation of the stable structural analog of ADP-sensitive phosphoenzyme of Ca2+-ATPase with occluded Ca2+ by beryllium fluoride: structural changes during phosphorylation and isomerization, J Biol Chem 284 (2009) 22722-22735.
[24] F.N. Briggs, K.F. Lee, A.W. Wechsler, L.R. Jones, Phospholamban expressed in slow-twitch and chronically stimulated fast-twitch muscles minimally affects calcium affinity of sarcoplasmic reticulum Ca(2+)-ATPase, J Biol Chem 267 (1992) 26056-26061.
[25] J. Fujii, J. Lytton, M. Tada, D.H. MacLennan, Rabbit cardiac and slow-twitch muscle express the same phospholamban gene, FEBS Lett 227 (1988) 51-55.
[26] D.A. Ferrington, Q. Yao, T.C. Squier, D.J. Bigelow, Comparable levels of Ca-ATPase inhibition by phospholamban in slow- twitch skeletal and cardiac sarcoplasmic reticulum, Biochemistry 41 (2002) 13289-13296.
[27] G. Hasenfuss, Alterations of calcium-regulatory proteins in heart failure, Cardiovasc Res 37 (1998) 279-289.
[28] J. Zamoon, A. Mascioni, D.D. Thomas, G. Veglia, NMR solution structure and topological orientation of monomeric phospholamban in dodecylphosphocholine micelles, Biophys J 85 (2003) 2589-2598.
[29] A.D. Wegener, L.R. Jones, Phosphorylation-induced mobility shift in phospholamban in sodium dodecyl sulfate-polyacrylamide gels. Evidence for a protein structure consisting of multiple identical phosphorylatable subunits, J Biol Chem 259 (1984) 1834-1841.
[30] H.S. Young, L.R. Jones, D.L. Stokes, Locating phospholamban in co-crystals with Ca(2+)-ATPase by cryoelectron microscopy, Biophys J 81 (2001) 884-894.

[31] H.K. Simmerman, Y.M. Kobayashi, J.M. Autry, L.R. Jones, A leucine zipper stabilizes the pentameric membrane domain of phospholamban and forms a coiled-coil pore structure, J Biol Chem 271 (1996) 5941-5946.
[32] D.H. MacLennan, Y. Kimura, T. Toyofuku, Sites of regulatory interaction between calcium ATPases and phospholamban, Ann N Y Acad Sci 853 (1998) 31-42.
[33] D.D. Thomas, L.G. Reddy, C.B. Karim, M. Li, R. Cornea, J.M. Autry, L.R. Jones, J. Stamm, Direct spectroscopic detection of molecular dynamics and interactions of the calcium pump and phospholamban, Ann N Y Acad Sci 853 (1998) 186-194.
[34] L.G. Reddy, L.R. Jones, D.D. Thomas, Depolymerization of phospholamban in the presence of calcium pump: a fluorescence energy transfer study, Biochemistry 38 (1999) 3954-3962.
[35] L.G. Reddy, J.M. Autry, L.R. Jones, D.D. Thomas, Co-reconstitution of phospholamban mutants with the Ca-ATPase reveals dependence of inhibitory function on phospholamban structure, J Biol Chem 274 (1999) 7649-7655.
[36] S.L. Robia, K.S. Campbell, E.M. Kelly, Z. Hou, D.L. Winters, D.D. Thomas, Forster transfer recovery reveals that phospholamban exchanges slowly from pentamers but rapidly from the SERCA regulatory complex, Circ Res 101 (2007) 1123-1129.
[37] J.P. Glaves, C.A. Trieber, D.K. Ceholski, D.L. Stokes, H.S. Young, Phosphorylation and mutation of phospholamban alter physical interactions with the sarcoplasmic reticulum calcium pump, J Mol Biol 405 (2011) 707-723.
[38] R. Aschar-Sobbi, T.L. Emmett, G.J. Kargacin, M.E. Kargacin, Phospholamban phosphorylation increases the passive calcium leak from cardiac sarcoplasmic reticulum, Pflugers Arch 464 (2012) 295-305.
[39] S. Smeazzetto, I. Schroder, G. Thiel, M.R. Moncelli, Phospholamban generates cation selective ion channels, Phys Chem Chem Phys 13 (2011) 12935-12939.
[40] R. Verardi, L. Shi, N.J. Traaseth, N. Walsh, G. Veglia, Structural topology of phospholamban pentamer in lipid bilayers by a hybrid solution and solid-state NMR method, Proc Natl Acad Sci U S A 108 (2011) 9101-9106.
[41] V.V. Vostrikov, K.R. Mote, R. Verardi, G. Veglia, Structural dynamics and topology of phosphorylated phospholamban homopentamer reveal its role in the regulation of calcium transport, Structure 21 (2013) 2119-2130.
[42] A. Mattiazzi, E.G. Kranias, The role of CaMKII regulation of phospholamban activity in heart disease, Front Pharmacol 5 (2014) 5.
[43] W. Luo, I.L. Grupp, J. Harrer, S. Ponniah, G. Grupp, J.J. Duffy, T. Doetschman, E.G. Kranias, Targeted ablation of the phospholamban gene is associated with markedly enhanced myocardial contractility and loss of beta-agonist stimulation, Circ Res 75 (1994) 401-409.
[44] B.D. Hoit, S.F. Khoury, E.G. Kranias, N. Ball, R.A. Walsh, In vivo echocardiographic detection of enhanced left ventricular function in gene-targeted mice with phospholamban deficiency, Circ Res 77 (1995) 632-637.
[45] G. Chu, J.W. Lester, K.B. Young, W. Luo, J. Zhai, E.G. Kranias, A single site (Ser16) phosphorylation in phospholamban is sufficient in mediating its maximal cardiac responses to beta -agonists, J Biol Chem 275 (2000) 38938-38943.

[46] W. Luo, G. Chu, Y. Sato, Z. Zhou, V.J. Kadambi, E.G. Kranias, Transgenic approaches to define the functional role of dual site phospholamban phosphorylation, J Biol Chem 273 (1998) 4734-4739.
[47] J. Colyer, J.H. Wang, Dependence of cardiac sarcoplasmic reticulum calcium pump activity on the phosphorylation status of phospholamban, J Biol Chem 266 (1991) 17486-17493.
[48] Y. Ji, W. Zhao, B. Li, J. Desantiago, E. Picht, M.A. Kaetzel, J. Schultz Jel, E.G. Kranias, D.M. Bers, J.R. Dedman, Targeted inhibition of sarcoplasmic reticulum CaMKII activity results in alterations of Ca2+ homeostasis and cardiac contractility, Am J Physiol Heart Circ Physiol 290 (2006) H599-606.
[49] A. Mattiazzi, C. Mundina-Weilenmann, L. Vittone, M. Said, E.G. Kranias, The importance of the Thr17 residue of phospholamban as a phosphorylation site under physiological and pathological conditions, Braz J Med Biol Res 39 (2006) 563-572.
[50] D.G. Allen, C.H. Orchard, The effects of changes of pH on intracellular calcium transients in mammalian cardiac muscle, J Physiol 335 (1983) 555-567.
[51] L. Vittone, C. Mundina-Weilenmann, M. Said, A. Mattiazzi, Mechanisms involved in the acidosis enhancement of the isoproterenol-induced phosphorylation of phospholamban in the intact heart, J Biol Chem 273 (1998) 9804-9811.
[52] C.A. Valverde, C. Mundina-Weilenmann, M. Reyes, E.G. Kranias, A.L. Escobar, A. Mattiazzi, Phospholamban phosphorylation sites enhance the recovery of intracellular Ca2+ after perfusion arrest in isolated, perfused mouse heart, Cardiovasc Res 70 (2006) 335-345.
[53] M. Said, L. Vittone, C. Mundina-Weilenmann, P. Ferrero, E.G. Kranias, A. Mattiazzi, Role of dual-site phospholamban phosphorylation in the stunned heart: insights from phospholamban site-specific mutants, Am J Physiol Heart Circ Physiol 285 (2003) H1198-1205.
[54] P. James, M. Inui, M. Tada, M. Chiesi, E. Carafoli, Nature and site of phospholamban regulation of the Ca2+ pump of sarcoplasmic reticulum, Nature 342 (1989) 90-92.
[55] T. Toyofuku, K. Kurzydlowski, M. Tada, D.H. MacLennan, Amino acids Lys-Asp-Asp-Lys-Pro-Val402 in the Ca(2+)-ATPase of cardiac sarcoplasmic reticulum are critical for functional association with phospholamban, J Biol Chem 269 (1994) 22929-22932.
[56] M. Asahi, Y. Kimura, K. Kurzydlowski, M. Tada, D.H. MacLennan, Transmembrane helix M6 in sarco(endo)plasmic reticulum Ca(2+)-ATPase forms a functional interaction site with phospholamban. Evidence for physical interactions at other sites, J Biol Chem 274 (1999) 32855-32862.
[57] T. Toyofuku, K. Kurzydlowski, M. Tada, D.H. MacLennan, Amino acids Glu2 to Ile18 in the cytoplasmic domain of phospholamban are essential for functional association with the Ca(2+)-ATPase of sarcoplasmic reticulum, J Biol Chem 269 (1994) 3088-3094.
[58] D.K. Ceholski, C.A. Trieber, H.S. Young, Hydrophobic imbalance in the cytoplasmic domain of phospholamban is a determinant for lethal dilated cardiomyopathy, J Biol Chem 287 (2012) 16521-16529.

[59] Y. Kimura, K. Kurzydlowski, M. Tada, D.H. MacLennan, Phospholamban regulates the Ca2+-ATPase through intramembrane interactions, J Biol Chem 271 (1996) 21726-21731.
[60] C.B. Karim, C.G. Marquardt, J.D. Stamm, G. Barany, D.D. Thomas, Synthetic null-cysteine phospholamban analogue and the corresponding transmembrane domain inhibit the Ca-ATPase, Biochemistry 39 (2000) 10892-10897.
[61] Y. Kimura, K. Kurzydlowski, M. Tada, D.H. MacLennan, Phospholamban inhibitory function is activated by depolymerization, J Biol Chem 272 (1997) 15061-15064.
[62] P.D. Adams, I.T. Arkin, D.M. Engelman, A.T. Brunger, Computational searching and mutagenesis suggest a structure for the pentameric transmembrane domain of phospholamban, Nat Struct Biol 2 (1995) 154-162.
[63] R.L. Cornea, J.M. Autry, Z. Chen, L.R. Jones, Reexamination of the role of the leucine/isoleucine zipper residues of phospholamban in inhibition of the Ca2+ pump of cardiac sarcoplasmic reticulum, J Biol Chem 275 (2000) 41487-41494.
[64] C.A. Trieber, M. Afara, H.S. Young, Effects of phospholamban transmembrane mutants on the calcium affinity, maximal activity, and cooperativity of the sarcoplasmic reticulum calcium pump, Biochemistry 48 (2009) 9287-9296.
[65] C. Toyoshima, M. Asahi, Y. Sugita, R. Khanna, T. Tsuda, D.H. MacLennan, Modeling of the inhibitory interaction of phospholamban with the Ca2+ ATPase, Proc Natl Acad Sci U S A 100 (2003) 467-472.
[66] A.M. Winther, M. Bublitz, J.L. Karlsen, J.V. Moller, J.B. Hansen, P. Nissen, M.J. Buch-Pedersen, The sarcolipin-bound calcium pump stabilizes calcium sites exposed to the cytoplasm, Nature 495 (2013) 265-269.
[67] B.L. Akin, T.D. Hurley, Z. Chen, L.R. Jones, The structural basis for phospholamban inhibition of the calcium pump in sarcoplasmic reticulum, J Biol Chem 288 (2013) 30181-30191.
[68] M.C. Hutter, J. Krebs, J. Meiler, C. Griesinger, E. Carafoli, V. Helms, A structural model of the complex formed by phospholamban and the calcium pump of sarcoplasmic reticulum obtained by molecular mechanics, Chembiochem 3 (2002) 1200-1208.
[69] J. Zamoon, F. Nitu, C. Karim, D.D. Thomas, G. Veglia, Mapping the interaction surface of a membrane protein: Unveiling the conformational switch of phospholamban in calcium pump regulation, Proc Natl Acad Sci U S A 102 (2005) 4747-4752.
[70] K. Seidel, O.C. Andronesi, J. Krebs, C. Griesinger, H.S. Young, S. Becker, M. Baldus, Structural characterization of Ca(2+)-ATPase-bound phospholamban in lipid bilayers by solid-state nuclear magnetic resonance (NMR) spectroscopy, Biochemistry 47 (2008) 4369-4376.
[71] C. Toyoshima, S. Iwasawa, H. Ogawa, A. Hirata, J. Tsueda, G. Inesi, Crystal structures of the calcium pump and sarcolipin in the Mg2+-bound E1 state, Nature 495 (2013) 260-264.
[72] Z. Chen, B.L. Akin, L.R. Jones, Ca2+ binding to site I of the cardiac Ca2+ pump is sufficient to dissociate phospholamban, J Biol Chem 285 (2010) 3253-3260.

[73] Z. Chen, D.L. Stokes, W.J. Rice, L.R. Jones, Spatial and dynamic interactions between phospholamban and the canine cardiac Ca2+ pump revealed with use of heterobifunctional cross-linking agents, J Biol Chem 278 (2003) 48348-48356.
[74] T. Morita, D. Hussain, M. Asahi, T. Tsuda, K. Kurzydlowski, C. Toyoshima, D.H. Maclennan, Interaction sites among phospholamban, sarcolipin, and the sarco(endo)plasmic reticulum Ca(2+)-ATPase, Biochem Biophys Res Commun 369 (2008) 188-194.
[75] M. Asahi, E. McKenna, K. Kurzydlowski, M. Tada, D.H. MacLennan, Physical interactions between phospholamban and sarco(endo)plasmic reticulum Ca2+-ATPases are dissociated by elevated Ca2+, but not by phospholamban phosphorylation, vanadate, or thapsigargin, and are enhanced by ATP, J Biol Chem 275 (2000) 15034-15038.
[76] N.C. Bal, S.K. Maurya, D.H. Sopariwala, S.K. Sahoo, S.C. Gupta, S.A. Shaikh, M. Pant, L.A. Rowland, E. Bombardier, S.A. Goonasekera, A.R. Tupling, J.D. Molkentin, M. Periasamy, Sarcolipin is a newly identified regulator of muscle-based thermogenesis in mammals, Nat Med 18 (2012) 1575-1579.
[77] S.K. Sahoo, S.A. Shaikh, D.H. Sopariwala, N.C. Bal, M. Periasamy, Sarcolipin protein interaction with sarco(endo)plasmic reticulum Ca2+ ATPase (SERCA) is distinct from phospholamban protein, and only sarcolipin can promote uncoupling of the SERCA pump, J Biol Chem 288 (2013) 6881-6889.
[78] C.B. Karim, T.L. Kirby, Z. Zhang, Y. Nesmelov, D.D. Thomas, Phospholamban structural dynamics in lipid bilayers probed by a spin label rigidly coupled to the peptide backbone, Proc Natl Acad Sci U S A 101 (2004) 14437-14442.
[79] Y. Nesmelov, D.D. Thomas, Protein structural dynamics revealed by site-directed spin labeling and multifrequency EPR., Biophysi Rev (2010) 91-99.
[80] M. Gustavsson, R. Verardi, D.G. Mullen, K.R. Mote, N.J. Traaseth, T. Gopinath, G. Veglia, Allosteric regulation of SERCA by phosphorylation-mediated conformational shift of phospholamban, Proc Natl Acad Sci U S A 110 (2013) 17338-17343.
[81] M. Gustavsson, N.J. Traaseth, G. Veglia, Probing ground and excited states of phospholamban in model and native lipid membranes by magic angle spinning NMR spectroscopy, Biochim Biophys Acta (2012).
[82] K.N. Ha, M. Gustavsson, G. Veglia, Tuning the structural coupling between the transmembrane and cytoplasmic domains of phospholamban to control sarcoplasmic reticulum Ca(2+)-ATPase (SERCA) function, J Muscle Res Cell Motil In Press (2012).
[83] C.B. Karim, Z. Zhang, E.C. Howard, K.D. Torgersen, D.D. Thomas, Phosphorylation-dependent conformational switch in spin-labeled phospholamban bound to SERCA, J Mol Biol 358 (2006) 1032-1040.
[84] J. Li, Z.M. James, X. Dong, C.B. Karim, D.D. Thomas, Structural and Functional Dynamics of an Integral Membrane Protein Complex Modulated by Lipid Headgroup Charge, J Mol Biol (2012).
[85] B. Mueller, C.B. Karim, I.V. Negrashov, H. Kutchai, D.D. Thomas, Direct detection of phospholamban and sarcoplasmic reticulum Ca-ATPase interaction in

membranes using fluorescence resonance energy transfer, Biochemistry 43 (2004) 8754-8765.
[86] P. Bidwell, D.J. Blackwell, Z. Hou, A.V. Zima, S.L. Robia, Phospholamban binds with differential affinity to calcium pump conformers, J Biol Chem 286 (2011) 35044-35050.
[87] S. Minamisawa, Y. Sato, Y. Tatsuguchi, T. Fujino, S. Imamura, Y. Uetsuka, M. Nakazawa, R. Matsuoka, Mutation of the phospholamban promoter associated with hypertrophic cardiomyopathy, Biochem Biophys Res Commun 304 (2003) 1-4.
[88] K. Haghighi, G. Chen, Y. Sato, G.C. Fan, S. He, F. Kolokathis, L. Pater, I. Paraskevaidis, W.K. Jones, G.W. Dorn, 2nd, D.T. Kremastinos, E.G. Kranias, A human phospholamban promoter polymorphism in dilated cardiomyopathy alters transcriptional regulation by glucocorticoids, Hum Mutat 29 (2008) 640-647.
[89] T.M. Lee, L.J. Addonizio, W.K. Chung, Dilated cardiomyopathy due to a phospholamban duplication, Cardiol Young (2014) 1-2.
[90] M. Medin, M. Hermida-Prieto, L. Monserrat, R. Laredo, J.C. Rodriguez-Rey, X. Fernandez, A. Castro-Beiras, Mutational screening of phospholamban gene in hypertrophic and idiopathic dilated cardiomyopathy and functional study of the PLN -42 C>G mutation, Eur J Heart Fail 9 (2007) 37-43.
[91] K. Haghighi, F. Kolokathis, L. Pater, R.A. Lynch, M. Asahi, A.O. Gramolini, G.C. Fan, D. Tsiapras, H.S. Hahn, S. Adamopoulos, S.B. Liggett, G.W. Dorn, 2nd, D.H. MacLennan, D.T. Kremastinos, E.G. Kranias, Human phospholamban null results in lethal dilated cardiomyopathy revealing a critical difference between mouse and human, J Clin Invest 111 (2003) 869-876.
[92] J.P. Schmitt, M. Kamisago, M. Asahi, G.H. Li, F. Ahmad, U. Mende, E.G. Kranias, D.H. MacLennan, J.G. Seidman, C.E. Seidman, Dilated cardiomyopathy and heart failure caused by a mutation in phospholamban, Science 299 (2003) 1410-1413.
[93] A. Medeiros, D.G. Biagi, T.J. Sobreira, P.S. de Oliveira, C.E. Negrao, A.J. Mansur, J.E. Krieger, P.C. Brum, A.C. Pereira, Mutations in the human phospholamban gene in patients with heart failure, Am Heart J 162 (2011) 1088-1095 e1081.
[94] D.K. Ceholski, C.A. Trieber, C.F. Holmes, H.S. Young, Lethal, hereditary mutants of phospholamban elude phosphorylation by protein kinase A, J Biol Chem 287 (2012) 26596-26605.
[95] K.N. Ha, L.R. Masterson, Z. Hou, R. Verardi, N. Walsh, G. Veglia, S.L. Robia, Lethal Arg9Cys phospholamban mutation hinders Ca2+-ATPase regulation and phosphorylation by protein kinase A, Proc Natl Acad Sci U S A 108 (2011) 2735-2740.
[96] K. Haghighi, F. Kolokathis, A.O. Gramolini, J.R. Waggoner, L. Pater, R.A. Lynch, G.C. Fan, D. Tsiapras, R.R. Parekh, G.W. Dorn, 2nd, D.H. MacLennan, D.T. Kremastinos, E.G. Kranias, A mutation in the human phospholamban gene, deleting arginine 14, results in lethal, hereditary cardiomyopathy, Proc Natl Acad Sci U S A 103 (2006) 1388-1393.
[97] M.G. Posch, A. Perrot, C. Geier, L.H. Boldt, G. Schmidt, H.B. Lehmkuhl, R. Hetzer, R. Dietz, M. Gutberlet, W. Haverkamp, C. Ozcelik, Genetic deletion of arginine

14 in phospholamban causes dilated cardiomyopathy with attenuated electrocardiographic R amplitudes, Heart Rhythm 6 (2009) 480-486.
[98] K. Haghighi, T. Pritchard, J. Bossuyt, J.R. Waggoner, Q. Yuan, G.C. Fan, H. Osinska, A. Anjak, J. Rubinstein, J. Robbins, D.M. Bers, E.G. Kranias, The human phospholamban Arg14-deletion mutant localizes to plasma membrane and interacts with the Na/K-ATPase, J Mol Cell Cardiol 52 (2012) 773-782.
[99] J.K. Gwathmey, L. Copelas, R. MacKinnon, F.J. Schoen, M.D. Feldman, W. Grossman, J.P. Morgan, Abnormal intracellular calcium handling in myocardium from patients with end-stage heart failure, Circ Res 61 (1987) 70-76.
[100] G. Hasenfuss, H. Reinecke, R. Studer, M. Meyer, B. Pieske, J. Holtz, C. Holubarsch, H. Posival, H. Just, H. Drexler, Relation between myocardial function and expression of sarcoplasmic reticulum Ca(2+)-ATPase in failing and nonfailing human myocardium, Circ Res 75 (1994) 434-442.
[101] M. Meyer, W. Schillinger, B. Pieske, C. Holubarsch, C. Heilmann, H. Posival, G. Kuwajima, K. Mikoshiba, H. Just, G. Hasenfuss, et al., Alterations of sarcoplasmic reticulum proteins in failing human dilated cardiomyopathy, Circulation 92 (1995) 778-784.
[102] U. Schmidt, R.J. Hajjar, C.S. Kim, D. Lebeche, A.A. Doye, J.K. Gwathmey, Human heart failure: cAMP stimulation of SR Ca(2+)-ATPase activity and phosphorylation level of phospholamban, Am J Physiol 277 (1999) H474-480.
[103] K.L. Koss, I.L. Grupp, E.G. Kranias, The relative phospholamban and SERCA2 ratio: a critical determinant of myocardial contractility, Basic Res Cardiol 92 (1997) 17-24.
[104] R.H. Schwinger, G. Munch, B. Bolck, P. Karczewski, E.G. Krause, E. Erdmann, Reduced Ca(2+)-sensitivity of SERCA 2a in failing human myocardium due to reduced serin-16 phospholamban phosphorylation, J Mol Cell Cardiol 31 (1999) 479-491.
[105] J.B. Sande, I. Sjaastad, I.B. Hoen, J. Bokenes, T. Tonnessen, E. Holt, P.K. Lunde, G. Christensen, Reduced level of serine(16) phosphorylated phospholamban in the failing rat myocardium: a major contributor to reduced SERCA2 activity, Cardiovasc Res 53 (2002) 382-391.
[106] T. Netticadan, R.M. Temsah, K. Kawabata, N.S. Dhalla, Sarcoplasmic reticulum Ca(2+)/Calmodulin-dependent protein kinase is altered in heart failure, Circ Res 86 (2000) 596-605.
[107] B. Huang, S. Wang, D. Qin, M. Boutjdir, N. El-Sherif, Diminished basal phosphorylation level of phospholamban in the postinfarction remodeled rat ventricle: role of beta-adrenergic pathway, G(i) protein, phosphodiesterase, and phosphatases, Circ Res 85 (1999) 848-855.
[108] S. Mishra, H.N. Sabbah, J.C. Jain, R.C. Gupta, Reduced Ca2+-calmodulin-dependent protein kinase activity and expression in LV myocardium of dogs with heart failure, Am J Physiol Heart Circ Physiol 284 (2003) H876-883.
[109] Y. Kawase, H.Q. Ly, F. Prunier, D. Lebeche, Y. Shi, H. Jin, L. Hadri, R. Yoneyama, K. Hoshino, Y. Takewa, S. Sakata, R. Peluso, K. Zsebo, J.K. Gwathmey, J.C. Tardif, J.F. Tanguay, R.J. Hajjar, Reversal of cardiac dysfunction

after long-term expression of SERCA2a by gene transfer in a pre-clinical model of heart failure, J Am Coll Cardiol 51 (2008) 1112-1119.
[110] S. Sakata, D. Lebeche, N. Sakata, Y. Sakata, E.R. Chemaly, L.F. Liang, T. Tsuji, Y. Takewa, F. del Monte, R. Peluso, K. Zsebo, D. Jeong, W.J. Park, Y. Kawase, R.J. Hajjar, Restoration of mechanical and energetic function in failing aortic-banded rat hearts by gene transfer of calcium cycling proteins, J Mol Cell Cardiol 42 (2007) 852-861.
[111] S. Sakata, D. Lebeche, Y. Sakata, N. Sakata, E.R. Chemaly, L. Liang, C. Nakajima-Takenaka, T. Tsuji, N. Konishi, F. del Monte, R.J. Hajjar, M. Takaki, Transcoronary gene transfer of SERCA2a increases coronary blood flow and decreases cardiomyocyte size in a type 2 diabetic rat model, Am J Physiol Heart Circ Physiol 292 (2007) H1204-1207.
[112] A.R. Lyon, M.L. Bannister, T. Collins, E. Pearce, A.H. Sepehripour, S.S. Dubb, E. Garcia, P. O'Gara, L. Liang, E. Kohlbrenner, R.J. Hajjar, N.S. Peters, P.A. Poole-Wilson, K.T. Macleod, S.E. Harding, SERCA2a gene transfer decreases sarcoplasmic reticulum calcium leak and reduces ventricular arrhythmias in a model of chronic heart failure, Circ Arrhythm Electrophysiol 4 (2011) 362-372.
[113] M.J. Cutler, X. Wan, K.R. Laurita, R.J. Hajjar, D.S. Rosenbaum, Targeted SERCA2a gene expression identifies molecular mechanism and therapeutic target for arrhythmogenic cardiac alternans, Circ Arrhythm Electrophysiol 2 (2009) 686-694.
[114] F. del Monte, D. Lebeche, J.L. Guerrero, T. Tsuji, A.A. Doye, J.K. Gwathmey, R.J. Hajjar, Abrogation of ventricular arrhythmias in a model of ischemia and reperfusion by targeting myocardial calcium cycling, Proc Natl Acad Sci U S A 101 (2004) 5622-5627.
[115] F. Prunier, Y. Kawase, D. Gianni, C. Scapin, S.B. Danik, P.T. Ellinor, R.J. Hajjar, F. Del Monte, Prevention of ventricular arrhythmias with sarcoplasmic reticulum Ca2+ ATPase pump overexpression in a porcine model of ischemia reperfusion, Circulation 118 (2008) 614-624.
[116] L. Hadri, R. Bobe, Y. Kawase, D. Ladage, K. Ishikawa, F. Atassi, D. Lebeche, E.G. Kranias, J.A. Leopold, A.M. Lompre, L. Lipskaia, R.J. Hajjar, SERCA2a gene transfer enhances eNOS expression and activity in endothelial cells, Mol Ther 18 (2010) 1284-1292.
[117] B. Greenberg, A. Yaroshinsky, K.M. Zsebo, J. Butler, G.M. Felker, A.A. Voors, J.J. Rudy, K. Wagner, R.J. Hajjar, Design of a Phase 2b Trial of Intracoronary Administration of AAV1/SERCA2a in Patients With Advanced Heart Failure: The CUPID 2 Trial (Calcium Up-Regulation by Percutaneous Administration of Gene Therapy in Cardiac Disease Phase 2b), JACC Heart Fail 2 (2014) 84-92.
[118] K. Zsebo, A. Yaroshinsky, J.J. Rudy, K. Wagner, B. Greenberg, M. Jessup, R.J. Hajjar, Long-term effects of AAV1/SERCA2a gene transfer in patients with severe heart failure: analysis of recurrent cardiovascular events and mortality, Circ Res 114 (2014) 101-108.
[119] L. Suckau, H. Fechner, E. Chemaly, S. Krohn, L. Hadri, J. Kockskamper, D. Westermann, E. Bisping, H. Ly, X. Wang, Y. Kawase, J. Chen, L. Liang, I. Sipo, R. Vetter, S. Weger, J. Kurreck, V. Erdmann, C. Tschope, B. Pieske, D. Lebeche,

H.P. Schultheiss, R.J. Hajjar, W.C. Poller, Long-term cardiac-targeted RNA interference for the treatment of heart failure restores cardiac function and reduces pathological hypertrophy, Circulation 119 (2009) 1241-1252.

[120] S. Minamisawa, M. Hoshijima, G. Chu, C.A. Ward, K. Frank, Y. Gu, M.E. Martone, Y. Wang, J. Ross, Jr., E.G. Kranias, W.R. Giles, K.R. Chien, Chronic phospholamban-sarcoplasmic reticulum calcium ATPase interaction is the critical calcium cycling defect in dilated cardiomyopathy, Cell 99 (1999) 313-322.

[121] F. del Monte, S.E. Harding, G.W. Dec, J.K. Gwathmey, R.J. Hajjar, Targeting phospholamban by gene transfer in human heart failure, Circulation 105 (2002) 904-907.

[122] D.M. Kaye, A. Preovolos, T. Marshall, M. Byrne, M. Hoshijima, R. Hajjar, J.A. Mariani, S. Pepe, K.R. Chien, J.M. Power, Percutaneous cardiac recirculation-mediated gene transfer of an inhibitory phospholamban peptide reverses advanced heart failure in large animals, J Am Coll Cardiol 50 (2007) 253-260.

[123] M. Hoshijima, Y. Ikeda, Y. Iwanaga, S. Minamisawa, M.O. Date, Y. Gu, M. Iwatate, M. Li, L. Wang, J.M. Wilson, Y. Wang, J. Ross, Jr., K.R. Chien, Chronic suppression of heart-failure progression by a pseudophosphorylated mutant of phospholamban via in vivo cardiac rAAV gene delivery, Nat Med 8 (2002) 864-871.

[124] Y. Iwanaga, M. Hoshijima, Y. Gu, M. Iwatate, T. Dieterle, Y. Ikeda, M.O. Date, J. Chrast, M. Matsuzaki, K.L. Peterson, K.R. Chien, J. Ross, Jr., Chronic phospholamban inhibition prevents progressive cardiac dysfunction and pathological remodeling after infarction in rats, J Clin Invest 113 (2004) 727-736.

[125] A.N. Carr, A.G. Schmidt, Y. Suzuki, F. del Monte, Y. Sato, C. Lanner, K. Breeden, S.L. Jing, P.B. Allen, P. Greengard, A. Yatani, B.D. Hoit, I.L. Grupp, R.J. Hajjar, A.A. DePaoli-Roach, E.G. Kranias, Type 1 phosphatase, a negative regulator of cardiac function, Mol Cell Biol 22 (2002) 4124-4135.

[126] A. Pathak, F. del Monte, W. Zhao, J.E. Schultz, J.N. Lorenz, I. Bodi, D. Weiser, H. Hahn, A.N. Carr, F. Syed, N. Mavila, L. Jha, J. Qian, Y. Marreez, G. Chen, D.W. McGraw, E.K. Heist, J.L. Guerrero, A.A. DePaoli-Roach, R.J. Hajjar, E.G. Kranias, Enhancement of cardiac function and suppression of heart failure progression by inhibition of protein phosphatase 1, Circ Res 96 (2005) 756-766.

[127] P. Nicolaou, P. Rodriguez, X. Ren, X. Zhou, J. Qian, S. Sadayappan, B. Mitton, A. Pathak, J. Robbins, R.J. Hajjar, K. Jones, E.G. Kranias, Inducible expression of active protein phosphatase-1 inhibitor-1 enhances basal cardiac function and protects against ischemia/reperfusion injury, Circ Res 104 (2009) 1012-1020.

[128] K.M. Fish, D. Ladage, Y. Kawase, I. Karakikes, D. Jeong, H. Ly, K. Ishikawa, L. Hadri, L. Tilemann, J. Muller-Ehmsen, R.J. Samulski, E.G. Kranias, R.J. Hajjar, AAV9.I-1c delivered via direct coronary infusion in a porcine model of heart failure improves contractility and mitigates adverse remodeling, Circ Heart Fail 6 (2013) 310-317.

[129] T.J. Pritchard, Y. Kawase, K. Haghighi, A. Anjak, W. Cai, M. Jiang, P. Nicolaou, G. Pylar, I. Karakikes, K. Rapti, J. Rubinstein, R.J. Hajjar, E.G. Kranias, Active inhibitor-1 maintains protein hyper-phosphorylation in aging hearts and halts remodeling in failing hearts, PLoS ONE 8 (2013) e80717.

[130] W. Becker, The bh TCSPC Handbook, 5th ed., 2012.
[131] T. Förster, Intermolecular energy migration and fluorescence, Ann. Phys. (Leipzig) 2 (1948) 55-75.
[132] L. Stryer, Fluorescence energy transfer as a spectroscopic ruler, Annu Rev Biochem 47 (1978) 819-846.
[133] J.N. Sachs, D.M. Engelman, Introduction to the membrane protein reviews: the interplay of structure, dynamics, and environment in membrane protein function, Annu Rev Biochem 75 (2006) 707-712.
[134] S. McLaughlin, D. Murray, Plasma membrane phosphoinositide organization by protein electrostatics, Nature 438 (2005) 605-611.
[135] M. Tada, M. Inui, Regulation of calcium transport by the ATPase-phospholamban system, J Mol Cell Cardiol 15 (1983) 565-575.
[136] T. Cantilina, Y. Sagara, G. Inesi, L.R. Jones, Comparative studies of cardiac and skeletal sarcoplasmic reticulum ATPases. Effect of a phospholamban antibody on enzyme activation by Ca2+, J Biol Chem 268 (1993) 17018-17025.
[137] H.K. Simmerman, L.R. Jones, Phospholamban: protein structure, mechanism of action, and role in cardiac function, Physiol Rev 78 (1998) 921-947.
[138] D.H. MacLennan, and Kranias, E. G., Phospholamban: a crucial regulator of cardiac contractility, Nature Reviews 4 (2003) 666-678.
[139] R.L. Cornea, L.R. Jones, J.M. Autry, D.D. Thomas, Mutation and phosphorylation change the oligomeric structure of phospholamban in lipid bilayers, Biochemistry 36 (1997) 2960-2967.
[140] N.J. Traaseth, L. Shi, R. Verardi, D.G. Mullen, G. Barany, G. Veglia, Structure and topology of monomeric phospholamban in lipid membranes determined by a hybrid solution and solid-state NMR approach, Proc Natl Acad Sci U S A 106 (2009) 10165-10170.
[141] E.E. Metcalfe, J. Zamoon, D.D. Thomas, G. Veglia, 1H/15N Heteronuclear NMR spectroscopy shows four dynamic domains for phospholamban reconstituted in dodecylphosphocholine micelles, Biophys J 87 (2004) 1205-1214.
[142] E.E. Metcalfe, N.J. Traaseth, G. Veglia, Serine 16 phosphorylation induces an order-to-disorder transition in monomeric phospholamban, Biochemistry 44 (2005) 4386-4396.
[143] Z. Chen, B.L. Akin, L.R. Jones, Mechanism of reversal of phospholamban inhibition of the cardiac Ca2+-ATPase by protein kinase A and by anti-phospholamban monoclonal antibody 2D12, J Biol Chem 282 (2007) 20968-20976.
[144] T.L. Kirby, C.B. Karim, D.D. Thomas, Electron paramagnetic resonance reveals a large-scale conformational change in the cytoplasmic domain of phospholamban upon binding to the sarcoplasmic reticulum Ca-ATPase, Biochemistry 43 (2004) 5842-5852.
[145] Y.E. Nesmelov, C.B. Karim, L. Song, P.G. Fajer, D.D. Thomas, Rotational dynamics of phospholamban determined by multifrequency electron paramagnetic resonance, Biophys J 93 (2007) 2805-2812.

[146] D. Kast, L.M. Espinoza-Fonseca, C. Yi, D.D. Thomas, Phosphorylation-induced structural changes in smooth muscle myosin regulatory light chain, Proc Natl Acad Sci U S A 107 (2010) 8207-8212.
[147] G.W. Hunter, S. Negash, T.C. Squier, Phosphatidylethanolamine modulates Ca-ATPase function and dynamics, Biochemistry 38 (1999) 1356-1364.
[148] L.G. Reddy, R.L. Cornea, D.L. Winters, E. McKenna, D.D. Thomas, Defining the molecular components of calcium transport regulation in a reconstituted membrane system, Biochemistry 42 (2003) 4585-4592.
[149] E.L. Lockamy, R.L. Cornea, C.B. Karim, D.D. Thomas, Functional and physical competition between phospholamban and its mutants provides insight into the molecular mechanism of gene therapy for heart failure, Biochem Biophys Res Commun 408 (2011) 388-392.
[150] W. Birmachu, F.L. Nisswandt, D.D. Thomas, Conformational transitions in the calcium adenosinetriphosphatase studied by time-resolved fluorescence resonance energy transfer, Biochemistry 28 (1989) 3940-3947.
[151] J.M. Muretta, A. Kyrychenko, A.S. Ladokhin, D. Kast, G.E. Gillispie, D.D. Thomas, High -performance time-resolved fluorescence by direct waveform recording, Rev Sci Instrum 81 (2010) 103101-103101 - 103101-103108.
[152] R.V. Agafonov, I.V. Negrashov, Y.V. Tkachev, S.E. Blakely, M.A. Titus, D.D. Thomas, Y.E. Nesmelov, Structural dynamics of the myosin relay helix by time-resolved EPR and FRET, Proc Natl Acad Sci U S A 106 (2009) 21625-21630.
[153] J.R. Lakowicz, Principles of fluorescence spectroscopy, 2nd ed., Kluwer Academic/Plenum, New York, 1999.
[154] K.N. Ha, N.J. Traaseth, R. Verardi, J. Zamoon, A. Cembran, C.B. Karim, D.D. Thomas, G. Veglia, Controlling the inhibition of the sarcoplasmic Ca2+-ATPase by tuning phospholamban structural dynamics, J Biol Chem 282 (2007) 37205-37214.
[155] M. Gustavsson, N.J. Traaseth, C.B. Karim, E.L. Lockamy, D.D. Thomas, G. Veglia, Lipid-Mediated Folding/Unfolding of Phospholamban as a Regulatory Mechanism for the Sarcoplasmic Reticulum Ca(2+)-ATPase, J Mol Biol (2011).
[156] R.J. Bick, L.M. Buja, W.B. Van Winkle, G.E. Taffet, Membrane asymmetry in isolated canine cardiac sarcoplasmic reticulum: comparison with skeletal muscle sarcoplasmic reticulum, J Membr Biol 164 (1998) 169-175.
[157] R.L. Cornea, D.D. Thomas, Effects of membrane thickness on the molecular dynamics and enzymatic activity of reconstituted Ca-ATPase, Biochemistry 33 (1994) 2912-2920.
[158] Y. Sonntag, M. Musgaard, C. Olesen, B. Schiott, J.V. Moller, P. Nissen, L. Thogersen, Mutual adaptation of a membrane protein and its lipid bilayer during conformational changes, Nat Commun 2 (2011) 304.
[159] E. Hughes, J.C. Clayton, D.A. Middleton, Cytoplasmic residues of phospholamban interact with membrane surfaces in the presence of SERCA: a new role for phospholipids in the regulation of cardiac calcium cycling?, Biochim Biophys Acta 1788 (2009) 559-566.
[160] A.G. Lee, Lipid-protein interactions in biological membranes: a structural perspective, Biochim Biophys Acta 1612 (2003) 1-40.

[161] M.B. Gustavsson, N.J. Traaseth, G. Veglia, Activating and Deactivating Roles of Lipid Bilayers on the Ca2+-Atpase/Phospholamban Complex, Biochemistry (2011).
[162] X. Guo, L. Huang, Recent advances in nonviral vectors for gene delivery, Acc Chem Res 45 (2012) 971-979.
[163] A. Kunze, S. Svedhem, B. Kasemo, Lipid transfer between charged supported lipid bilayers and oppositely charged vesicles, Langmuir 25 (2009) 5146-5158.
[164] C.B. Karim, Z. Zhang, D.D. Thomas, Synthesis of TOAC spin-labeled proteins and reconstitution in lipid membranes, Nat Protoc 2 (2007) 42-49.
[165] J.M. Muretta, A. Kyrychenko, A.S. Ladokhin, D.J. Kast, G.D. Gillispie, D.D. Thomas, High-performance time-resolved fluorescence by direct waveform recording, Rev Sci Instrum 81 (2010) 103101.
[166] D.M. Bers, S. Despa, Cardiac myocytes Ca2+ and Na+ regulation in normal and failing hearts, J Pharmacol Sci 100 (2006) 315-322.
[167] G. Inesi, F. Tadini-Buoninsegni, Ca/H exchange, lumenal Ca release and Ca /ATP coupling ratios in the sarcoplasmic reticulum ATPase, J Cell Commun Signal (2013).
[168] A. Mattiazzi, C. Mundina-Weilenmann, C. Guoxiang, L. Vittone, E. Kranias, Role of phospholamban phosphorylation on Thr17 in cardiac physiological and pathological conditions, Cardiovasc Res 68 (2005) 366-375.
[169] J.K. Gwathmey, A. Yerevanian, R.J. Hajjar, Targeting sarcoplasmic reticulum calcium ATPase by gene therapy, Hum Gene Ther 24 (2013) 937-947.
[170] M. Jessup, B. Greenberg, D. Mancini, T. Cappola, D.F. Pauly, B. Jaski, A. Yaroshinsky, K.M. Zsebo, H. Dittrich, R.J. Hajjar, Calcium Upregulation by Percutaneous Administration of Gene Therapy in Cardiac Disease (CUPID): A Phase 2 Trial of Intracoronary Gene Therapy of Sarcoplasmic Reticulum Ca2+-ATPase in Patients With Advanced Heart Failure, Circulation 124 (2011) 304-313.
[171] Z.M. James, J.E. McCaffrey, K.D. Torgersen, C.B. Karim, D.D. Thomas, Protein-protein interactions in calcium transport regulation probed by saturation transfer electron paramagnetic resonance, Biophys J 103 (2012) 1370-1378.
[172] S.J. Gruber, S. Haydon, D.D. Thomas, Phospholamban mutants compete with wild type for SERCA binding in living cells, Biochem Biophys Res Commun (2012) epublished.
[173] J.L. Fernandez, M. Rosemblatt, C. Hidalgo, Highly purified sarcoplasmic reticulum vesicles are devoid of Ca2+- independent ('basal') ATPase activity, Biochim Biophys Acta 599 (1980) 552-568.
[174] D.L. Stokes, N.M. Green, Three-dimensional crystals of CaATPase from sarcoplasmic reticulum. Symmetry and molecular packing, Biophys J 57 (1990) 1-14.
[175] J.E. Bishop, T.C. Squier, D.J. Bigelow, G. Inesi, (Iodoacetamido)fluorescein labels a pair of proximal cysteines on the Ca2+-ATPase of sarcoplasmic reticulum, Biochemistry 27 (1988) 5233-5240.

[176] A. Mascioni, C. Karim, J. Zamoon, D.D. Thomas, G. Veglia, Solid-state NMR and rigid body molecular dynamics to determine domain orientations of monomeric phospholamban, J Am Chem Soc 124 (2002) 9392-9393.
[177] B. Buck, J. Zamoon, T.L. Kirby, T.M. DeSilva, C. Karim, D. Thomas, G. Veglia, Overexpression, purification, and characterization of recombinant Ca-ATPase regulators for high-resolution solution and solid-state NMR studies, Protein Expr Purif 30 (2003) 253-261.
[178] J.R. Lakowicz, Principles of Fluorescence Spectroscopy, 3rd ed., Springer Science + Business Media, LLC, New York, 2006.
[179] Z. Hou, E.M. Kelly, S.L. Robia, Phosphomimetic mutations increase phospholamban oligomerization and alter the structure of its regulatory complex, J Biol Chem 283 (2008) 28996-29003.
[180] D.M. Bers, Calcium cycling and signaling in cardiac myocytes, Annu Rev Physiol 70 (2008) 23-49.
[181] L.M. Espinoza-Fonseca, D.D. Thomas, Atomic-level characterization of the activation mechanism of SERCA by calcium, PLoS One 6 (2011) e26936.
[182] Z. Hou, S. Hu, D.J. Blackwell, T.D. Miller, D.D. Thomas, S.L. Robia, Two-color calcium pump reveals closure of the cytoplasmic headpiece with calcium binding., PLoS ONE (2012) accepted.
[183] R.W. Gross, Identification of plasmalogen as the major phospholipid constituent of cardiac sarcoplasmic reticulum, Biochemistry 24 (1985) 1662-1668.
[184] N.J. Traaseth, K.N. Ha, R. Verardi, L. Shi, J.J. Buffy, L.R. Masterson, G. Veglia, Structural and dynamic basis of phospholamban and sarcolipin inhibition of Ca(2+)-ATPase, Biochemistry 47 (2008) 3-13.
[185] A.R. Marks, Calcium cycling proteins and heart failure: mechanisms and therapeutics, J Clin Invest 123 (2013) 46-52.
[186] J.S. Pattison, J.R. Waggoner, J. James, L. Martin, J. Gulick, H. Osinska, R. Klevitsky, E.G. Kranias, J. Robbins, Phospholamban overexpression in transgenic rabbits, Transgenic Res 17 (2008) 157-170.
[187] H.K. Simmerman, J.H. Collins, J.L. Theibert, A.D. Wegener, L.R. Jones, Sequence analysis of phospholamban. Identification of phosphorylation sites and two major structural domains, J Biol Chem 261 (1986) 13333-13341.
[188] B.L. Akin, L.R. Jones, Characterizing phospholamban to sarco(endo)plasmic reticulum Ca2+-ATPase 2a (SERCA2a) protein binding interactions in human cardiac sarcoplasmic reticulum vesicles using chemical cross-linking, J Biol Chem 287 (2012) 7582-7593.
[189] J. Li, B.H. Jia, J. Sun, X.L. Lou, S.J. Hu, Phospholamban antisense RNA improves SR Ca2+-ATPase activity and left ventricular function in STZ-induced diabetic rats, Biomed Environ Sci 26 (2013) 577-583.
[190] J. Li, D.J. Bigelow, T.C. Squier, Phosphorylation by cAMP-dependent protein kinase modulates the structural coupling between the transmembrane and cytosolic domains of phospholamban, Biochemistry 42 (2003) 10674-10682.
[191] N.A. Steenaart, J.R. Ganim, J. Di Salvo, E.G. Kranias, The phospholamban phosphatase associated with cardiac sarcoplasmic reticulum is a type 1 enzyme, Arch Biochem Biophys 293 (1992) 17-24.

[192] L.K. MacDougall, L.R. Jones, P. Cohen, Identification of the major protein phosphatases in mammalian cardiac muscle which dephosphorylate phospholamban, Eur J Biochem 196 (1991) 725-734.
[193] G. Jakab, E.G. Kranias, Phosphorylation and dephosphorylation of purified phospholamban and associated phosphatidylinositides, Biochemistry 27 (1988) 3799-3806.
[194] J. Colyer, Phosphorylation states of phospholamban, Ann N Y Acad Sci 853 (1998) 79-91.
[195] S. Wang, B. Ziman, I. Bodi, M. Rubio, Y.Y. Zhou, K. D'Souza, N.H. Bishopric, A. Schwartz, E.G. Lakatta, Dilated cardiomyopathy with increased SR Ca2+ loading preceded by a hypercontractile state and diastolic failure in the alpha(1C)TG mouse, PLoS ONE 4 (2009) e4133.
[196] M. Said, R. Becerra, C.A. Valverde, M.A. Kaetzel, J.R. Dedman, C. Mundina-Weilenmann, X.H. Wehrens, L. Vittone, A. Mattiazzi, Calcium-calmodulin dependent protein kinase II (CaMKII): a main signal responsible for early reperfusion arrhythmias, J Mol Cell Cardiol 51 (2011) 936-944.
[197] A. Mattiazzi, E.G. Kranias, CaMKII regulation of phospholamban and SR Ca2+ load, Heart Rhythm 8 (2011) 784-787.
[198] S.D. Miyamoto, B.L. Stauffer, S. Nakano, R. Sobus, K. Nunley, P. Nelson, C.C. Sucharov, Beta-adrenergic adaptation in paediatric idiopathic dilated cardiomyopathy, Eur Heart J 35 (2014) 33-41.
[199] R. Dash, K.F. Frank, A.N. Carr, C.S. Moravec, E.G. Kranias, Gender influences on sarcoplasmic reticulum Ca2+-handling in failing human myocardium, J Mol Cell Cardiol 33 (2001) 1345-1353.
[200] J.G. Oh, J. Kim, S.P. Jang, M. Nguen, D.K. Yang, D. Jeong, Z.Y. Park, S.G. Park, R.J. Hajjar, W.J. Park, Decoy peptides targeted to protein phosphatase 1 inhibit dephosphorylation of phospholamban in cardiomyocytes, J Mol Cell Cardiol 56 (2013) 63-71.
[201] Y. Wang, S. Tandan, J. Cheng, C. Yang, L. Nguyen, J. Sugianto, J.L. Johnstone, Y. Sun, J.A. Hill, Ca2+/calmodulin-dependent protein kinase II-dependent remodeling of Ca2+ current in pressure overload heart failure, J Biol Chem 283 (2008) 25524-25532.
[202] N.A. Ablorh, T. Miller, F. Nitu, S.J. Gruber, C. Karim, D.D. Thomas, Accurate quantitation of phospholamban phosphorylation by immunoblot, Anal Biochem (2012).
[203] S.C. Calaghan, E. White, J. Colyer, Co-ordinated changes in cAMP, phosphorylated phospholamban, Ca2+ and contraction following beta-adrenergic stimulation of rat heart, Pflugers Archiv European Journal of Physiology 436 (1998) 948-956.
[204] S. Calaghan, E. White, J. Colyer, Preservation of the in vivo phosphorylation status of phospholamban in the heart: evidence for a site-specific difference in the dephosphorylation of phospholamban, Biochem Biophys Res Commun 248 (1998) 701-705.

[205] S. Calaghan, L. Kozera, E. White, Compartmentalisation of cAMP-dependent signalling by caveolae in the adult cardiac myocyte, Journal of Molecular and Cellular Cardiology 45 (2008) 88-92.
[206] S. Grote-Wessels, H.A. Baba, P. Boknik, A. El-Armouche, L. Fabritz, H.J. Gillmann, D. Kucerova, M. Matus, F.U. Muller, J. Neumann, M. Schmitz, F. Stumpel, G. Theilmeier, J. Wohlschlaeger, W. Schmitz, U. Kirchhefer, Inhibition of protein phosphatase 1 by inhibitor-2 exacerbates progression of cardiac failure in a model with pressure overload, Cardiovasc Res 79 (2008) 464-471.
[207] P.J. Guinto, T.E. Haim, C.C. Dowell-Martino, N. Sibinga, J.C. Tardiff, Temporal and mutation-specific alterations in Ca2+ homeostasis differentially determine the progression of cTnT-related cardiomyopathies in murine models, Am J Physiol Heart Circ Physiol 297 (2009) H614-626.
[208] W.A. Jackson, J. Colyer, Translation of Ser16 and Thr17 phosphorylation of phospholamban into Ca 2+-pump stimulation, Biochem J 316 (Pt 1) (1996) 201-207.
[209] X. Loyer, A.M. Gomez, P. Milliez, M. Fernandez-Velasco, P. Vangheluwe, L. Vinet, D. Charue, E. Vaudin, W. Zhang, Y. Sainte-Marie, E. Robidel, I. Marty, B. Mayer, F. Jaisser, J.J. Mercadier, S. Richard, A.M. Shah, J.P. Benitah, J.L. Samuel, C. Heymes, Cardiomyocyte overexpression of neuronal nitric oxide synthase delays transition toward heart failure in response to pressure overload by preserving calcium cycling, Circulation 117 (2008) 3187-3198.
[210] M. Tada, M. Inui, M. Yamada, M. Kadoma, T. Kuzuya, H. Abe, S. Kakiuchi, Effects of phospholamban phosphorylation catalyzed by adenosine 3':5'-monophosphate- and calmodulin-dependent protein kinases on calcium transport ATPase of cardiac sarcoplasmic reticulum, J Mol Cell Cardiol 15 (1983) 335-346.
[211] L. Raeymaekers, F. Hofmann, R. Casteels, Cyclic GMP-dependent protein kinase phosphorylates phospholamban in isolated sarcoplasmic reticulum from cardiac and smooth muscle, Biochem J 252 (1988) 269-273.
[212] H. Towbin, T. Staehelin, J. Gordon, Electrophoretic transfer of proteins from polyacrylamide gels to nitrocellulose sheets: procedure and some applications, Proc Natl Acad Sci U S A 76 (1979) 4350-4354.
[213] C.B. Karim, M.G. Paterlini, L.G. Reddy, G.W. Hunter, G. Barany, D.D. Thomas, Role of cysteine residues in structural stability and function of a transmembrane helix bundle, J Biol Chem 276 (2001) 38814-38819.
[214] N.A. Lockwood, R.S. Tu, Z. Zhang, M.V. Tirrell, D.D. Thomas, C.B. Karim, Structure and function of integral membrane protein domains resolved by peptide-amphiphiles: application to phospholamban, Biopolymers 69 (2003) 283-292.
[215] Y. Ji, E. Loukianov, T. Loukianova, L.R. Jones, M. Periasamy, SERCA1a can functionally substitute for SERCA2a in the heart, Am J Physiol 276 (1999) H89-97.
[216] W. Zhao, K.F. Frank, G. Chu, M.J. Gerst, A.G. Schmidt, Y. Ji, M. Periasamy, E.G. Kranias, Combined phospholamban ablation and SERCA1a overexpression result in a new hyperdynamic cardiac state, Cardiovasc Res 57 (2003) 71-81.

[217] L. Lipskaia, E.R. Chemaly, L. Hadri, A.M. Lompre, R.J. Hajjar, Sarcoplasmic reticulum Ca(2+) ATPase as a therapeutic target for heart failure, Expert Opin Biol Ther 10 (2010) 29-41.
[218] M. Hoshijima, Gene therapy targeted at calcium handling as an approach to the treatment of heart failure, Pharmacol Ther 105 (2005) 211-228.
[219] D.M. Bers, CaMKII inhibition in heart failure makes jump to human, Circ Res 107 (2010) 1044-1046.
[220] S. Sossalla, N. Fluschnik, H. Schotola, K.R. Ort, S. Neef, T. Schulte, K. Wittkopper, A. Renner, J.D. Schmitto, J. Gummert, A. El-Armouche, G. Hasenfuss, L.S. Maier, Inhibition of elevated Ca2+/calmodulin-dependent protein kinase II improves contractility in human failing myocardium, Circ Res 107 (2010) 1150-1161.